Technische Universität München

Fakultät für Chemie

Institut für Wasserchemie und Chemische Balneologie

Lehrstuhl für Analytische Chemie und Wasserchemie

Application of Raman Microscopy For a Rapid Antibiotic Susceptibility Test and the Investigation of Dormant Mycobacteria

David Bauer

Vollständiger Abdruck der von der Fakultät für Chemie der Technischen Universität München zur Erlangung des akademischen Grades eines

Doktors der Naturwissenschaft (Dr. rer. nat.)

genehmigten Dissertation.

Vorsitzender:	Prof. Dr. Martin Elsner
Prüfer der Dissertation:	1. apl. Prof. Dr. Christoph Haisch
	2. Prof. Dr. Wolfgang Frieß

Die Dissertation wurde am 17.05.2021 bei der Technischen Universität München eingereicht und durch die Fakultät für Chemie am 30.06.2021 angenommen.

„Je mehr der Mensch die Wirklichkeit und die Welt erkennt, desto besser erkennt er sich selbst in seiner Einmaligkeit, während sich für ihn immer drängender die Frage nach dem Sinn der Dinge und seines eigenen Daseins stellt. Alles, was als Gegenstand unserer Erkenntnis erscheint, wird daher selbst Teil unseres Lebens.“

Papst Johannes Paul II, Enzyklika “fides et ratio”

ACKNOWLEDGMENTS

First of all, I want to thank my supervisor and mentor Professor Dr. Christoph Haisch. Without his efforts and initiative this scientific research work would not exist. Thank you for the topics, the profound and enlightening discussions, which again and again gave me a direction and helped me to go my scientific way. I am also grateful for your confidence and the freedom you gave me in order to try out my own approaches.

Further thanks for the constant support, with advice and the design of experiments for everything dealing with microbiology and clinical infections and mycobacteria to PD Dr. med. Andreas Wieser. Thank you also for the good working environment interesting side topics and instructive and interesting digressions on 3D printing and microfluidic design.

Special thanks go also to my dear colleague Dr. Karin Wieland, for your time, creativity, datascientific support and the motivation. The paper was a real cowork and I learnt a lot! Thank you also for good talks during coffee and lunch breaks.

Here I also want to thank my other colleagues, Anna-Cathrine Neumann-Cip, Alexander Rinkenburger, Emilio Ambra, Genny Pang, Jessica Beyerl, Li Qiu and Klemens Thaler, as well as Ruben Weiss, Philipp Anger, Lisa Göpfert, Elli von der Esch, many more, all the students and other members of the institute.

Further special thanks for great support with the practical lab work goes to Gabi Liegl, Niculina Kriewall, Sarah Sternkopf and Christine Benning. Thank you!

Last but not least I want to thank my wonderful wife for her love, patience and confidence as well as my whole family and especially my parents who always supported me.

PUBLICATIONS

Parts of this work have been published:

Bauer, D.*; Wieland, K.*; Qiu, L.; Neumann-Cip, A.-C.; Magistro, G.; Stief, C. G.; Wieser, A.; Haisch, C., Heteroresistant Bacteria Detected by an Extended Raman-based Antibiotic Susceptibility Test. *Analytical Chemistry* **2020**.

Bauer, D.; Qiu, L.; Wieland, K.; Neumann-Cip, A.-C.; Wieser, A.; Magistro, G.; Stief, C.; Haisch, C., Deuterium uptake in combination with Raman spectroscopy as a tool to investigate antibiotic susceptibility of bacteria. *SPIE BiOS* **2020,** *11223*.

Neumann, A. C.; **Bauer, D.**; Hoelscher, M.; Haisch, C.; Wieser, A., Identifying Dormant Growth State of Mycobacteria by Orthogonal Analytical Approaches on a Single Cell and Ensemble Basis. *Analytical Chemistry* **2019,** *91* (1), 881-887.

Further publications to which I contributed with measurements and data analysis:

Qiu, L.; Pang, G. A.; Zheng, G.; **Bauer, D.**; Wieland, K.; Haisch, C., Kinetic and Mechanistic Investigation of the Photocatalyzed Surface Reduction of 4-Nitrothiophenol Observed on a Silver Plasmonic Film via Surface-Enhanced Raman Scattering. *Acs Appl Mater Inter* **2020,** *12* (18), 21133-21142.

Ploetz, E.; Zimpel, A.; Cauda, V.; **Bauer, D.**; Lamb, D. C.; Haisch, C.; Zahler, S.; Vollmar, A. M.; Wuttke, S.; Engelke, H., Metal–Organic Framework Nanoparticles Induce Pyroptosis in Cells Controlled by the Extracellular pH. *Adv Mater* **2020,** *32* (19), 1907267.

Dina, N. E.; Gherman, A. M. R.; Chis, V.; Sarbu, C.; Wieser, A.; **Bauer, D.**; Haisch, C., Characterization of Clinically Relevant Fungi via SERS Fingerprinting Assisted by Novel Chemometric Models. *Analytical Chemistry* **2018,** *90* (4), 2484-2492.

Alaoui Tahiri, A.; El Bali, B.; Lachkar, M.; Wilson, C.; **Bauer, D.**; Haisch, C., Crystal structure, IR, Raman and UV-Vis studies of $[Co(H_2P_2O_7)_2(H_2O)_2][CH_3)_3C\text{-}NH_3)]_2\cdot 2H_2O$. Inorganic Chemistry Communications **2021**, 108541.

*These authors contributed equally to this work.

ABSTRACT

The use of Raman spectroscopy in microbiology has increased dramatically over the past years, as improvements in the instruments and higher computing capabilities have made chemometric methods and automated measurements more efficient. In this thesis, Raman spectroscopy in combination with multivariate data analysis was used in order to develop Raman-based analytical approaches for two different research fields of microbiology. First, a fast and reliable antibiotic susceptibility test (AST) for advanced detection of heteroresistance was realized. Second, the dormant state of *Mycobacterium smegmatis* was investigated.

Antibiotics are one of the most effective ways of fighting bacterial infections, but the number of resistant germs is increasing, so it is even more important at this time to develop reliable and fast AST methods. In this work, Raman spectroscopy in combination with the stable isotope deuterium was used for this purpose. In the form of heavy water (D_2O), deuterium can be added to cultivation media and then be metabolized and incorporated by bacteria. By looking for the band of the carbon deuterium (CD) stretching vibration between 2100 and 2400 cm^{-1} in the Raman spectra of the cells due to the newly formed bond, the incorporation of the isotope can be monitored and consequently the metabolic activity can be measured. In preliminary experiments, two bacterial strains (Gram-negative *Escherichia coli* (*E. coli*) ATCC 9637 and Gram-positive *Enterococcus faecalis* (*E. faecalis*) ATCC 29212) were investigated. As a prerequisite for a reproducible and fast measurement, the sample preparation was optimized in order to obtain a concentrated and dried spot of biomass. This allows a time-efficient, automatable and straightforward measurement. Experiments of *E. coli* with ampicillin, ciprofloxacin and meropenem, as well as *E. faecalis* with ampicillin and vancomycin, proved the necessity of a 90-minute treatment with the antibiotic before addition of deuterium in the form of D_2O. Thus, an AST assay that allowed an unambiguous and reliable differentiation between resistant and sensitive bacteria was set up. The comparison of the intensity of the CD band with a parallel control culture then provides information about the sensitivity of the bacterium to the antibiotic. In total, the test takes 3.5 hours compared to 16 - 24 hours for conventional ASTs like broth dilution or disk diffusion tests. The applicability of the protocol was then

tested on 52 clinical isolates (30 *E. coli*, 10 *E. faecalis* and 12 *E. faecium*). All of these could be correctly identified. However, five heteroresistant isolates required an extended testing time. Still, compared to state-of-the-art AST methods, which are often not able to detect heteroresistance at all, the herein developed method proves to be advantageous. In heteroresistant cultures, a subpopulation of the bacterial cells exhibits a resistant phenotype, which often remains unnoticed in conventional tests. This mainly depends on the frequency of resistance, which lies between 10^{-2} and 10^{-7} in clinically relevant cultures. The fact that this kind of resistance is difficult to detect represents one of the greatest threats to patients with such infections, as this could lead to failure of antibiotic treatment. In this work, however, even these isolates were successfully identified as resistant within 5 - 6 hours. Furthermore, heteroresistant cultures with frequencies between 10^{-1} and 10^{-4} were experimentally modelled and investigated with the Raman-deuterium-based method. It was demonstrated that this comparably simple approach allows an estimation of the frequency of heteroresistance.

In addition to the antibiotic testing, the identification was performed using the obtained Raman spectra. A “support vector machine”, which is a supervised machine learning algorithm, was used to assign the spectra to the corresponding species with an accuracy of 95.7%.

Scientific investigation of *Mycobacteria* is another field of great importance, since tuberculosis, one of the deadliest bacterial infections, is caused by *Mycobacterium tuberculosis*. The dormant state of these bacteria is a state of persistence in which the bacteria have a reduced metabolism and therefore antibiotic treatment is ineffective. In this work, Raman spectra of single cells of dormant and non-dormant bacteria were recorded and evaluated by hierarchical cluster analysis. As reference analysis, electron microscopy, mass spectrometry and microbiological measurements were used.

ZUSAMMENFASSUNG

Die Anwendung der Raman-Spektroskopie in der Mikrobiologie hat aufgrund instrumenteller Fortschritte und verbesserter Möglichkeiten multivariater Datenauswertung, stark zugenommen. So ist die Verwendung von Raman-Mikroskopen zwar nichts Neues, leistungsstarke chemometrische Methoden und automatisierbare Messungen können aber erst seit kurzem nützlich und zeiteffizient verknüpft werden. Diese innovative Kombination wurde in dieser Arbeit in zwei unterschiedlichen Forschungsthemen der Mikrobiologie eingesetzt. Einmal wurde die Entwicklung eines schnellen und zuverlässigen Antibiotika-Empfindlichkeitstest vorangebracht. Zum anderen wurde der dormante Zustand von *Mycobacterium smegmatis* untersucht.

Antibiotika sind die Medikamente der Wahl, um bakterielle Infektionen zu behandeln und bislang mangelt es an echten Alternativen dafür. Ebenso steigt die Anzahl an resistenten Keimen in bedenklichem Maße und damit auch die Gefahr, dass Infektionen sogar tödlich enden. Ein Grund für den Anstieg resistenter Bakterien ist die Verschreibung typischer Antibiotika, ohne Laborbefund in Hinblick auf die Antibiotika-Empfindlichkeit. Diese Untersuchung ist normalerweise frühestens am nächsten Tag verfügbar, die Behandlung akuter Infektionen kann jedoch nicht aufgeschoben werden. Durch Behandlung mit nicht wirksamen Antibiotika kann sich eine Resistenz jedoch weiter manifestieren. Ein wichtiger Schritt um dieses Problem in den Griff zu bekommen ist die gezielte Verschreibung der Medikamente erst nach der Testung im Labor. Dafür ist es allerdings dringend erforderlich, schnellere Untersuchungsmethoden zu entwickeln. In dieser Arbeit wurde dazu die Raman-Spektroskopie im Zusammenspiel mit dem stabilen Isotop Deuterium verwendet. In Form von schwerem Wasser (D_2O) kann es Nährmedien unkompliziert zugegeben und dann von Bakterien aufgenommen werden. In den Raman-Spektren der Zellen kann anhand der neu entstehenden Bande der Kohlenstoff-Deuterium (CD) Streckschwingung zwischen 2100 und 2400 cm^{-1} der Einbau des Isotops in verschiedene Biomoleküle der Zellen und somit die Stoffwechselaktivität gemessen werden. In Vorversuchen wurden zwei Bakterienstämme (Gram-negative *Escherichia coli* ATCC 9637 und Gram-positive *Enterococcus faecalis* ATCC 29212) untersucht. Als Voraussetzung für eine reproduzierbare und besonders schnelle Messung wurde die Probenvorbereitung optimiert.

Ausgehend von der Bakterienkultur wurde die Zellmasse vor der Messung gereinigt, aufkonzentriert und getrocknet. Durch Wachstumsexperimente bei D_2O-Konzentrationen von 0%, 25% und 50% und Untersuchungen der Einwirkdauer verschiedener Antibiotika vor der D_2O-Zugabe konnte ein allgemein anwendbares Protokoll erstellt werden, das die zuverlässige Unterscheidung in resistente und empfindliche Bakterien erlaubt. Dazu wurden die Bakterien bei einer definierten Antibiotika-Konzentration in Nährmedium, welches kein D_2O enthält, 90 Minuten lang bei 37°C inkubiert und bei ansonsten gleichbleibenden Bedingungen wurde die D_2O-Konzentration auf 50% erhöht und nach einer weiteren Stunde die Probe genommen. Der Vergleich der Intensität der CD-Bande zu einer parallel durchgeführten Kontroll-Kultur liefert dann eine Aussage über die Empfindlichkeit des Bakteriums gegenüber dem Antibiotikum. Insgesamt dauert die Durchführung dieses Tests bis zum Ergebnis 3,5 Stunden. Im Vergleich dazu benötigt man für die Antibiotika Testung mittels herkömmlicher Tests, wie dem Epsilometer-Test, 16 bis 24 Stunden. Die Anwendbarkeit des Protokolls wurde an 52 klinischen Isolaten (30 *E. coli,* 10 *E. faecalis* und 12 *E. faecium*) erprobt. Hier kam der große Vorteil des Protokolls gegenüber anderen bisher entwickelter Methoden bei sogenannten heteroresistenten Keimen zum Tragen. Dies sind genetisch identische Bakterien, bei denen ein gewisser Anteil an Zellen jedoch einen resistenten Phänotyp aufweist. Typische klinisch relevante Frequenzen resistenter Zellen liegen dann zwischen 10^{-2} und 10^{-7}. Entsprechend bleibt dieses Phänomen jedoch je nach Testmethode unbemerkt und stellt somit eine der größten Gefahren für eine erfolgreiche Antibiotika-Behandlung dar. In dieser Arbeit konnten jedoch auch diese gefährlichen Isolate innerhalb von 5 bis 6 Stunden erfolgreich als resistent erkannt werden. In einem Experiment wurden zudem heteroresistente Kulturen mit Frequenzen zwischen 10^{-1} und 10^{-4} modelliert und es konnte gezeigt werden, dass die Raman-Deuterium basierte Testung eine Abschätzung der Frequenz ermöglicht. Ebenso wurde in einer Simulation aufgrund der experimentellen Ergebnisse gezeigt, dass Frequenzen bis zu 10^{-7} innerhalb von 7 bis 8 Stunden detektiert werden können.

Zusätzlich zur Antibiotika-Testung wurde die Identifikation der Bakterienspezies anhand der erhaltenen Spektren durchgeführt. Hierzu wurde ein maschineller Lern-Algorithmus, eine „Support Vector Machine“ angewendet um die Spektren den entsprechenden Spezies mit einer Genauigkeit von 95.7% zuzuordnen.

Die Erforschung von Mykobakterien hat große Bedeutung, da Tuberkulose, die tödlichste bakterielle Infektion, durch *Mycobacterium tuberkulosis* verursacht wird. Der dormante Zustand dieser Bakterien ist ein Überdauerungszustand, in dem die Bakterien aufgrund des verminderten Stoffwechsels nur eingeschränkt auf die Behandlung mit Antibiotika reagieren. Im Rahmen dieser Arbeit wurden Raman Spektren einzelner Zellen von dormanten und nicht-dormanten Bakterien aufgenommen und mittels Cluster-Analyse ausgewertet. Als Referenzanalytik wurden Elektronenmikroskopie, Massenspektrometrie und mikrobiologische Messungen angewendet.

TABLE OF CONTENTS

Page

1 INTRODUCTION

Antibiotics are the most effective means for the treatment of bacterial infections and they are one of the most important discoveries and fundaments of modern medicine and our healthcare system. However, the drastic increase of antibiotic-resistant bacteria is a fatal consequence of the wrong and careless use of the drugs.[1, 2] According to the World Health Organization (WHO), antimicrobial resistance constitutes a critical public health issue.[3] One important way to tackle the spread of resistant bacteria is the rapid diagnosis of antibiotic susceptibility with analytical tools that help to monitor and understand the mechanisms of resistance.

Thus, the focus of this work lies on the development of reliable and rapid analytical tests in the field of bacterial infections based on Raman spectroscopy. The fundamental working principle is the detection of inelastically scattered light due to vibrations of molecules under excitation by monochromatic light, which is typically provided by a laser. In this way, information about the molecular structure of the sample can be obtained. In combination with a microscope, it is even possible to examine single bacterial cells.[4] The instruments for this have become increasingly more sensitive and faster, especially in recent years. Together with enhanced computing power and the possibility of fast multivariate data analysis, further possibilities for the application of this analytical method were and are currently being established.

The objective of this work was to apply Raman spectroscopy in two important areas of clinical microbiology: the development of a rapid antibiotic susceptibility test for typical pathogens of urinary tract infections (*Escherichia coli* and *Enterococcus faecalis* and *faecium*) and the investigation of mycobacteria.

Advances in the diagnosis and treatment of urinary tract infections (UTIs) are of utmost interest, since it is among the most prevalent bacterial infections in the world. On average, every other woman contracts a UTI during her lifetime. Accordingly high are the costs to the healthcare system.[5] In the USA alone, the costs per year are in the range of \$2.7 – 3.5 billion.[6] It is widely known that antibiotics are the first choice for the treatment of bacterial infections. However, we also know that not every antibiotic is equally effective against

each bacterium. Among the multitude of existing bacteria, there are some with natural resistance mechanisms against certain antibiotics as well as some with acquired ones as a result of mutation and selection. The evolution of the latter kind is especially enhanced due to the unnecessary and improper use of the drugs. Of utmost concern for the global health systems in this context are evolving multi-drug resistant germs.[3] Only by thorough antibiotic susceptibility testing (AST), and consequent targeted treatment, can this situation be improved. However, the tests currently approved by the regulatory authorities (in Europe, for example, the European Committee on Antimicrobial Susceptibility Testing) are carried out on agar plates or in culture media and demand long incubation times of about 16 hours in order to give a profound test result.[7] This is too long for immediate treatment. In addition, many of the multi-resistant germs include an increasing number of heteroresistant bacteria.[8] They come with a subpopulation (typically one in 10^2 - 10^7 cells) that shows resistance to a certain antibiotic, whereas the majority of the cells are susceptible. Consequently, the supposedly effective antibiotic is prescribed and the few resistant cells can still grow. This leads to a persistent or repeated infection, with partly fatal consequences for the patients. Such heteroresistant pathogens can only be identified by repeated testing and therefore a suitable antibiotic is often indicated only very late. Therefore, the development of faster test procedures is urgently needed.

Another part of this work is about mycobacteria and their investigation with Raman spectroscopy. These kind of bacteria are also playing an important part in the context of infectious diseases.[9, 10] They represent a group of bacteria to which the pathogen causing tuberculosis, *Mycobacterium tuberculosis*, belongs. It is one of the most deadly bacterial infections for humans, currently causing 1.8 million deaths per year, and therefore deserves special attention.[11] In addition to a particularly robust cell wall, slow growth and the associated protracted treatment, they can reach a metabolic state known as dormancy.[12, 13] These are the reasons for frequent therapy complication and failure. The focus of this work lies on the characterization of this dormant state in which only a reduced metabolism takes place. This specific metabolic state leads to a passivation towards drugs that are usually effective against the bacteria. So far, aside from time-intensive and elaborate cultivation methods and ATP measurements, no fast and reliable analytical methods to distinguish the metabolic states of mycobacteria are established.[13] Here too, Raman spectroscopy might

be a straightforward alternative. Thus, in the second part of this work, the non-pathogenic *Mycobacterium smegmatis* was used to investigate the suitability of single-cell Raman spectroscopy in combination with hierarchical cluster analysis for classifying the metabolic state.

2 SCIENTIFIC FUNDAMENTALS

2.1 Raman Spectroscopy

The interaction of electromagnetic radiation and molecules is a huge area of research. One important branch is the investigation and application of different scattering processes. Of those, the two fundamental types are the elastic and the inelastic scattering of light. They are known as Rayleigh and Raman scattering, respectively, named after the scientists John William Strutt (3rd Baron Rayleigh) and Sir C. V. Raman, who first observed and described these effects experimentally in 1871 and 1928, respectively.[14-16] While no change in the wavelength can be observed for elastically scattered photons, a change in wavelength can be observed for inelastically scattered ones as a result of the interaction with the vibrations of molecules. Here, two options exist for the photons. They can either absorb the energy of a molecular vibrational mode, or they can excite it. These two kinds of scattering are known as anti-Stokes and Stokes scattering, respectively. A scheme of the dispersion of light at interaction with a sample and the energy scheme to describe these different processes is helpful and is given in Figure 1.

Raman spectroscopy is a powerful spectroscopic method for the characterization of molecules and is the cornerstone of this work. Already the first experimental observation of the inelastic scattering of liquids by Sir C. V. Raman in 1928 and experiments performed at the same time by G. Landsberg and L. Mandelstam in crystals allowed to characterize the corresponding materials down to the molecular level.[14, 17]

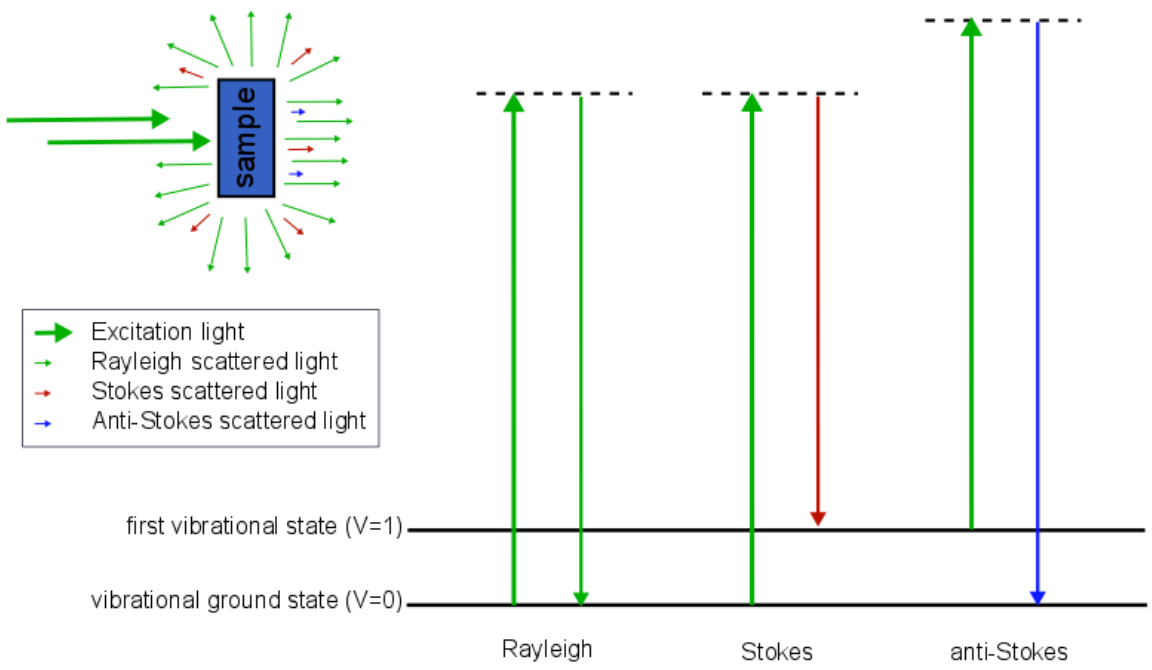

Figure 1: Schematic types of dispersed light that happen when coherent light hits a sample. The regarding energy-level diagrams of Raman (Stokes and anti-Stokes) scattering and Rayleigh scattering. Vibrational ground state at V = 0 and the first vibrational excited state at V = 1. Dotted lines: virtual energy states.

To describe the theoretical aspects of Raman scattering in an approximation, the molecule, which is excited by light can be considered as a dipole in an electromagnetic field. The induced dipole moment p is directly proportional to the polarizability α and the electrical field E as expressed in equation (1).

$$p = \alpha \cdot E \tag{1}$$

The polarizability depends on the molecular structure and especially the chemical bonds. The fundamental criterion for a molecule to be Raman active is that its polarizability changes during a vibration while obeying the expression in equation (2):[18]

$$\frac{\delta(\alpha)}{\delta(q)} \neq 0, \tag{2}$$

with δ(α), being the change in polarizability and δ(q) the spatial change of atoms from their coordinates in the ground state. According to the scheme depicted in Figure 1, the energy of scattered light can be expressed by means of the induced dipole moment with equation (3).

$$p = p(\nu_0) + p(\nu_0 + \nu_v) + p(\nu_0 - \nu_v) \quad (3)$$

Here, ν_0 is the frequency of the incident light and ν_v the frequency of the molecular vibration. From this equation, the three different possibilities of scattering can also be deducted. The first term represents Rayleigh scattering, the second term anti-Stokes and the third term Stokes scattering. If not otherwise specified, a Raman spectrum represents the Stokes scattered signals.

In Raman spectroscopy, the recorded signals are usually shown as the Raman shift in wavenumbers, i.e. in relative cm^{-1}. The Raman shift is calculated from the recorded wavelength λ_n and the wavelength of the light used for excitation λ_0 using equation (4).

$$\Delta\tilde{\nu}[cm^{-1}] = \frac{10^7}{\lambda_0\,[nm]} - \frac{10^7}{\lambda_n\,[nm]} \quad (4)$$

The energy range of the molecular vibrations commonly investigated in Raman spectroscopy lies in the range of 10 – 3500 cm^{-1}.[19] The position in terms of wavenumbers of a band in the Raman spectrum, which corresponds to the frequency of vibration of a molecular bond, can be approximated by the harmonic oscillation of a spring. The equation to calculate the respective frequency ν_v of such a vibration can be expressed as

$$\nu_v = \frac{1}{2\cdot\pi} \cdot \sqrt{\frac{\kappa}{\mu}}, \quad (5)$$

with κ being the force constant of the corresponding bond and μ the reduced mass.[18, 20] The latter can be calculated for a diatomic molecule using the masses m_1 and m_2 of the two involved atoms as shown in equation (6).

$$\mu = \frac{1}{m_1} + \frac{1}{m_2} \quad (6)$$

Thus, a comprehensive overview of typical Raman bands of typical molecular vibrations is given in Table 1 with the corresponding range of the vibration and the relative Raman intensity.

Table 1: Typical Raman bands of inorganic and organic functional groups with the corresponding vibrational mode (ν – stretching, δ - bending) and the spectral range in cm^{-1}. The relative intensity is abbreviated as follows: w – weak, m – medium, s – strong, vs – very strong.[18, 19, 21-25]

Functional group	Vibration mode	Spectral range in cm^{-1}	Relative intensity
Lattice vibrations in crystals	longitudinal modes	10 – 200	s
Metal-Oxygen	$\nu(X_{metal}\text{-}O)$	150 – 450	s
O–H stretch	ν(O–H)	3650 – 3000	w
N–H stretch	ν(N–H)	3500 – 3300	m
C–H stretch of alkenes	ν(=C–H)	3100 – 3000	s
C–H stretch of alkanes	ν(–C–H)	3000 – 2750	s
C≡C stretch of alkynes	ν(C≡C)	2250 – 2100	vs
C=C stretch of alkenes	ν(C=C)	1750 – 1450	vs – m
C–C stretch of aliphatic chains and cycloalkanes	ν(C–C)	1150 – 950	s – m
CC stretch of aromatics	ν(CC)	1600, 1580	s – m
	"ring-breathing"	1000	s
C=O stretch	ν(C=O)	1870 – 1650	s – w
Symmetrical C–O–C stretch	$\nu_{sym}(COC)$	970 – 800	s – m
CH_2 bending vibrations, antisymmetric CH_3 bend	$\delta(CH_2)$,$\delta_{asym}(CH_3)$	1470 – 1400	m
Symmetric CH_3 bend	$\delta_{sym}(CH_3)$	1380	m – w
Amide I band (CONH stretch)	Amide I	1670 – 1630	m – w
Amide III band (C-N stretch, coupled with opening of the CNH angle)	Amide III	1350 – 1250	m – w

The table already demonstrates that Raman spectroscopy allows identifying and characterizing molecules in detail. Hence, it is a powerful analytical tool and applied in many fields of research as well as for the identification of synthetic and natural materials in forensics, industry, geology and medicine.

Despite its many areas of application, Raman spectroscopy also has two main restrictions to its use. First, Raman scattering is a weak effect compared to other spectroscopic events such as Rayleigh scattering, absorption or fluorescence. It has a low scattering cross section corresponding to one Raman-scattered photon in 10^6 photons of incident light.[26-30] Second, at the typical excitation wavelengths of below 700 nm, fluorescence emission also occurs and interferes with the measurement. With about 10^5 orders of magnitude higher quantum efficiency than Raman scattering, fluorescence usually exceeds Raman scattering in terms of signal intensity and often covers a broad range of the entire spectrum. To prevent fluorescence, sample pretreatment, change of excitation wavelength or photobleaching can be performed.[31]

2.2 Fundamentals of Microscopy and Confocal Microscopy

Raman spectroscopy is often used in combination with a microscope in order to allow for the measurement of micrometer-sized samples.[30] Thus, the spectra can be collected from an accordingly small-sized spot. Raman hyperspectral imaging of microscopic structures. A typical setup for Raman microscopy is shown in Figure 2 on the left side. The light path is indicated in green. As light source, continuous wave lasers with typical wavelengths of 488, 532, 633 or 785 nm are usually used. The laser beam is guided into the microscope by mirrors or a combination of optical fibers and mirrors and is focused onto the sample via the objective. The scheme on the right side of Figure 2 shows how the backscattered light is then guided through a pinhole and into a spectrometer. The pinhole is important in order to have a confocal system.[30] As can be seen in the scheme, only light from the focal plane passes the pinhole, while the light from below ("reference plane") is blocked. This leads to a better spatial resolution compared to a non-confocal system. The size of the pinhole is commonly in the range of 25 – 200 μm. The light is guided to a spectrometer either by mirrors or by optical fibers. As detector, a charge-coupled device (CCD) is

typically used. It consists of a two-dimensional array of light-sensitive silicon photodiodes, also referred to as “pixels”, connected to a capacitor and allows the quantitative conversion of photons into electronic signals.[30, 32]

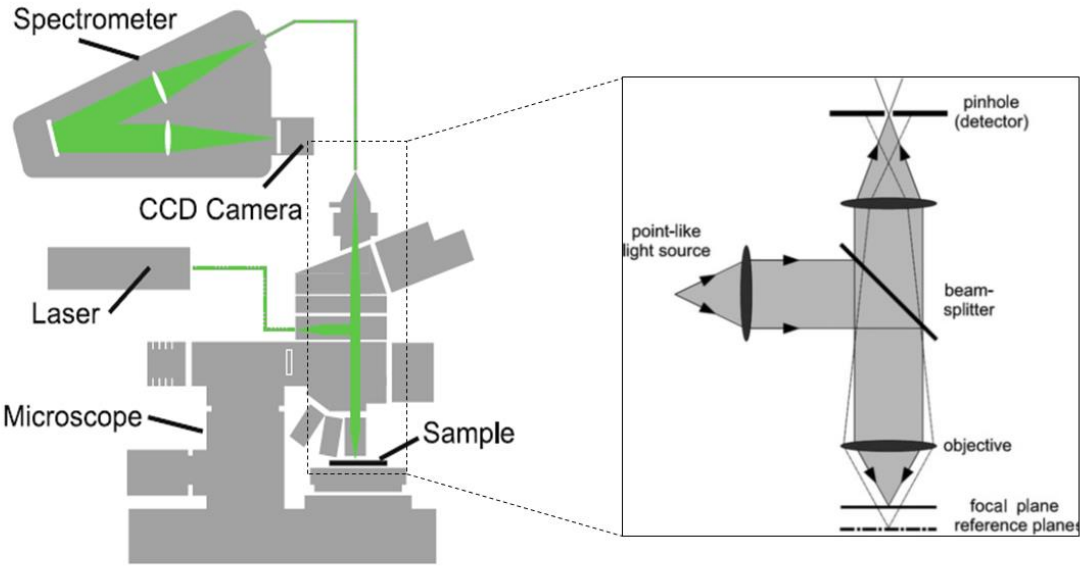

Figure 2: Left: Raman microscope setup with the different optical and spectroscopical components and the light path of the laser indicated in green. Right: More detailed view of the optical components of a confocal setup. Reprinted with permisssion from “Confocal Raman Microscopy”, chapter 1, by O. Hollricher and W. Ibach.[30]

In a given system, the selection of microscope objectives determines the focal volume from which the spectrum is collected. Here, not only the magnification but, most importantly, the numerical aperture (NA) of the objective contribute to the size of the focal volume. With equations (7) and (8), the lateral and axial resolution R_{lat} and R_{ax}, respectively, can be calculated for a given optical wavelength, in accordance with the Rayleigh criterion.[33]

$$R_{lat} = \frac{0.51 \cdot \lambda}{NA} \tag{7}$$

$$R_{ax} = \frac{0.88 \cdot \lambda}{n - \sqrt{(n^2 - NA^2)}} \tag{8}$$

In Table 2, the theoretical axial and lateral resolutions are given for different NAs of typically used objectives using the above given equations (7 and 8) for 532, 633 and 785 nm. These are the wavelengths of the most frequently used lasers in Raman spectroscopy.[18] While the first three objectives (50x, 60x, and 100x) are so-called metallurgical objectives that are used for direct measurement of the sample through air, the 63x objective is corrected for use with oil immersion.[34-37] The maximum NA is dependent on the refractive index of the medium in which the objective is used. Air has a refractive index of ~1.00, while that of a typical immersion oil equals 1.52.[36, 38, 39] With oil immersion objectives, a thin glass slide is used to cover the sample and a drop of oil is spread between the glass and the objective lens. Thus, a much higher NA and a better resolution can be obtained compared to metallurgical objectives.[40] Adar *et al.*[41, 42], Everall *et al.*[34-37] and Vyörykkä *et al.*[40] published studies in which they experimentally examined the resolution capabilities of confocal Raman microscopes. The values for the depth resolution were assessed by means of the full width at half maximum of the Raman intensity of a prominent band of the analyzed material (either polymer layers/beads with well-defined geometry or silicon wafers) during a z-scan. In their study from 2007, Everall *et al.* discussed in detail the depth resolutions of different objectives when performing a z-scan on silicon with a 532 nm laser and a confocal pinhole of 200 μm.[36] The depth resolution that results for different objectives is listed in Table 2 in the last column.

Table 2: Spatial resolution in nanometer calculated with the Rayleigh criterion for different NAs of typically used objectives (magnification/NA = 50x/0.55, 60x/0.7, 100x/0.9, 63x oil immersion/1.4) and for wavelengths of 532 and 631 nm.

Objective Magn./NA	λ = 532/633 nm		Everall 2007 (532 nm)
	Lateral Resolution	Axial Resolution	Objective/z-Resolution
50x/0.55	493/587	**2840**/3379	**11400**
60x/0.7	388/461	**1638**/1949	**6500**
100x/0.9	302/359	**830**/988	**2100**
63x (oil)/1.4 (n_{oil} = 1.518)	194/231	**503**/598	**2800**

When comparing those experimentally achieved with the calculated values, the experimental ones are at least by a factor of 2.5 higher. While the lateral resolution can be reached with a Raman microscope, it is difficult for the axial resolution.[30, 43, 44] Among the most important factors influencing the resolution in context of confocal Raman microscopy is the size of the confocal pinhole. However, a smaller pinhole size also reduces the amount of collected light and consequently leads to a decrease in Raman signal intensity. A compromise needs to be made here. Still, the best depth resolution published so far for bare silicon using a 532 nm laser, a 25 μm confocal pinhole size and a 100-fold objective with NA = 0.9 is 1.98 μm.[41, 42] Further influencing factors are the refraction properties of the sample that can lead to a different depth resolution than theoretically expected.[36, 37, 45] Precise depth profiling of polymer layers can be carried out if the thickness is in the range of 20 – 100 μm.[35, 36, 41, 46] Since elaborate experiments are necessary to pin down the depth resolution and would need to be carried out for each kind of sample material and microscopic setup, the exact depth resolution of a measurement is usually not known. However, during the last few years Raman microscopic systems were further improved and optimized and the manufacturers state depth resolutions of down to 1 μm for their Raman microscopes.[30, 37, 45, 47-49]

2.3 Processing of Raman Spectra

2.3.1 Acquisition and Basic Processing of Spectra

In order to acquire a Raman spectrum on a Raman microscope, as just explained, one step is the x-, y-, z-focusing on the sample. Furthermore, the selection of a suitable wavelength of the laser, the adjustment of its intensity and the selection of a proper integration time (i.e. the time for light accumulation at the detector) are necessary. Raman microscopy is usually used to investigate solid samples. If they are not completely pure elements or single chemical compounds but environmental samples or biological cells or tissue, they come with a rather heterogeneous chemical composition. Due to the small volume from which a spectrum is acquired, it is therefore necessary to record multiple spectra from different locations on the sample in order to characterize it entirely by means of Raman

spectroscopy. Thus, the Raman microscopic measurement of a single sample usually consists of a big dataset of several Raman spectra. To extract the necessary information about the sample, further processing steps are necessary. First, signals of cosmic rays need to be removed. They originate from high energy particles in the atmosphere and interfere with Raman measurements. Thus, they can be observed in spectra as very intense and sharp signal artefacts, covering one to three pixels of the CCD, and do not represent an actual signal of the sample.[30, 50-52] This kind of artefact can be determined by repeated measurement of the same spot on the sample and removed by an algorithm comparing the intensity of every single data point of the spectrum with the adjacent ones.[51, 52] If the intensity lies above a certain threshold compared to the average intensity, it is adjusted accordingly.[30, 52]

Depending on the sample material and the acquisition settings used, a more or less strongly changing background, originating from fluorescence can be recorded. Furthermore, Raman signals of the glass slide or material on which the sample is placed or, in the case of a dispersed sample, the dispersion medium might also be recorded. Hence, in order to evaluate the intensity of a Raman band of interest, the background has to be determined and removed. This is one of the critical steps during the processing of the spectra and is prone to errors, especially if an automated processing of multiple spectra is carried out.[53-55] The goal of any background subtraction is to estimate the background as precisely as possible without including any feature of the Raman spectrum of the sample. Subsequently, it can be simply subtracted from the raw spectrum. Mainly three different kinds of algorithms are used in Raman spectroscopy: the single-pass polynomial, the moving average and wavelet transformation based techniques.[53, 56-60] In this work, an algorithm provided by Vincent Mazet as a Matlab function ("backcor") was applied.[61] It uses a polynomial function of varying order in combination with a non-quadratic cost function to fit the baseline of the spectrum. Furthermore, a threshold value, which determines the level of noise that is taken into account for the fitting, needs to be set. A corresponding example

of the graphical selection of optimum parameters for a spectrum of *E. coli* (blue) is given in Figure 3.

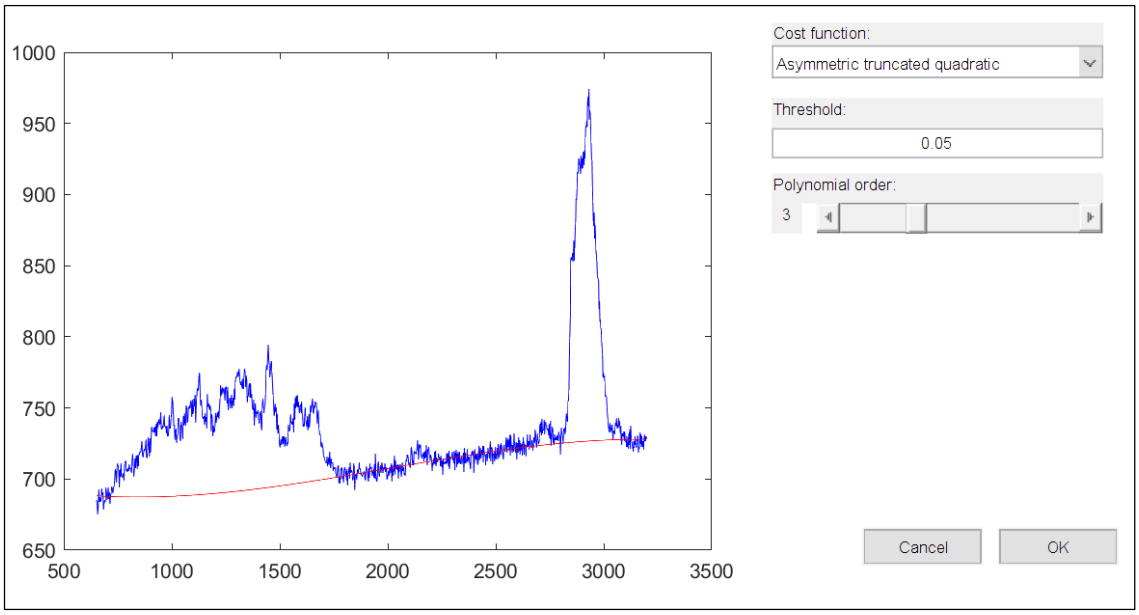

Figure 3: Example of the background correction with the Matlab function "backcor" for a spectrum of *E. coli* with CD band (blue). The parameters "cost function", "threshold" and "polynomial order" can be changed with the drop-down menu, the input field and the slider shown on the right, respectively. The currently visible parameters result in the curve drawn as a red line.

As can be seen, the selected parameters describe a good estimate of the baseline (red). However, when using large datasets, the variance of the background is high and spectra with high differences in signal-to-noise ratio (SNR) have to be processed. Hence, when using polynomial fitting, it is advantageous and more reproducible to divide the spectrum into smaller ranges.[62] Depending on the purpose or further use of the Raman spectrum, it can be reconstructed after the background correction or the single spectral sections can be used. In the first part of this work for example, solely the CD and CH stretching bands (2050- 2250 cm^{-1} and 2850 – 3050 cm^{-1}, respectively) are of interest. Thus, only the spectral range between 1900 and 3100 cm^{-1} was used for further processing.

2.3.2 Normalization

Depending on the intended use of the acquired data, normalization might be necessary. In general, normalization means the adjustment of the intensities of a spectrum by multiplication with a factor in order to equalize the value of a certain spectral feature of a

number of spectra. This feature can be the intensity of a specific band, the maximum band in the spectrum, the area under the curve or the vector length of the spectrum.[58] It is of utmost importance that the fluctuating background is subtracted in advance of normalization.

Under certain circumstances, normalization is necessary in order to use the spectra, for example, for quantitative analysis or multivariate data analysis.[53-55, 58] In general, the intensity of the Raman signal is proportional to the amount of sample and can be used for quantitative measurements.[58, 63-66] This is true if the focal volume is filled out homogeneously and completely with the sample, which can easily be ensured for measurements of liquid solutions in cuvettes or in measuring chambers that are larger than the focal volume.[66-74] A different, more complex case is the measurement of solid samples. The signal of crystals, for example, depends on the angle of incident light to their different crystal planes, on the refraction behavior of the beam of light due to edges and impurities and many more factors.[35, 45, 70, 75-80 56] Furthermore, a solid sample does not necessarily fill out the total focal volume, and the depth of penetration of a specific material by a laser depends also on the wavelength of the laser and the properties of the sample. After these aspects have been considered and the purpose of the measurements has been thoroughly thought through, it has to be decided whether normalization of the spectra is necessary or not.

2.3.3 Multivariate Chemometric Analysis

Linear Regression Analysis

Linear regression analysis is a good mathematical tool for combined quantitative and qualitative interpretation and analysis of Raman spectra. A prerequisite to its carrying out is knowledge about the composition of the spectra.[68, 73, 77, 81, 82] In general, regression analysis is a process in which a dependent variable is approximated by the linear combination of one or more independent variables, or so-called predictor variables, by means of the principle of least squares.[83, 84] The basis for the linear regression analysis is an equation of the form

$$y = a_0 + a_1 \cdot x_1 + a_2 \cdot x_2 + \cdots + a_n \cdot x_n + \epsilon, \quad (9)$$

with y being the dependent variable, $a_{0\ldots n}$ coefficients, $x_{1..n}$ the predictor variables and ε the residual. The approximation of the dependent variable is most times realized by fitting a linear combination of the independent variables in a least squares algorithm.[74, 77] In the case of more than one predictor, a multiple linear regression (MLR) is used. The goodness of the regression model is typically evaluated by the analysis of variance.[77, 85] In the context of Raman spectroscopy, the independent variable is usually the spectrum of a mixture of two or more different chemical compounds, and the predictors are the corresponding spectra of the pure chemical compounds.

Support Vector Machines

In analytical chemistry, often a large amount of multivariate, i.e. multidimensional, data is obtained from one measurement, or alternatively a series of experiments and measurements. In this context, computationally laborious data analysis can be carried out with programming environments like Matlab, Spyder (based on Python), R, or software provided by manufacturers of analytical instruments to analyze the respective data. In the context of Raman spectroscopy data analysis techniques are typically used in order to identify different chemical compounds by marginal differences between spectra. In general, two approaches of multivariate data analysis exist, supervised and unsupervised methods. While unsupervised methods (for example principal component analysis or cluster analysis) work without prior conditioning of the algorithm, supervised methods adapt a classification algorithm in order to lead to a predefined output.[30, 75, 77, 86, 87] One of the supervised algorithms that is often used for Raman and IR spectroscopy-based classification is the support vector machine (SVM).[25, 88-90] Its fundamental idea is based on algorithms of pattern recognition first suggested by R.A. Fisher back in 1936.[91] However, V.N. Vapnik published methods to modify and generalize this algorithm much later, in the 1990s, when personal computers with sufficient computing power were available.[91-94] As depicted in Figure 4, a dataset of two groups of data is used as training dataset and a so called kernel function, which describes a decision vector (abbreviated dv in Figure 4), forms a maximum margin between the data of the two classes. The most adjacent data

points define the support vector. The resulting kernel function can then be used to classify new data into one of the groups.

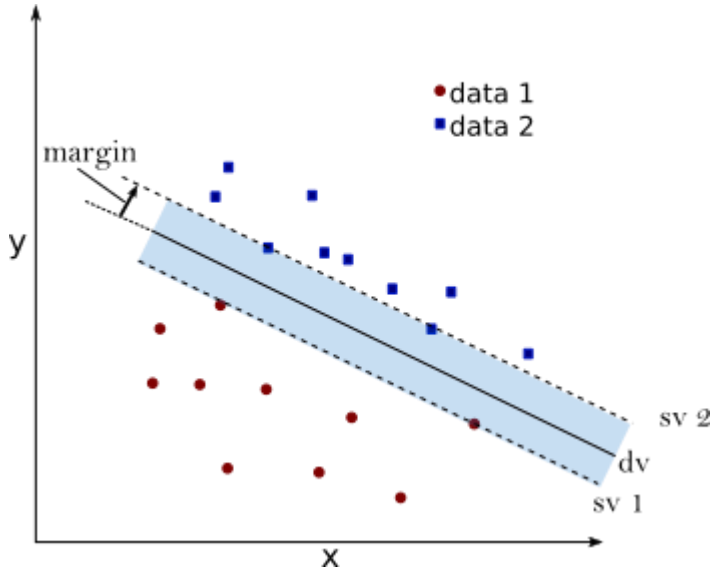

Figure 4: Scheme of the support vector machine. The two support vectors sv 1 and sv 2 have the largest possbile margin from the decision vector (dv). Scheme drawn according to Burges.[94]

In Figure 4, two simple examples for such supporting vectors are depicted for a two-dimensional problem. Using a larger dataset with higher dimensional data results in finding several support vectors, forming a plane. Consequently, the kernel function needs to describe a decision hyperplane. However, among classification strategies, SVM comes with high accuracy and demands comparably low computing power. Therefore, it is one of the most applied techniques in classification problems.[94] It can also be used for classification of more than two groups.[91, 92] To realize this, the multiclass problem is reduced into multiple binary classification problems by different strategies. One of them, called “one-versus-all”, works by separation of the multi-class training data into one group containing a single class and another group containing the rest of the classes.[94] Thus, a binary problem can again be solved. This is repeated for the complete number of classes so that each comprises the single class once. In a second approach called “one-versus-one”, pairs of classes are formed and classified against each other. Error-correcting output codes (ECOC) form a framework by which to solve these multiple binary classifications in a reasonable amount of time.[95-97] Although the reader is referred to the corresponding specialized literature for further details, the number of publications on the use of SVMs in

the field of Raman spectroscopy is steadily increasing. SVMs are especially popular for the Raman based identification of bacteria down to the strain level.[25, 88, 98-100]

Cluster Analysis

Cluster analysis can be used to group data according to their similarity and is an unsupervised classification method.[30, 84, 87, 101] The two main steps are the calculation of a similarity measure from each data point and the use of the measures in a clustering algorithm. Depending on the algorithm, the visualization can be realized as a colored schematic or a dendrogram.

There are different ways to find similarities in a numeric dataset like multiple spectral data. Typical metric distances are often based on the general Minkowski distance d_{XY}, which gives the distance between vectors X and Y using the equation (10)[102]

$$d_{XY} = \sqrt[p]{\sum_{j=1}^{n} |X_j - Y_j|^p}, \tag{10}$$

with p being an integer or ∞. For p = 1, the equation represents the Manhattan distance; for p = 2, the Euclidean distance; and for p = ∞, the Chebyshev distance.[102] These are also the most commonly used distances for numeric cluster analysis. Figure 5 depicts the Euclidean distance and the Manhattan distance for two points A(1,2) and B(2,1) in Cartesian coordinates.

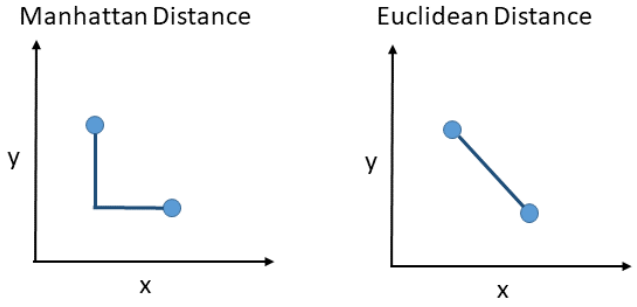

Figure 5: Graphical representation of Manhattan and Euclidean distance for two points in simplified Cartesian coordinates (modified scheme according to Brereton[87]).

Among the clustering algorithms, the agglomerative hierarchical clustering and the partitioning k-means clustering are mainly used.[30, 87, 102]

2.3.4 Raman Spectroscopy of Bacteria

Raman spectroscopy allows the identification of molecules based on their unique composition and the intensity distribution of their respective spectral bands. An extensive study by De Gelder *et al.* gives a good overview of Raman spectra of the most important biological molecules like DNA, RNA, lipids, sugars, and many more.[103] However, analysis and identification of bacteria is more challenging than the identification of a single, pure, highly concentrated substance, since they are composed of a complex mixture of biomolecules. According to Delgado *et al.,* dry cells of *E. coli* consist of 50-55% proteins, 20% RNA, 7-9% Lipids and 3% DNA, depending on their state of growth.[104]

Table 3 summarizes the most relevant spectral features of biologically relevant molecules.[105-108] However, many studies reported not just the discrimination of bacteria even down to the strain level by Raman spectroscopy and multivariate data analysis but also that the growth phases and cultivation condition play a significant role for analysis, since they have a strong influence on the Raman spectra.[98, 106, 109-112] Consequently, the cultivation procedure, sample collection and preparation of the sample need to be well defined before using spectra of bacteria for any purpose in order to prevent false classification caused by differences in the growth state or experimental condition.[105, 106, 113]

Table 3: List of characteristic group vibrations of biologically relevant molecules as taken from Neugebauer et al.[105, 106]

Biomolecular group	Molecular vibration	Raman shift/cm^{-1}
Nucleic Acids (Cytosine, Uracil)	ring breathing	785
Phenylalanine	ring breathing	1002
Phosphate Backbone	O-P-O stretching	1095
Amide III	N-H, C-N and skeleton stretch	1230 -1300
CH_2/CH_3	deformation vibration	1425 - 1475
Amide II	C-N stretching	1480 - 1580

Nucleic Acids (Adenine, Guanine)	C=C stretching	1570 - 1580
Amide I	C=O stretching	1600 - 1690
Lipids and Phospholipids	C=O stretching	1745
C-H	C-H stretching	2800 - 3020

While an advantage of the combination of Raman spectroscopy and confocal microscopy is the possibility to investigate even single cells, it is a time-consuming technique. Usually, the time for the acquisition of a single cell spectrum, with a good SNR, lies in the range of 1 to 20 seconds. While this seems rather short, the additional time for exact positioning and focusing also requires approximately between 3-10 seconds per bacterium, depending on the used instrument and objective. If a large number of cells of one culture needs to be analyzed, for example in order to obtain a thorough clinical test result, the measurement of a highly concentrated assembly of cells might be more efficient.[64]

2.4 Microbiological Background

2.4.1 Antimicrobial Agents

Successful treatment of bacterial infections has been one of the most important tasks for doctors and medical practitioners, even in the early days.[114-116] However, systematic studies and synthesis of the specific molecules that inhibit growth of bacteria were not done until the end of the 19th century.[116, 117] Research around antibacterial drugs was and is one of the great success stories of our time and helps to save millions of lives each year.[118] These drugs can be grouped according to the molecular target of the bacterial cell they act on. Figure 6 shows the relevant binding sites of antibiotics and lists the corresponding types of drugs. They can inhibit cell wall synthesis, formation of the plasma membrane or the DNA or RNA synthesis, act destructively on the ribosomes in which protein synthesis occurs or disrupt other metabolic pathways.[119-121] In this work, ampicillin, meropenem, ciprofloxacin and vancomycin were used. Their use and properties will be explained here in detail.

Further information on other such compounds can be found in the corresponding textbooks and literature.[119, 122, 123]

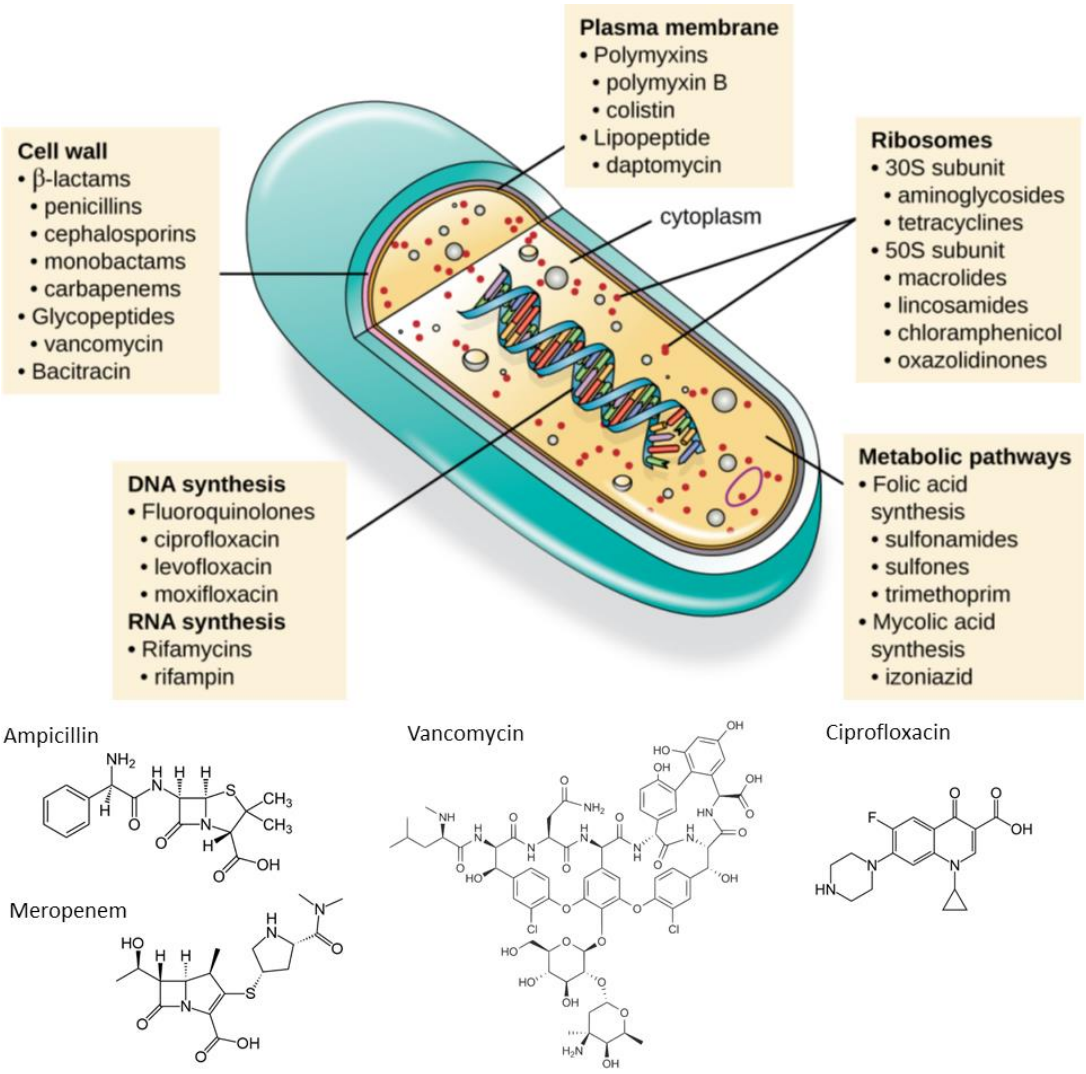

Figure 6: Top: Scheme of a bacterial cell with the different types of antiobtics and the molecular targets in the cell.[119] Bottom: molecular structures of ampicillin, meropenem, vancomycin and ciprofloxacin, the four antibiotics used in this work.

Ampicillin and meropenem belong to the β-lactams, named after the four-membered ring common to their chemical structures.[123] This ring contains a nitrogen atom attached to a β-carbon, that is, a carbon in beta position to the carbonyl ($R_2C=O$) group. While ampicillin is a penicillin derivate, meropenem belongs to the class of drugs called carbapenems. Both show a very different effectiveness against bacteria, since their chemical stability, cell diffusion kinetics, side effects and various other physical and chemical properties are very different.[124-126] However, the effect on bacteria is the same. Like most β-lactams, they

prevent cell wall synthesis during the first binary fission, by inhibiting the enzyme transpeptidase. As a consequence, lysis of the cells occurs.[127]

Vancomycin is a glycopeptide that can be obtained biotechnologically from the bacterium *Amycolatopsis orientalis* or synthetically.[119, 123] It has a larger molecular structure than ampicillin or meropenem, as can be seen in Figure 6. Nevertheless, it also affects the cell wall synthesis, although only of Gram-positive bacteria. Due to its hydrophilic nature, it binds strongly to D-alanyl-D-alanine, which forms the terminal moiety of *N*-acetylmuramic acid and *N*-acetylglucosamine. They are the major constituents of the bacterial cell wall of Gram-positive bacteria. The binding of vancomycin prevents the successful formation of the cell wall and consequently the growth of bacteria.

The fourth antibiotic of interest is ciprofloxacin, a fluoroquinolone. It inhibits gyrase, which is an enzyme that takes part in the process of winding up the DNA, by inducing formation of an enzyme-ciprofloxacin-DNA complex. In this way, replication of the DNA and consequently reproduction of the bacterium is prevented.[119, 123]

2.4.2 Antibiotic Resistance

As already mentioned, not every antibiotic is effective against all bacteria. In general, two main groups of bacteria exist: Gram-positive and Gram-negative. They have very different cell wall structures. As explained for vancomycin, certain antibiotics target certain molecular structures within the cell wall and are therefore specific for one of the abovementioned bacteria types and ineffective for the others. Furthermore, penetration of certain chemicals can be blocked due to the cell wall composition and structure.[119] Another reason for antibiotic treatment failure can be the presence of efflux pumps, which are enzyme complexes that move specific molecules out of the cell.[128] Two more mechanisms that could lead to failure of an antibiotic treatment exist. Inactivation of the drug by enzymes like β-lactamase and modification of the cell target. These mechanisms of resistance are called inherent resistance, since they are naturally present in the wild type of certain bacteria or arise from the specific cell wall structure of the bacterium. However, as in all organisms, genetic mutations can occur and resistance can thus be acquired. The routine and frequent use of antibiotics induces selective pressure and increases the number

of resistant bacteria.[2, 3] Thus, bacteria that are resistant against a large number of antibiotics exist. They are known as multi-drug resistant bacteria, and they are one of the most threatening issues in our modern healthcare system.[3] Therefore, effort is increasingly being put into studies to find new strategies for treating bacterial infections. One important step, and also the focus of this work, is to provide faster testing methods for finding the most suitable antibiotic in a given case. In this context, a particular threat to successful testing and treatment are so-called heteroresistant bacteria.[8, 129-131] With these bacteria, a certain portion of the population, i.e. a subpopulation, shows reduced susceptibility towards a specific antibiotic. This ratio of resistant to susceptible cells is also referred to as "frequency" of resistance.[132-136] The clinically relevant frequencies are in the range of 10^{-2} to 10^{-7}.[129, 137]

One important property in this context is the stability of heteroresistance.[8, 129, 130, 137, 138] A "stable" culture means that the frequency of resistant cells remains constant. However, isolates that cause detection and treatment failure are often not stable. Thus, several biochemical processes connected to resistance mechanisms are accompanied by a high cost of fitness and reduced growth rates. Consequently, they are only activated in the presence of an antibiotic and in a low number of cells (i.e. a low frequency). The resistance will therefore only be noted after repeated and prolonged growth in the presence of the antibiotic. Further complicating the detection, the expression of the resistance gene is not activated in the absence of the antibiotic, and the bacteria may appear susceptible in a later antibiotic test. To pin down heteroresistant cultures with low frequency and unstable resistance patterns, time-intensive genetic studies involving frequently repeated genetic testing, cultivation and plate counting is usually needed. To conclude, a method that allows the reliable and fast determination of heteroresistance, the corresponding frequency of resistance and its stability is urgently needed.

2.4.3 Antibiotic Susceptibility Testing

One of the main reasons for the increase of multi-drug resistant bacteria is the overuse of antibiotics. Thus, a crucial prerequisite to its prevention is the careful use of these drugs. This requires systematic testing of the patients. A thorough diagnosis of a bacterial

infection requires not only the identification of the organism but also the performance of antibiotic susceptibility testing (AST). An international standard procedure (ISO 20776-2:2007) to carry out such tests exists. Corresponding guidelines and data for laboratories to carry out these tests are provided by regional authorities like the Clinical and Laboratory Standards Institute (CLSI) in the United States and the European Committee on Antibiotic Susceptibility Testing (EUCAST) for Europe.[7, 139-142] According to the guidelines of EUCAST and CLSI, one of the main prerequisites of an AST test is phenotypic evidence of the susceptibility of an organism towards an antibiotic. This means that a clear inhibition of growth needs to be observed at a certain concentration of the drug. Official breakpoints (BPs) have been determined for the most common combinations of pathogens and antibiotics. These BPs are threshold concentration values that allow the classification of an organism as resistant or susceptible. They are defined by a committee of experts based on a huge number of parameters such as "resistance mechanisms, MIC distributions, zone diameter distributions […] pharmacodynamics and epidemiological cutoff values".[143] Lists of various bug-drug combinations with corresponding BPs are published by the responsible committees on their websites and are updated yearly (see for example http://www.eucast.org/clinical_breakpoints/). The final classification of a specific isolate as susceptible or resistant is done by comparison of its minimum inhibitory concentration (MIC) with the BP. The MIC is defined as the lowest concentration of antibiotic at which inhibition of growth can be observed. The gold standard methods to measure it, are the disk diffusion test according to Bauer and Kirby[144], the Epsilometer test (E-test) and the broth dilution method (depicted in Figure 7 A-C, respectively).[142, 145] In the agar plate-based tests (Figure 7 B and C), a concentration gradient of antibiotic is formed by diffusion of antibiotic from a disk, or a strip in the case of the E-test, containing defined concentrations of the drug. The bacteria are spread on the agar plate, and in the case of susceptibility, a certain diameter of the zone of growth inhibition can be observed. The corresponding value of the diameter can be correlated to a certain concentration of antibiotic, i.e. the MIC. In the E-test, a test strip embedded and printed with a gradient of antibiotic concentrations is placed on the plate and the MIC can be directly read from it. As can be seen in Figure 7 C, for the broth dilution, a series of tubes with growth medium

and increasing concentrations of antibiotic is prepared and growth is monitored by turbidity. The concentration at which no visible growth is observed gives the MIC.

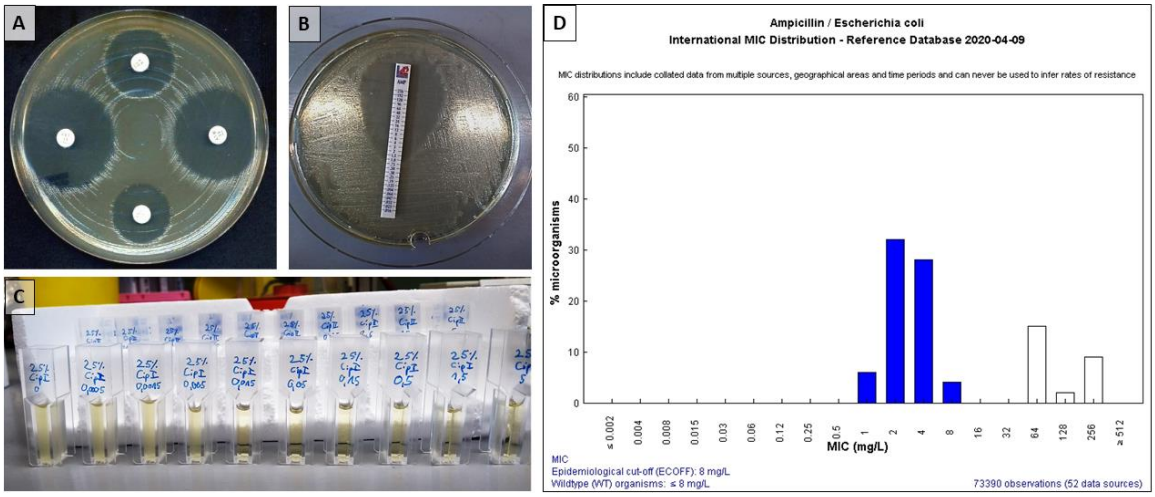

Figure 7: (A-C) Gold standard methods for antibiotic susceptibility testing according to CLSI and EUCAST guidelines. (A) Disk diffusion; (B) Epsilometer test; (C) broth dilution. (D) EUCAST MIC distribution graph for ampicillin – *E. coli*. The blue bars represent the MIC value distribution of the wild type and the white bars that of the resistant isolates. The corresponding dataset consists of 73390 clinical observations from 52 laboratories.[146]

Depending on the microorganism used, the necessary incubation time for the test is 16 hours. Testing platforms like the BD Phoenix ™, Vitek® 2 or MicroScan Walkaway try to minimize the time and material needed for preparation.[147-150] They can be used to identify the organism and determine the MIC within 5 to 12 hours after insertion of the bacterial suspension. However, for urgent treatment, as in the case of sepsis, the results are needed even sooner. Furthermore, they have only a poor performance in determination of heteroresistance. Therefore, several new methods are on the rise and advances towards accomplishing successful testing within a few hours are being made.[145, 151-153] Among them, a promising approach is based on Raman spectroscopy. However, most studies that have been published over the last few years focus on a very limited number of bug-drug combinations. While up to date only the feasibility was demonstrated the aspect of an automation of the measurement has not been discussed in detail and therefore application in a clinical environment and with a large number of samples has not yet been realized.[113, 152, 154-169] Thus, a robust, cheap and automatable method that is valid for a large variety of bug-drug combinations has to be developed.

2.4.4 Effect of Deuterium on Bacterial Growth and Its Metabolic Uptake

In this work, a Raman spectroscopy-based approach for the fast detection of antibiotic susceptibility was developed. The fact that the Raman shift of a molecular group vibration is strongly dependent on the mass of the atoms in the group can be exploited to monitor the incorporation of stable isotopes in organisms.[170-172] In this way, metabolic activity can be measured and consequently the effect of antibiotics on the metabolism can be studied. Suitable stable isotopes are those of atoms that are frequent in biomolecules. These are ^{2}H, ^{13}C, ^{15}N or ^{18}O. In the context of Raman spectroscopy, replacing hydrogen (^{1}H) by deuterium (^{2}H, abbreviated as "D") is especially of interest, since the difference of mass is large in proportion.[165, 167, 173, 174] Consequently, the shift of the group frequency is accordingly large. Thus, the -CH_2/-CH_3 stretching vibration, which is recorded at 2800 – 3100 cm^{-1} is shifted to 2000 – 2300 cm^{-1}, for the -CD_2/-CD_3 stretching vibration. Furthermore, there are no other group vibrations present in this range of the Raman spectrum, so unambiguous detection is possible.

Another advantage of using deuterium is its relatively low price compared to the other mentioned stable isotopes and its general applicability, for example D_2O, can be used in place of H_2O. Even though, the ability of bacteria to grow in media containing up to 85% D_2O was proved by Lester *et al.*[175], as well as Lovett[176], as early as the 1960s, D_2O remained a tool for scientific inquiry. The combination of growth of bacteria in D_2O and Raman spectroscopy is a useful tool for metabolic activity monitoring and was increasingly used for the purpose of carrying out rapid antibiotic tests during the past few years.

Thus, Berry *et al.* presented a comprehensive study in 2015 on the use of heavy water to identify metabolically active bacteria.[174] In their experiments, the use of 50% of D_2O (50% H_2O) showed no effect on growth of bacteria, while use of 100% D_2O significantly reduced growth. In 2017, Tao *et al.* used 50% D_2O on different bacteria and mentioned difficulty silencing the CD band completely, even when using concentrations of 60-fold the MIC of ampicillin with *Streptococcus mutans*.[162] Nevertheless, discrimination of resistant and susceptible bacteria was already possible after 30 minutes of incubation by analysis of the CD band intensity. Other works showed similar results but always on a limited number of bacteria and antibiotics.[177, 178] A study of a broader range of bug-drug combinations was

performed by Yang *et al.* in 2019.[169] Here, the application of the method on bacteria directly obtained from a patients' urine sample narrowed down the assay time to 2.5 hours. However, only Gram-negative bacteria were investigated in this study. The relevance for Gram-positive bacteria as uropathogens and of bacteria causing many other infections was not discussed. A protocol that is generally applicable for the most important uropathogens should include at least the Gram-positive Enterococci, which make up 5 – 25% of the causative uropathogens.[179] Another scientifically discussed aspect of a protocol using D_2O in the growth medium is its impact on the metabolism and growth rate of the organism of interest. While several studies suggest that very low concentrations (0.05 to 0.5%) of heavy water even enhance the growth, levels up to 50% partly decrease it.[175, 176, 180-182] However, the complete replacement of water by D_2O was often reported to completely inhibit growth.[109] Thus, a generally applicable protocol for Gram-positive and Gram-negative bacteria, as well as the influence of the amount of D_2O on the antibiotic effect, needs to be developed in order to achieve a clinically applicable protocol.

2.4.5 Mycobacteria and Their Metabolic Dormant State

Another topic of this work is the application of Raman spectroscopy on mycobacteria and the characterization of their metabolic state.[21, 183-190] Mycobacteria pose a special group of bacteria with a particular composition of the cell wall.[128, 185, 191-193] The most noticeable representative is *Mycobacterium tuberculosis*, which causes tuberculosis, since it leads to the most deaths per year among the bacterial infections.[11, 194, 195] One of the reasons for this negative record is the special structure of the cell wall. It is composed of a thick layer of lipids and mycolic acid that is similar for all *Mycobacteria*.[12] This specific chemical composition makes them resistant against many typical antibiotics and requires treatment of their infections with a limited number of special drugs sometimes declared as antimycobacterials.[128, 196] Another reason these microorganisms are dangerous is the fact that they can reach a so-called dormant state.[128, 193, 197, 198] In this state, their metabolism shows reduced activity and drugs are therefore even less effective. However, as indicated by the term "dormant", they can recover ("wake up") and grow again. *Mycobacterium smegmatis* (*M. smegmatis*) is frequently used as a model organism for studying

mycobacteria, since it is not pathogenic and, with 3 hours generation time, is also fast-growing compared to *M. tuberculosis* and many other *Mycobacteria.* Its typical doubling times are in the range of 15 – 20 hours.[186] *M. smegmatis* also reaches the dormant state and can therefore be used to investigate methods for its determination and therapy.[191, 199]

3 EXPERIMENTAL

3.1 Chemicals and Preparation of Cultivation Media and Antibiotic Solutions

Table 4 comprises a list of chemicals and media used for the experiments in this work. Where it applies, the purity is given and in the third column the supplier. All experiments were carried out under strict sterile conditions, where good laboratory and microbiological practice oblige it.

Table 4: List of chemicals used in this work.

Compound Name	Purity	Supplier
Deuteriumoxid (D_2O)	99.9 Atom%	Sigma-Aldrich, Germany
Ampicillin Sodium	BioReagent	Sigma-Aldrich, Germany
Meropenem	Pharmaceutical Secondary Standard	Sigma-Aldrich, Germany
Vancomycin Hydrochloride	Pharmaceutical Secondary Standard	Sigma-Aldrich, Germany
Ciprofloxacin	≥ 98.0% (HPLC)	Sigma-Aldrich, Germany
Formaldehyde solution	36.5-38%	Sigma-Aldrich, Germany
Yeas extract	grade for molecular biology	Sigma-Aldrich, Germany
Trypton	grade for molecular biology	Carl Roth, Germany
Sodium Chloride	>99%	Carl Roth, Germany
Mueller-Hinton Medium	powder	Becton Dickinson, US
Tryptic Soy Broth	powder	Becton Dickinson, US
M7H9 medium	Powder	Becton Dickinson, US
Nutrient Broth	Powder	Becton Dickinson, US
K_2HPO_4	ACS reagens, ≥ 98%	Sigma-Aldrich, Germany
$MgSO_4 \cdot 7H_2O$	ACS reagens, ≥ 98%	Sigma-Aldrich, Germany
NaH_2PO_4	BioXtra, ≥ 99.0%	Sigma-Aldrich, Germany

L-asparagine	≥ 98%	Sigma-Aldrich, Germany
glycerol	for molecular biology, ≥ 99.0%	Sigma-Aldrich, Germany
ferric ammonium citrate	reagent grade	Sigma-Aldrich, Germany
citric acid	≥ 99.5%	Sigma-Aldrich, Germany
Tween-80	10% low peroxide	Sigma-Aldrich, Germany
Middlebrook OADC	for microbiology	Sigma-Aldrich, Germany
MilliQ Water	18.2 MΩ·cm (25°C)	Merck-Millipore
HCl	1 M	Sigma-Aldrich, Germany
NaOH	>98%	Sigma-Aldrich, Germany

Cultivation media (Müller Hinton – MH; Lysogeny Broth – LB; Tryptic Soy Broth – TB; Nutrient Broth – NB) were prepared by dissolution of the corresponding powders in case of MH, TSB, NB and M7H9 medium (supplemented with OADC and 0.05% Tween-80) and mixtures of compounds in case of LB medium and Sautons medium in the corresponding volume ratio of MilliQ water/ 99.9% D_2O. LB medium contained per liter: 5 g/L yeast extract; 10 g/L Trypton; 1 g/L NaCl; Sautons medium contained per liter: K_2HPO_4, 0.18 g; $MgSO_4 \cdot 7H_2O$, 0.166 g; NaH_2PO_4, 0.056 g; L-asparagine, 1.33 g; glycerol, 20 mL; ferric ammonium citrate, 0.017 g; citric acid, 0.66 g; polysorbate 80, 0.833 g. The pH was adjusted to 6.0 in case of Sautons medium and to 7.0 for LB medium, using 1 M HCl or NaOH. The final Sautons medium was supplemented with 0.05% Tween-80. After preparation all media were sterilized by autoclaving.

Antibiotic stock solutions with a concentration of 2.00 mg/mL were prepared by dissolution of 10.0 mg of the respective chemical compound in 5.00 mL 0.9% NaCl solution followed by filtration through a sterile Millex-GV syringe filter (Sigma Aldrich, Taufkirchen, Germany) with 0.22 µm pores. In case of ciprofloxacin, 50 µL of 0.9% NaCl solution were replaced by 1 mol/L HCl in order to dissolve the powder.

3.2 Microorganisms

All microorganisms used in this work were provided from the stock of the Max von Pettenkofer Institute (MVP) for Hygiene and Medical Microbiology of the Ludwig-Maximilians University Munich. Before the experiments, cells of the corresponding bacterial strain were drawn from the -80°C stock of the MVP, streaked out on Columbia agar plates with 5% sheep blood (Becton Dickinson, US) in order to check for purity and then cultivated in liquid culture. Stock aliquots (-20°C, 10% glycerol) with an optical density OD_{600} (i.e. the absorption of light with wavelength of 600 nm) of 2 to 3 were prepared from these liquid cultures. For all experiments, overnight cultures, grown for 16 hours in liquid media at 37°C and 140 rounds per minute (rpm), were used. In case of *E. faecalis* and *E. faecium,* 3 mL TSB were inoculated with 5 µL of stock suspension, while *E. coli* was grown by adding 5 µL stock to 10 mL LB.

3.3 Growth Study, Broth Dilution and Preincubation

Growth studies with media containing 0, 25 and 50% D_2O were made, using the bacterial reference strains, *E. coli* ATCC 9637 and *E. faecalis* ATCC 29212. While *E. coli* was grown in LB, *E. faecalis* was cultivated in TB in triplicates at 37°C and 140 rpm. In case of the Gram-negative bacteria, aliquots of 500 µL were taken out after 0, 0.5, 1, 1.5, 2, 2.5, 3, 4 and 6 hours and of the Gram-positive ones after 0, 1, 2, 3, 4, 6 and 8 hours. Progress of growth was monitored by optical density measurements and the samples washed and prepared in order to carry out Raman measurements.

Broth dilution was used to investigate the minimum inhibitory concentration of reference strains. *E. coli* ATCC 9637 was treated with ampicillin, ciprofloxacin and meropenem and *E. faecalis ATCC 29212* with ampicillin and vancomycin. Here, the MIC was determined by the standard broth dilution procedure using MH medium containing a varying volume percentage (0, 25, 50 %) of D_2O. Using a dilution series of freshly prepared antibiotics, cultivation tubes with 3 mL of medium were inoculated with 5 µL of bacterial overnight culture. The MIC was determined by visual investigation of the turbidity after 16 h growth at 37°C on a shaking plate (140 rpm). Experiments were performed in triplicates. The MIC

values were determined according to ISO standard 20776-1 and the corresponding EUCAST guideline and thus, determined as the lowest concentration of antibiotic that completely inhibited growth of bacteria as detected by the unaided eye.[140, 200]

Preincubation. After the baseline experiments on the effect of deuterium on the bacterial growth, the time and potential of antibiotics to suppress the metabolic activity and thus the influence of the antibiotic treatment on the uptake of deuterium was investigated. So far, such a preliminary investigation has not been looked at before by other publications. In all of the earlier published studies, bacteria were simply treated with antibiotics directly in D_2O containing medium. However, troubles to 'silence down' the CD-band in certain cases were reported.[162] Hence, antibiotic treatment of the bacteria before the addition of D_2O, referred to as 'preincubation time' in this work, was carried out at increasing periods of time (15, 30, 60 and 90 minutes) and was compared to the direct (i.e. 0 minutes preincubation time) addition of D_2O. This systematic experiments pose the key novelty in our AST protocol, compared to earlier publications. It allows to determine the influence of antibiotic treatment on the CD-band evolution for the bug-drug combinations used in this work. The experimental procedure was as follows for each of them. Antibiotic stock solution was added to autoclaved media shortly before the experiments in order to obtain the final concentrations of 150 mg/L for ampicillin, 50 mg/L for ciprofloxacin, 75 mg/L for meropenem and 30 mg/L for vancomycin. These concentrations were derived from the clinical breakpoints (BP) given by EUCAST.[139] All bacteria treated with antibiotics were compared to a control culture that was prepared in parallel using the same bacteria sample and medium but treated with a solution containing 0.9% NaCl instead of the drug. For the inoculum overnight grown cultures were used and adjusted to an optical density of 0.05 respective to the final volume of medium. The cultures were incubated at 37°C on a shaking plate for 0, 15, 30, 60 and 90 minutes in medium supplied with antibiotic or 0.9% NaCl (in case of the control) but without D_2O. After the respective preincubation time, medium containing D_2O was added in order to obtain a final D_2O concentration of 50%. Subsequently, incubation for further 60 minutes was carried out.

3.4 Clinical Samples – AST

In order to test the Raman-based AST protocol on clinical samples, 52 clinical isolates of *E. coli*, *E. faecalis* and *Enterococcus faecium* (*E. faecium*) were obtained from the MVP microbiology department of the LMU Munich university hospital. The protocol was carried out in accordance with the procedure described in the paragraph before (preincubation study), but only 90 minutes preincubation time were used. Table 5 comprises a list of those clinical isolates with the resulting MIC value according to E-Tests. They were carried out using test strips, purchased from Liofilchem (Teramo, Italy). The MIC was determined according to the EUCAST guidelines and instructions provided by the supplier. Thus, bacteria were evenly spread on MH-agar plates with an inoculation swab from a bacterial suspension with an OD_{600} of 0.1 (equivalent to 0.5 McFarland standard). The resulting MIC was determined after 16 hours growth at 37°C.

Table 5: List of clinical isolates with results of the E-test and number of recorded Raman spectra (control/antibiotic) of clinical isolates of *E. coli* and *Enterococci* (continued on next page). ** Heteroresistant isolates with corresponding MIC values; * *E. faecium*.

E. coli								
Ampicillin			Ciprofloxacin			Meropenem		
Label	MIC (mg/L)	# specs	Label	MIC (mg/L)	# specs	Label	MIC (mg/L)	# specs
EC Amp 1	1.3	53/62	EC Cip 1	0.012	67/72	EC Mer 1	0.023	56/42
EC Amp 2	2	36/63	EC Cip 2	0.016	53/58	EC Mer 2	0.016	70/51
EC Amp 3	1.3	56/54	EC Cip 3	0.023	60/75	EC Mer 3	< 0.016	67/41
EC Amp 4	1.8	73/65	EC Cip 4	0.016	50/72	EC Mer 4	< 0.016	66/63
EC Amp 5	2	53/47	EC Cip 5	0.016	71/60	EC Mer 5	< 0.016	72/53
EC Amp 6	> 256	40/68	EC Cip 6	**0.032(1)	74/66	EC Mer 6	4	59/48
EC Amp 7	> 256	53/67	EC Cip 7	> 32	74/67	EC Mer 7	1	63/41
EC Amp 8	> 256	58/48	EC Cip 8	> 32	63/61	EC Mer 8	**0.5 (32)	53/56
EC Amp 9	> 256	53/63	EC Cip 9	> 32	74/71	EC Mer 9	8	53/31
EC Amp 10	> 256	38/51	EC Cip 10	>32	71/72			

E. faecalis/ faecium (*)					
Ampicillin			Vancomycin		
Label	MIC (mg/L)	# specs	Label	MIC (mg/L)	# specs
EF Amp 1	0.75 - 1	79/73	EF* Van 1	1.5	67/61
EF Amp 2	1	78/57	EF Van 2	2	68/71
EF Amp 3	0.38	74/87	EF Van 3	1.7	79/52
EF Amp 4	0.5	74/51	EF Van 4	1.5	67/89
EF Amp 5	1	52/85	EF Van 5	0.38	70/75
EF* Amp 6	2	72/53	EF Van 6	0.5	74/76
EF* Amp 7	> 256	46/69	EF Van 7	> 256	59/61
EF* Amp 8	> 256	62/55	EF Van 8	> 256	77/67
EF* Amp 9	> 256	72/76	EF* Van 9	> 256	64/55
EF* Amp 10	> 256	72/67	EF* Van 10	> 256	76/73
EF* Amp 11	> 256	55/111	EF* Van 11	> 256	68/76

3.5 Raman Measurement and Spectra Processing

Sample Preparation of the bacteria for Raman measurements was carried out by using an aliquot of 750 – 900 µL bacterial suspension. They were purified by centrifugation (9300 g, 3 min, 4 °C). The supernatants were replaced by 200 µL of sterile ultrapure water (Ampuwa, Fresenius Kabi Deutschland GmbH). The bacterial pellet was re-suspended, vortexed and the centrifugation step was repeated. The pellet was subsequently re-suspended in a minimum amount (5 – 20 µL) of water to obtain a concentrated bacterial suspension, from which 1.5 µL were placed on a hydrophobic glass slide (Paul Marienfeld GmbH, Lauda-Konigshofen, Germany) and left in a desiccator until it was dry. Raman spectra were recorded from the dry samples using a WITec alpha300 R confocal system (WITec GmbH, Ulm, Germany), equipped with a Cobolt DPL 532 nm solid state laser (Cobolt AB, Solna, Sweden) and a true-power module ensuring a stable laser power of

10 mW. The laser light was focused onto the sample employing a 50x objective (Zeiss C Plan-Apochromat 50x/0.75; Carl Zeiss AG, Germany). The scattered Raman photons were collected in reflection mode. After passing an edge filter, the red shifted Stokes light was detected via a fiber-coupled spectrometer (UHTS 300, f/4, 300 mm focal length) including a 600 l/mm grating and a Newton 970 EMCCD camera (Andor Technology Ltd., Belfast, UK). From each sample, 60 to 80 spectra covering the spectral range from 200 to 3500 cm^{-1} were acquired from different locations selected randomly over the entire sample spot. Typically, single spectra were acquired accumulating 3 scans with an integration time of 5 s. For the clinical samples, the integration time was reduced to 3 s in order to further reduce the assay time.

In order to select spectra with a significant spectrum of the biomass and deselect those with high fluorescence or without containing spectral information, a signal-to-noise filtering was performed. For this purpose, spectra were used after background subtraction. As value for the signal, the mean of the three highest intensities between 2880 and 2950 cm^{-1} (the CH-stretching band) was chosen. For the value of the noise the standard deviation of the spectrum between 2550 and 2650 cm^{-1}, where typically no Raman band occurs, was used.

3.6 Experimental Modeling of Heteroresistant Cultures

For simulation of heteroresistant cultures with different frequencies of resistance gene inductions, mixed cultures with defined proportions were generated. Therefore, one ampicillin susceptible and one ampicillin resistant strain of *E. coli* cultures were cultivated overnight. They were both diluted with LB-medium to an OD_{600} of 1.0 (suspension denoted V_1 in Table 6). The suspension of resistant bacteria was further diluted with sodium chloride solution in a serial dilution in order to obtain the suspensions denoted V_{-1}, V_{-2}, V_{-3} in Table 6 (1:10, 1:100 and 1:1000 dilution respectively). With those suspensions, cultures for an antibiotic test were inoculated in volume ratios as given in Table 6 to obtain a starting cell-ratio of susceptible to resistant bacteria of 1:10, 1:50, 1:100, 1:1000 and 1:10000. Each culture was added to 1.555 mL of LB medium with and without 150 mg/L ampicillin prior to preincubation for 90 minutes in cultivation tubes placed on a shaker (140 rpm; 37 °C). Finally, 1.945 mL LB medium containing 90% D_2O were added. Further cultivation in the

incubator was carried out and aliquots of 900 µL were drawn at time points listed in the last column in the table below and prepared for Raman measurements.

Table 6: Composition of the simulated heteroresistant samples. Column 'Ratio R/S' gives the ratio of resistant to susceptible cells. Following columns contain the volume of bacteria suspension used for inoculation. The corresponding OD_{600} is given in the subscript. (S) – susceptible, (R) – resistant. The last column 'aliquots' lists the time points of incubation after 90 min preincubation and addition of D_2O at which a sample was taken for Raman spectroscopic measurements.

R/S	V_1(S)	V_1(R)	V_{-1} (R)	V_{-2} (R)	V_{-3} (R)	aliquots
10^{-1}	157.5 µL	17.5 µL				1h
$2 \cdot 10^{-2}$	171.5 µL	3.5 µL				1, 2 h
10^{-2}	157.5 µL		17.5 µL			1, 2, 3 h
10^{-3}	157.5 µL			17.5 µL		1, 2, 3, 4 h
10^{-4}	157.5 µL				17.5 µL	1, 2, 3, 4 h

3.7 Clinical Isolates of Heteroresistant Bacteria

For isolates identified as heteroresistant via repeated E-testing and comparison with the microbiological database, antibiotic treatment was repeated with additional incubation times of 2, 3 and 4 hours and different concentration of antibiotic as listed in Table 7

Table 7: List of clinical isolates that were tested with enhanced incubation time and varying concentration of antibiotic. Column 'Isolate' contains the label of the isolate, 'MIC1/2 (HR)' represents the MICs in mg/L obtained from the first and if given, the second e-test as well as the MIC of the heteroresistant cultures in brackets. Then the 'Antibiotic' that was used is given, 'DP-R-AST conc' stands for deuterium probing Raman-AST concentration, which lists the concentrations that were used in the Raman-AST in mg/L and finally the incubation times in hours.

Isolate	MIC1/2(HR) / mgL^{-1}	Antibiotic	DP-R-AST conc. /mgL^{-1}	incub. time / h
EC-Mer 6	4/6 (8-24)	meropenem	0, 15, 30, 75	1, 2, 3, 4 h
EC-Mer 7	1/1.5(12)			1, 2, 3, 4 h

EC-Mer 8	0.5(32)/0.5(6)			1, 2, 3, 4 h
EC-Mer 1	0.032			1, 4 h
EC-Mer 2	0.016			1, 4 h
EC-Mer 3	<0.016			1, 4 h
EC-Cip 6	0.5/0.5(32)	ciprofloxacin	0, 0.5, 5, 50	1, 2, 3, 4 h
EC-Cip 1	0.012			1, 2, 3, 4 h
EF-Van 8	2(64)	vancomycin	0, 4, 16, 30	1, 2, 3, 4 h
EF-Ref	0.1			1, 2, 3, 4 h

3.8 Cultivation of *Mycobacterium smegmatis*

Wild type (WT) *M. smegmatis* (strain MC^2 155) was cultivated overnight in M7H9 medium supplemented with 10 mmol/mL OADC and 0.05% Tween-80 at 37°C and shaking at 140 rpm. The protocol to generate dormant mycobacteria from this strain, required a first cultivation step of incubation in nutrient broth at 37°C at 140 rpm for 24 h. Consequently, 1 mL of this culture was given to 100 mL of Sauton's medium with a pH-value adjusted to 6.0. This culture was incubated subsequently for 20 days at 37°C and 140 rpm before measurements.

3.9 Raman Measurement of *Mycobacterium smegmatis*

A volume of 500 µL of a *M. smegmatis* liquid culture (wild-type or dormant) was centrifuged for 4 min at 5000g and 4 °C, the supernatant was discarded, and the cell pellet was resuspended in 500 µL of 0.5% NaCl solution. After brief vortex mixing, the sample was centrifuged a second time and the pellet finally resuspended in 250 µL of 0.9% NaCl solution. Exploiting the hydrophobic nature of the mycobacteria, commercially available hydrophobic glass slides (Paul Marienfeld GmbH, Lauda-Konigshofen, Germany) were

used in order to fix the bacteria. This was enabled in a straightforward way by dipping the glass slide into the bacterial suspension. Thus, not only a fast and reliable fixation of mycobacteria under physiological conditions could be achieved, but also Raman analysis via an oil immersion objective with a high numerical aperture (NA = 1.4, working distance 0.15 mm) was possible. After positioning the glass slide with the fixed bacteria onto the microfluidic measurement chamber, it was immediately filled with physiologic NaCl solution (0.9%) and sealed with wax to avoid drying out of the chamber during the measurement.

The Raman spectra were recorded on the above mentioned WITec AlphaR300 using the 532 nm laser and the 63× oil immersion objective (Zeiss C Plan-Apochromat 63 × 1.4 Oil; Carl Zeiss AG, Germany). The spectra were acquired from single bacterial cells, applying 10 mW laser power, 5 s integration time, and three accumulations, recording a spectral range from 200 to 3200 cm^{-1}. A threshold value for the signal-to-noise ratio of the CH-stretching vibration was used in order to select spectra with high intensities. Those were processed using MATLAB 2018 (The MathWorks Inc., Natick, MA). Background subtraction and normalization were carried out by the functions msbackadj and msnormalize.

3.10 Electron Microscopy Sample Preparation and Analysis

In order to obtain scanning electron microscopy (SEM) images of the bacterial cells, their fixation was achieved by adding the necessary volume of 37 wt.% formalin to the bacterial cultures so that a final concentration of 3.7 wt. % of formalin was achieved in the suspension. After centrifugation for 5 min at 4500 rpm and 20 °C the cell pellet was resuspended in 3.7% formalin solution. Ten microliters of this suspension was spotted on stretched 0.7 mm aluminum foil and dried slightly at 37°C, just until the visible liquid film evaporated. Dehydration of the cells was subsequently performed by stepwise replacement of the water with ethanol. This was done by laying the foil into solutions with increasing concentrations of ethanol (10%, 30%, 70%, and 100% v/v, 7 min each). Finally, the sample was dried at room temperature and stored inside a desiccator until electron microscopy measurement was carried out.

Samples were investigated on a Zeiss Sigma VP field emission scanning microscope (Carl Zeiss Microscopy GmbH, Germany) under high vacuum, with 3.1 mm working distance and a 30 µm objective lens aperture. Images were collected using a secondary electron detector, with a voltage of 3 kV. In case of *M. smegmatis*, the length of bacteria was analyzed by manual evaluation, using the software Fiji[201] (open source image processing software) on the electron microscopic images.[201] The pixel aspect ratio was determined using the scale bar tool followed by marking the clearly distinguishable bacteria with the "draw line" and "measure size" function.

4 RESULTS AND DISCUSSION

4.1 Raman-Based AST and Classification of Clinical Isolates

4.1.1 Bulk Approach Compared to Single Cell Measurement

The gold standard for antibiotic susceptibility testing is still the plate-based approach. In order to fight the spread and evolution of multi-resistant bacteria, swiftness of the AST is an important step, especially since the use of the wrong antibiotic may even support the growth of resistant bacteria.[3, 202-205] Only with an effective antibiotic can the optimum treatment of an infection be achieved and the corresponding causative pathogens be killed. In case of patients with sepsis and high health risks, this can even be life-saving. Thus, the development of faster AST procedures is important. Numerous attempts have already been made to realize a protocol for rapid AST based on Raman spectroscopy.[152, 155, 157-160, 163, 168, 169] They exploit the fact that antibiotics lead to changes in the molecular composition of bacterial cells if they are susceptible. Consequently, significant differences in certain Raman bands are obtained for resistant versus susceptible bacteria. Thus, a result can be obtained within between 2.5 hours and, in the case of *E. coli* treated with ciprofloxacin, even 30 minutes.[157, 166, 206, 207] However, one main drawback here is that these changes in the spectra are highly specific for a certain bug-drug combination. Thus, such methods are not applicable for a general AST, as would be desirable. Another problem that has to be overcome is the time-consuming aspect of the measurement itself. Often measurements of single cells are performed. In order to obtain a spectrum with a good signal-to-noise ratio, roughly five to ten seconds should be estimated for each cell. Furthermore, it is known that a set of multiple Raman spectra obtained from even one single bacterial cell shows a certain variability in spectral features.[110, 168, 174]

With the aim of reducing the measurement time and of realizing the acquisition of spectra from a multitude of cells in one step, a bulk measurement of a concentrated bacterial cell mass was employed in this work.

One further aspect that has not been investigated so far in Raman-based AST is the phenomenon of heteroresistance of bacteria towards an antibiotic. Nevertheless, it is proposed to be one of the main reasons for antibiotic treatment failure. Thus, it needs to be taken into account for the development of an advanced AST. In the case of heteroresistant bacteria, only a certain percentage of cells is resistant compared to cultures with a clear phenotype (i.e. either fully susceptible or fully resistant). Typically, clinically relevant frequencies of resistant cells are in the range of 1 in 10^2-10^7 susceptible cells. Since in this case, the corresponding number of cells that needs to be investigated is high, single cell measurement is not suitable for finding the resistant ones.

In the context of antibiotic-treated cells, the physical appearance also hampers the acquisition of Raman spectra of single cells. After treatment with β-lactam antibiotics, lysis, deformation and increased fluorescence can occur. Consequently, the time of measurement drastically increases. This is another reason why in this work, the measurement of a bulk sample, and hence the acquisition of a spectrum of multiple bacteria, was favored. In order to realize such a measurement, development of an optimized procedure for concentrating the bacteria was necessary. Usually, bacteria are prepared on a simple microscopic glass slide by letting a drop of the corresponding bacterial suspension evaporate until it is dry. The result of such a sample preparation can be seen in Figure 8A. It is a widely spread drop allowing observation of a single bacterium (see Figure 8B and C).

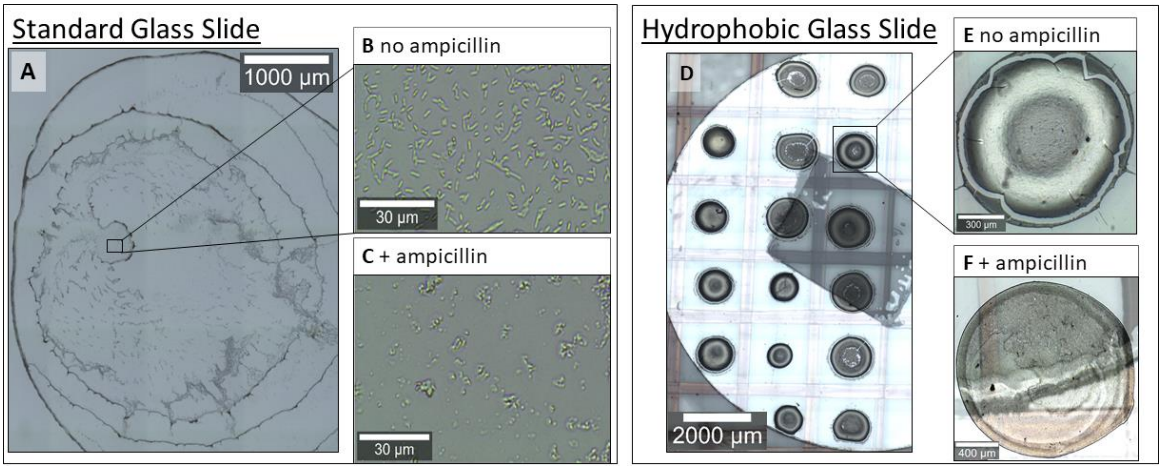

Figure 8: Sample preparation for measurements of bacteria on glass. (A) A dried drop on a normal glass slide allows obtainment of single cells of untreated (B) or ampicillin-treated bacteria (C). (D) On hydrophobic glass, bacteria are concentrated as distinct spots due to the high surface tension. Compared to untreated bacteria (D), the treatment with ampicillin leads to a drop like in (F).

However, in order to achieve a concentrated bacterial sample spot, hydrophobic glass was used instead of the standard hydrophilic glass. On this, the cells accumulate within a small spot due to the different surface properties of the glass and the aqueous sample. Figure 8 A and D allow a direct visual comparison of a dried 1.5-µL drop of bacterial suspension on a normal and a hydrophobic glass slide. While the drop spreads on the normal glass, the surface tension on the hydrophobic glass leads to dense accumulation of bacteria in spots. Furthermore, as already mentioned, treatment with certain antibiotics, for example ampicillin, leads to cell lysis. The corresponding result is visible in Figure 8 C. Here, only deformed remains of cells are obtained. In case of the hydrophobic slide, a difference between treated and untreated cells is also observed, as can be seen when comparing Figure 8F and E. Here, concentration of the biomass is achieved on the edge of the spot. This allows fast acquisition of spectra with minimum time delay between measurements.

4.1.2 Spectral Processing and CD band Evaluation

One main objective of this study was the development of an automated evaluation of the data. Hence, after establishing a robust sample preparation, allowing reproducible measurements, the settings for the acquisition of the spectra were optimized and a processing script that allows the reproducible and robust evaluation of the data was implemented in Matlab. All measurements were carried out using a 50x objective with 0.75 NA and a 532 nm laser of 10 mW and collecting signals in the spectral region between 100 and 3500 cm^{-1}. Especially when bacteria were treated with antibiotics compared to those of untreated bacteria, a greater portion of the spectra showed strong fluorescence. In these spectra the signal of Raman scattered photons is superimposed by fluorescence, which often covers a large part of the entire spectrum and leads to Raman spectra with a low SNR after background subtraction. In order to deselect those spectra and use only the ones with sufficient Raman intensity, a selection criterion based on the SNR of the CH-stretching band proved to be useful. As described in paragraph 3.5 on page 33, a robust method for SNR calculation was by division of the mean of the three maximum signals between 2880 and 2950 cm^{-1} (the CH-stretching band) and the standard deviation of the spectrum between 2550 and 2650 cm^{-1} (spectral region where typically no Raman band occurs).

As a next step, a background correction of the spectra was carried out. The prior partition of the spectra into fingerprint (650 – 1800 cm^{-1}) and CD/CH region (1800 and 3150 cm^{-1}), gave robust results for the application of the Matlab function for background estimation "backcor". It was used with a 5th order polynomial, 0.05 as noise threshold value and an asymmetric truncated quadratic function was chosen as the cost function.[61] Normalization was then carried out using the Euclidean vector length of the spectrum. The stitched spectra are depicted in the graphs in Figure 9 A and B for one sample of *E. coli* ATCC 9637 and *E. faecalis* ATCC 29212, respectively.

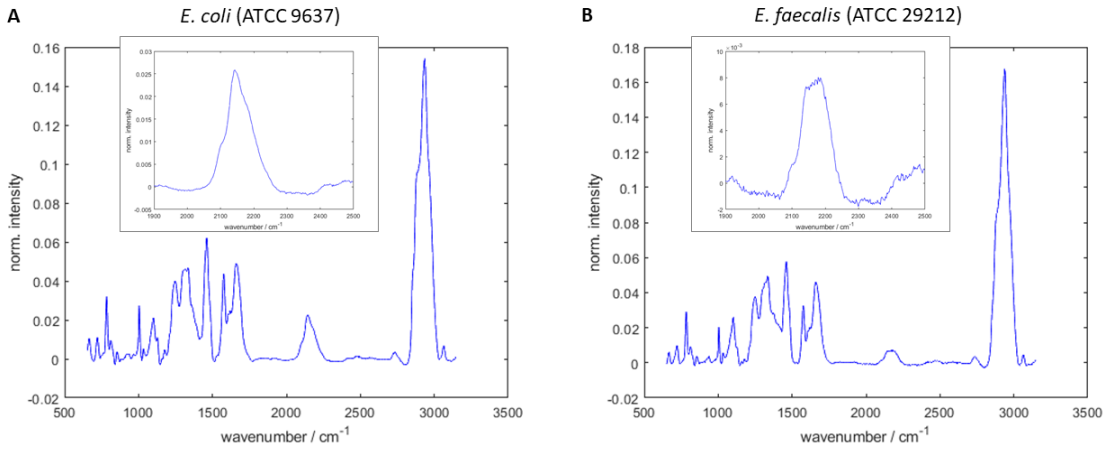

Figure 9: Spectra of reference bacteria (A: *E. coli*, B: *E. faecalis*) after 3 hours growth in medium containing 50% D_2O. The range of the CD band used as predictor for the linear regression analysis is shown enlarged.

The analysis of the CD band intensity was carried out using a linear regression analysis. As predictor variables, the CD band of either *E. coli* ATCC 9637 or *E. faecalis* ATCC 29212 grown in medium containing 50% D_2O for 3 hours (corresponding spectra in Figure 9 A and B) were used for the analysis of the spectra of the respective kind of bacteria. Thus, all plots in this work that give the CD content represent the value of the regression coefficient of those predictor spectra without explicit physical units.

As can be seen in the upper row in Figure 10, the first spectra of a control measurement are depicted in blue. The corresponding predictor spectrum for the CD band multiplied by the coefficient is drawn in red.

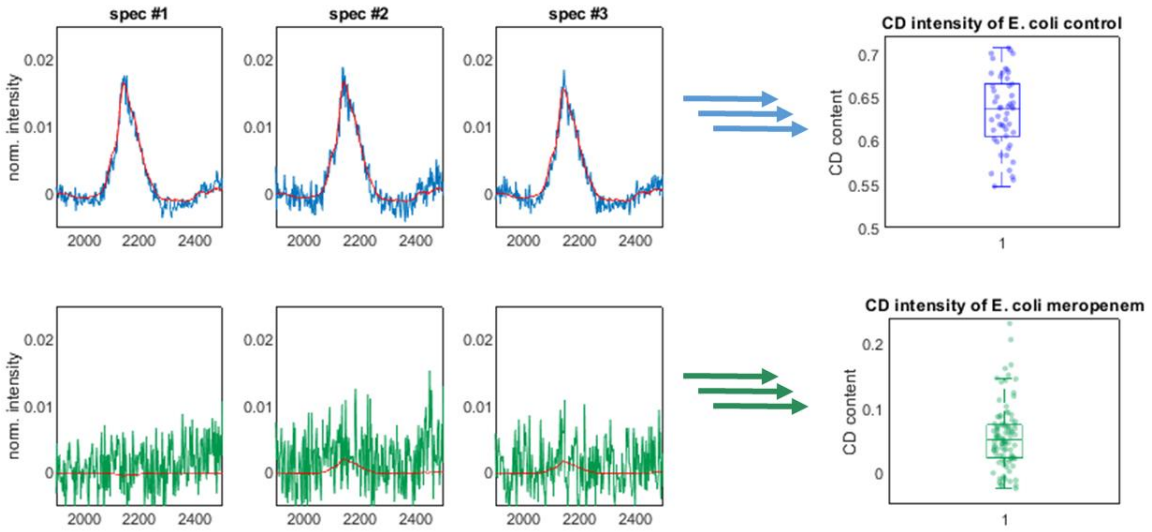

Figure 10: Regression analysis of the CD band of single spectra of *E. coli* control (upper row) and antibiotic-treated (bottom row), recorded with a 532nm laser, 10mW laserpower, 3s integration time and 3 accumulations after incubation in 50% D_2O-containing medium for 1h and pretreatment with 75 mg/L meropenem/NaCl (in the case of the control) without D_2O for 30 minutes. On the right, the respective boxplots of the regression coefficients with the corresponding single datapoints are depicted.

On the right side, a boxplot depicts the values of regression coefficients of all spectra recorded from the sample. The line in the middle of the box represents the median and the lower and upper range of the box indicate the 25th and 75th percentile (also known as lower and upper quartile, Q1 and Q3, respectively). The further horizontal lines are called whiskers and are positioned at the most extreme values of the data that are not declared outliers. In this work, data with an interquartile range (i.e. value of the Q1 subtracted from Q3) 1.5-fold below Q1 or above Q3 is defined as an outlier.

At the bottom of Figure 10, the corresponding spectra and data of susceptible *E. coli*, treated with meropenem is given. The corresponding spectral region given in green is dominated by noise. However, the value of the regression coefficient is not zero. As the corresponding boxplot shows, the values of the regression coefficients are in the range of 0 to 0.15, which is small compared to the values of the control, which lie between 0.55 and 0.70.

4.1.3 Deuterium Uptake of Bacteria

A fundamental question in development of an AST using deuterium is the appropriate amount of heavy water. It is known that at an increasing deuterium content, the growth rate of the microorganisms is changing.[175, 176] However, for reasons of comparability it should not deviate significantly from growth patterns in non-deuterated medium. At the same time the incorporation of the heavier isotope should result in a pronounced CD band and within a short time. In order to find an optimum deuterium content, reference strains of *E. coli* (ATCC 9637) and *E. faecalis* (ATCC 29212) were used as representatives of typical Gram-negative and Gram-positive uropathogens (i.e. bacteria causing urinary tract infection), respectively. The two strains were cultivated in triplicate in the respective optimal medium (LB and TSB) containing defined amounts (0%, 25% or 50%) of heavy water. Along with the growth, single cells were investigated phenotypically via SEM. Their overall appearance, such as shape and size, are compared with increasing deuterium concentration in the growth media (Figure 11 A and B). At all levels, the bacteria show the same phenotype expected for the corresponding microorganism. These images prove that even 50% D_2O content does not have any influence on the cell shape phenotype.

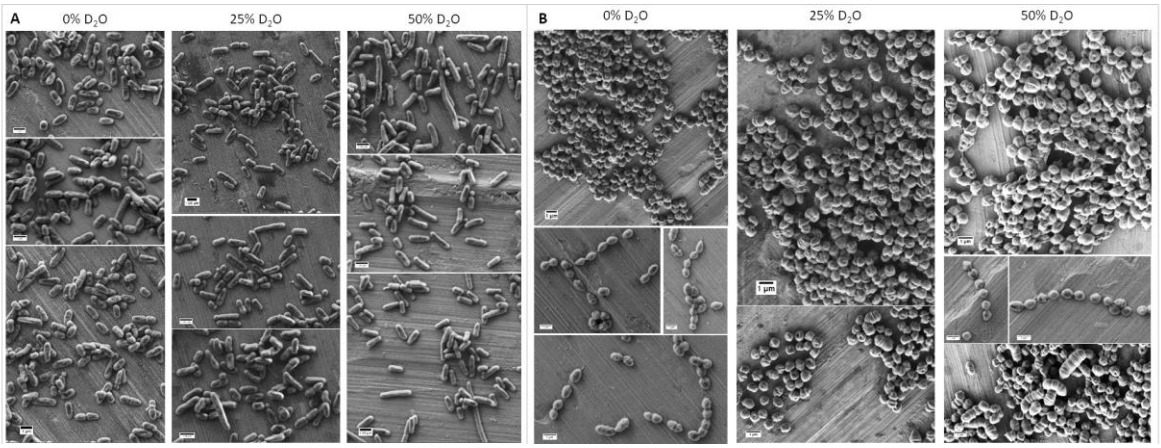

Figure 11: (A) SEM images of *E. coli* (ATCC 9367) and (B) *E. faecalis* (ATCC 29212) grown for 3 hours in 0%, 25% or 50% D_2O, respectively.

In accordance to previous studies, bacteria can not only withstand the replacement of hydrogen by deuterium but also adapt to these conditions well enough that their metabolic activity can be studied.[175, 176, 208, 209] However, most of the time, a decrease in the growth rate is reported with increasing deuterium concentration.[165, 173, 174, 177]

In Figure 12, the CD content (Figure 12A) and growth curves (Figure 12B) as well as the Raman spectra (Figure 12C) are shown for *E. coli*. A significant increase in CD band intensity for 50% D_2O (Figure 12A, data in black) is achieved compared to 25% D_2O (Figure 12A, data in red). For each point in time, at least 45 individual spectra were recorded for each biological replicate, and the corresponding mean and standard deviation are plotted. In parallel, the growth curves based on photometric measurements of the optical density at 600 nm (OD_{600}) were recorded and are given in Figure 12B. They show that the growth rate of *E. coli* is only minimally reduced when increasing the D_2O content of the medium.

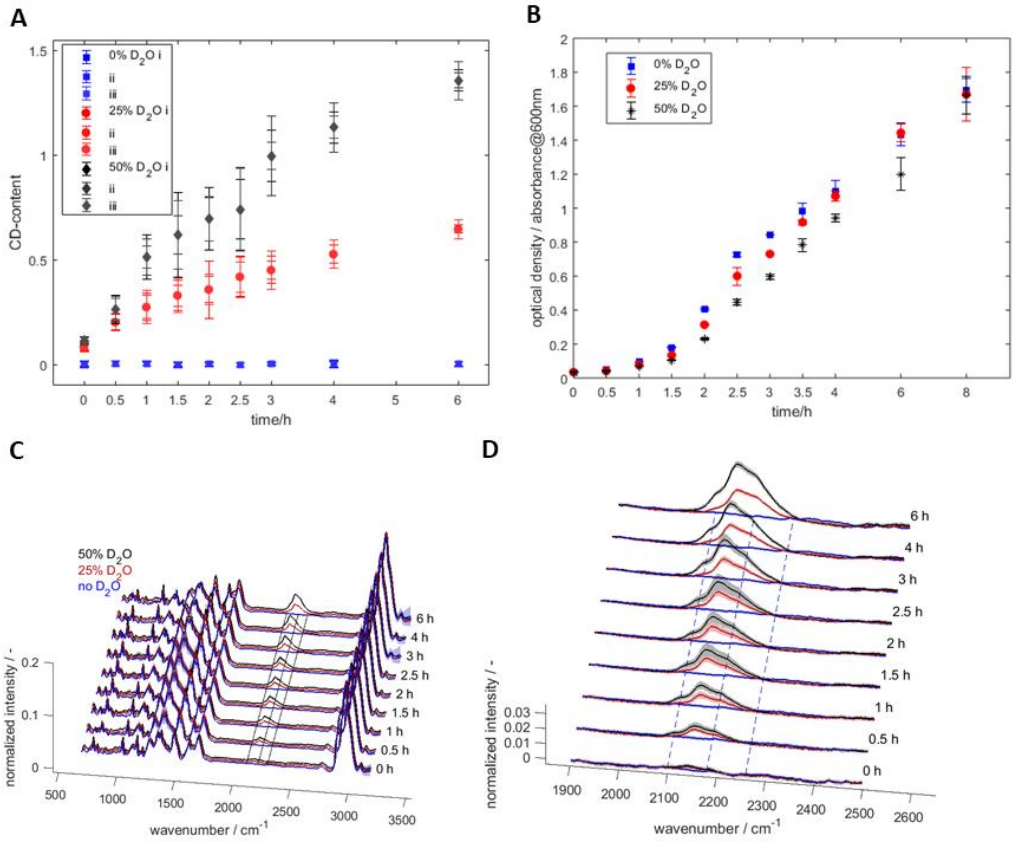

Figure 12: Timeline of growth of *E. coli* in 0%, 25% and 50% D_2O. (A) CD band intensity for triplicate data of each concentration. (B) Data of optical density by absorbtion at 600 nm. (C) Raman spectra for each timepoint (mean and standard deviation). (D) Spectra enlarged to the range of the CD band.

All individual spectra for each time point and for the three D_2O concentrations are shown in Figure 12C. Figure 12D gives a detailed view of the range between 1900 and 2500 cm^{-1}.

Together with the plots in Figure 12A, it is clearly visible that a significant increase of the CD band intensity can already be detected after only 30 minutes of growth.

The results of the equivalent measurements for *E. faecalis* are given in Figure 13. However, while *E. coli* has a generation time of approximately 20 minutes, the Gram-positive microorganism reaches a generation time of 35 minutes.[210-212] Thus, the time points for testing were stretched out a bit longer, namely to 0, 1, 2, 3, 4, 6 and 8 hours. Comparing the spectra of the two types of bacteria, it is furthermore noteworthy that the shape of the CD band is obviously different. While the CD band in the spectra of *E. coli* shows a maximum at 2140 cm^{-1}, that of *E. faecalis* forms a saddle point-like shape in the range of 2140 – 2190 cm^{-1}. This is obviously due to different metabolic pathways for the deuterium incorporation. Furthermore, as can be seen in Figure 13A, the intensity of the CD band and the course of increase over time differ for both kinds of bacteria. In the case of the Gram-positive species, the intensity of the CD band is flat after 3 hours, while in the case of the Gram-negative one, it continuously increases. Since the growth of *E. faecalis* reaches a steady state only after 5 to 6 hours according to the OD_{600} measurements, inhibition of deuterium uptake after a point is indicated.

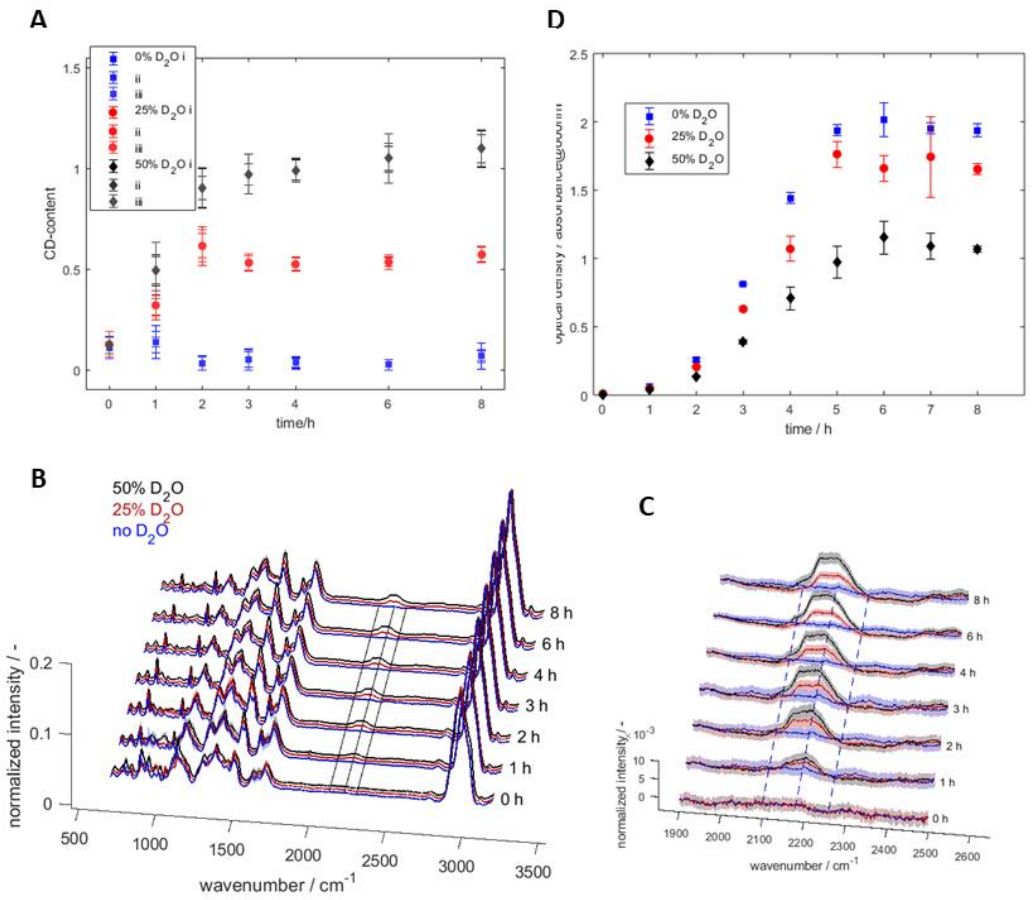

Figure 13: Timeline of growth of *E. faecalis* in 0%, 25% and 50% D_2O. (A) CD band intensity for triplicate data of each concentration. (B) Data of optical density by absorbtion at 600 nm. (C) Raman spectra for each timepoint (mean and standard deviation). (D) Spectra enlarged to the range of the CD band.

In addition, the impact of an increasing D_2O level in the medium on the growth is higher for *E. faecalis* than for *E. coli*, as can be seen in the OD_{600} curves (Figure 13B and Figure 12B). After 6 hours, it reached a maximum value of 2.02 ±0.12 for the normal medium and only 1.15 ±0.12 when 50% D_2O was added.

The data is in agreement with other published studies regarding the influence of D_2O on the growth rate.[162, 165, 169, 173, 174, 177, 178] It confirms that a tolerable D_2O content and the uptake kinetics should be tested for each organism in order to develop a suitable protocol for metabolic activity measurements. The use of 100% D_2O has been reported several times to strongly inhibit or even prevent growth of many bacteria and should therefore not be applied.[165, 173, 174, 177, 180] In conclusion, 50 % D_2O in the medium was determined as a good

compromise between effect on the growth rate and sufficient deuterium incorporation for unambiguous results and, hence, was chosen for all experiments.

4.1.4 Development of a Raman-Based AST

Although other studies have implemented a Raman-based AST by probing deuterium uptake, none of them investigated the influence of the amount of D_2O on the MIC. In this work, a study of the change in MIC for *E. coli* with ampicillin, ciprofloxacin or meropenem as well as for *E. faecalis* with ampicillin or vancomycin was carried out. The media contained 0%, 25% or 50% D_2O. The broth dilution method was performed according to the EUCAST guidelines, using Mueller-Hinton (MH) broth with the respective amount of D_2O.[7, 141] The results for the different bug-drug combinations are listed in Table 8.

Table 8: MIC for *E. coli* – ampicillin, ciprofloxacin or meropenem and *E. faecalis* – ampicillin or vancomycin in MH medium containing 0%, 25% or 50% D_2O.

MIC (mg/L)	*E. coli*			*E. faecalis*	
D_2O conc.	Amp	Cip	Mer	Amp	Van
0%	3.2 ± 1.3	0.038 ± 0.016	0.5 ± 0.0	0.6 ± 0.0	2.1 ± 0.6
25%	2.0 ± 0.0	0.015 ± 0.000	0.1 ± 0.0	0.6 ± 0.0	1.2 ± 0.0
50%	1.5 ± 0.0	0.005 ± 0.000	0.1 ± 0.0	0.8 ± 0.3	1.2 ± 0.0

These results indicate a decrease of the MIC of up to 57% for medium containing 50% D_2O compared to 0% D_2O, except for *E. faecalis* treated with ampicillin, for which the incorporation of deuterium leads to an inhibition of the antibiotic effect and the MIC at 50% D_2O is higher than for lower deuterium levels.

However, the primary goal of this work was to develop a test that results in a binary resistant/susceptible classification. Consequently, high concentrations of antibiotics well above clinical breakpoints were used to obtain an unequivocal identification of highly resistant bacteria. In a first attempt, *E. coli* was confronted with 150 mg/L ampicillin and also without ampicillin as control, both in triplicate. Aliquots were taken every 30 minutes

over a time of 180 minutes and Raman spectra were acquired. The corresponding CD content is shown in Figure 14A along with the complete spectra (Figure 14B).

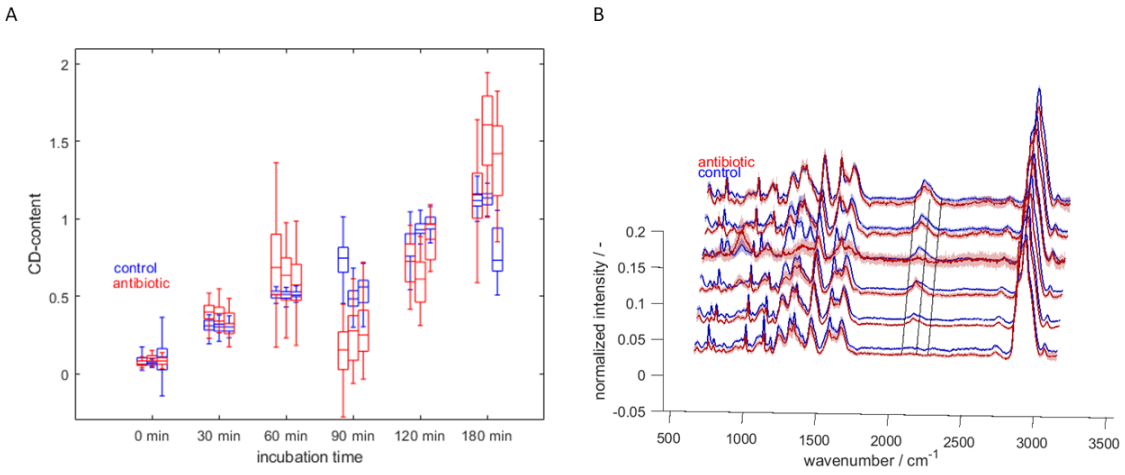

Figure 14: Treatment of *E. coli* with 150 mg/L ampicillin (red) and without antibiotic for control (blue) in triplicate. (A) Boxplots representing CD content and (B) the corresponding processed Raman spectra of one replicate.

Surprisingly, no reduction in CD band intensity due to antibiotic treatment was observed. However, higher values for the CD content than expected were measured. Tao *et al.* reported on the difficulty when trying to "silence down" the CD band in the case of *Streptococcus mutans*. [162] In their study, they treated the bacteria with ampicillin at a concentration of 60-fold the MIC. One aim of this work was to find the reason for these misleading results. In this work the hypothesis that the metabolic state of the bacteria used for inoculation is the main reason for this behavior was investigated. It is good laboratory practice to take bacteria from an overnight culture (i.e. after 16 – 18 hours of growth). After growth for such a period of time in normal medium, most bacteria are in the stationary phase in which the growth- and death-rate are equilibrated.[106, 120, 210, 213-216] Thus only one part of the cells is actively dividing while the other one is rather in a passive condition but still metabolically active.[217, 218] Since ampicillin, as a β-lactam, only acts on actively dividing cells, the immediate confrontation with the antibiotic does not obviously affect the metabolic activity of a major portion of the bacteria.[120, 128, 214] Therefore, deuterium uptake can be observed. To prove that bacteria need to be actively dividing in order to achieve metabolic inactivation, treatment of *E. coli* in the growth phase was carried out. Bacteria from an overnight culture were inoculated on medium (start OD_{600} = 0.01 - 0.05)

and cultivated for three hours. At this point, the OD_{600} equals 0.3 and the exponential growth phase is reached.[110, 112, 120, 214] The bacteria were treated with 150 mg/L ampicillin; the control was not. The Raman spectra were taken after one and two hours, and the obtained CD content is shown in Figure 15A and B, respectively. The red boxplots represent the data of the antibiotic-treated samples, and the blue ones the control samples.

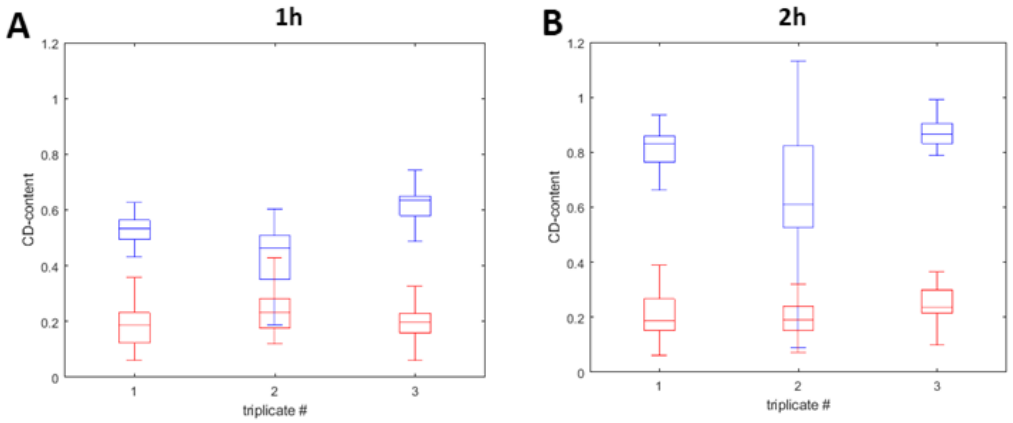

Figure 15: CD content of bacteria treated in the growth phase in triplicate. Boxplots of regression coefficients for the CD band after 1 (A) and 2 hours (B).

The CD content of bacteria treated with ampicillin remains at a low level of 0.2, even for two hours incubation (Figure 15B). However, the CD bands of the controls are higher and increase between one (Figure 15A) and two hours (Figure 15B).

Another approach to prevent false positives in terms of CD band increase was tested in another experimental setup. Here, incubation of the bacteria with antibiotic was performed before addition of D_2O. Different time intervals for this “preincubation” were tested to determine the time needed for the antibiotic to show an effect on the cells and thus inhibit uptake of deuterium. The experimental setup is shown in the scheme in Figure 16.

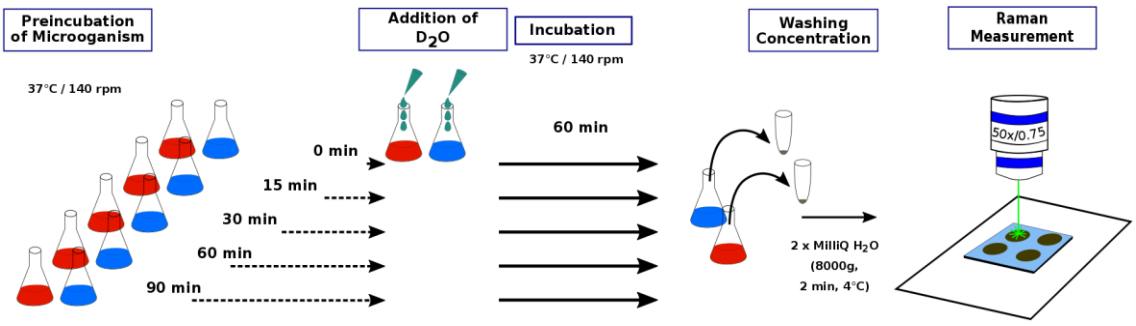

Figure 16: Scheme of the experimental approach to finding the necessary preincubation time with antibiotic before addition of D_2O-containing medium to prevent formation of a CD band that results after addition.

Again, antibiotic treatment was compared to a control where no antibiotic was used in order to obtain the CD band intensity of the corresponding non-inhibited case. Preincubation times of 0, 15, 30, 60 and 90 minutes were used and the previously already listed bug-drug combinations (*E. coli* – ampicillin/ciprofloxacin/meropenem and *E. faecalis* – ampicillin/vancomycin) were tested in triplicates at high concentrations of the antibiotic.

Looking at the data of *E. coli* and ampicillin with 0 and 15 minutes of preincubation time in Figure 17A, the same problem as discussed above can be observed. The CD band of bacteria treated with antibiotic features the same intensity range as the control. With longer preincubation time, the CD band intensity is drastically reduced until it reaches a minimum at 60 minutes, with values for the CD content of 0.05 to 0.1. Accordingly, in the Raman spectra given in Figure 17B, no CD band is visible in the spectra of the antibiotic-treated samples (red) for longer incubation times. Meanwhile, the CD band is clearly visible in the spectra of the control (blue). In order to set up an unbiased and general criterion, a statistical comparison between the CD content of the control and of the antibiotic-treated sample was established. Thus, for a set of data from one sample, the two-fold standard deviation (two-sigma) of the measured CD band intensities was chosen for the AST decision. The upper two-sigma interval of the antibiotic treated sample ($mean_A + 2\sigma_A$) needs to be smaller than the lower two-sigma of the control ($mean_c - 2\sigma_c$) to indicate susceptibility (S). When it is the other way around, the microorganism is classified as resistant (R). This is expressed mathematically in equation (11).

$$\begin{aligned} mean_A + 2\sigma_A &< mean_C - 2\sigma_C \quad \rightarrow (S) \\ mean_A + 2\sigma_A &\geq mean_C - 2\sigma_C \quad \rightarrow (R) \end{aligned} \tag{11}$$

The data from the preincubation experiments for each of the control/antibiotic pairs are shown in the boxplots in Figure 17 and Figure 18 for for *E. coli* and *E . faecalis*, respectively. They are labeled on top of the boxplot graph with the corresponding antibiotic. The result of the AST decision using the two-sigma criterion is given for each control/antibiotic pair within the graph.

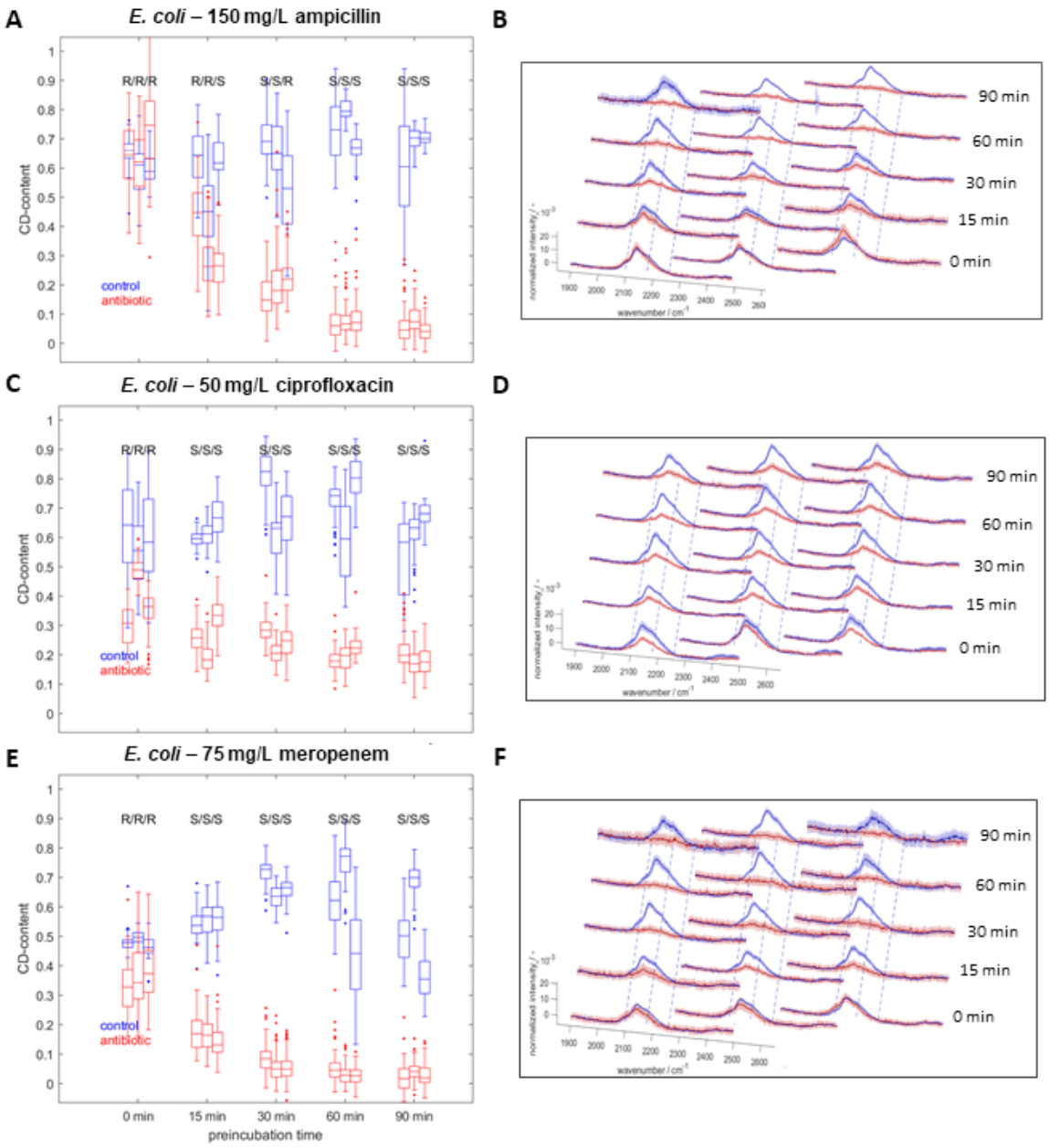

Figure 17: Preincubation study of *E. coli* with ampicillin, ciprofloxacin and meropenem with the corresponding boxplots of the triplicates and the CD band region of the Raman spectrum (A-F respectively).

Based on the MIC values given in Table 8 on page 48, the bacteria are known to be susceptible to all of these drugs. However, looking at the boxplots of all the first triplicate pairs at zero minutes of preincubation time, the correct classification fails for all bug-drug combinations. In the case of *E. coli* – ampicillin (Figure 17A), after 30 minutes, one replicate is still classified as resistant, thus contradicting the MIC data. For it to be in

accordance takes at least 60 minutes of preincubation. A different picture results for the data of the experiment with ciprofloxacin, shown in Figure 17C. While the classification as “susceptible” is already obtained with the 15-minute sample, the CD content still lies around 0.2 after 90 minutes. This is obviously different from the other antibiotics, where a steady decline for the CD band is observed. Accordingly, the CD band is still visible in the Raman spectra in Figure 17D but not in Figure 17B and F. This might be due to the different mechanism of action of ciprofloxacin and of the other two antibiotics. Ciprofloxacin is a gyrase inhibitor and thus blocks only this specific enzyme, which is involved in the structural organization of DNA wrapping.[219] A certain degree of metabolic activity of other enzymes that leads to deuterium uptake is obviously still going on. The data of meropenem shown in the graph in Figure 17E leads to a correct classification as “susceptible” when 30 minutes of preincubation is applied.

The data of the Gram-positive bacteria in Figure 18 on the next page gives an AST result in accordance with the MIC test already for the samples with zero minutes preincubation time. The CD band of antibiotic-treated bacteria is significantly smaller than the control. However, as can be seen in the boxplots and the spectra, the CD band has not completely disappeared. Instead, a continuous decrease of the CD band can be observed here too and a clear reduction only for longer preincubation times. The only exception is the data of the 90-minute samples of *E. faecalis*-ampicillin in Figure 18A and B where a slight increase of the CD content from 60-minute to 90-minute can be noted. However, this is rather due to the high level of noise and the consequently curved baseline in these spectra. In comparison, in the data of Enterococci treated with vancomycin in Figure 18C and D, a clear decline of the CD content with increasing incubation time is observed.

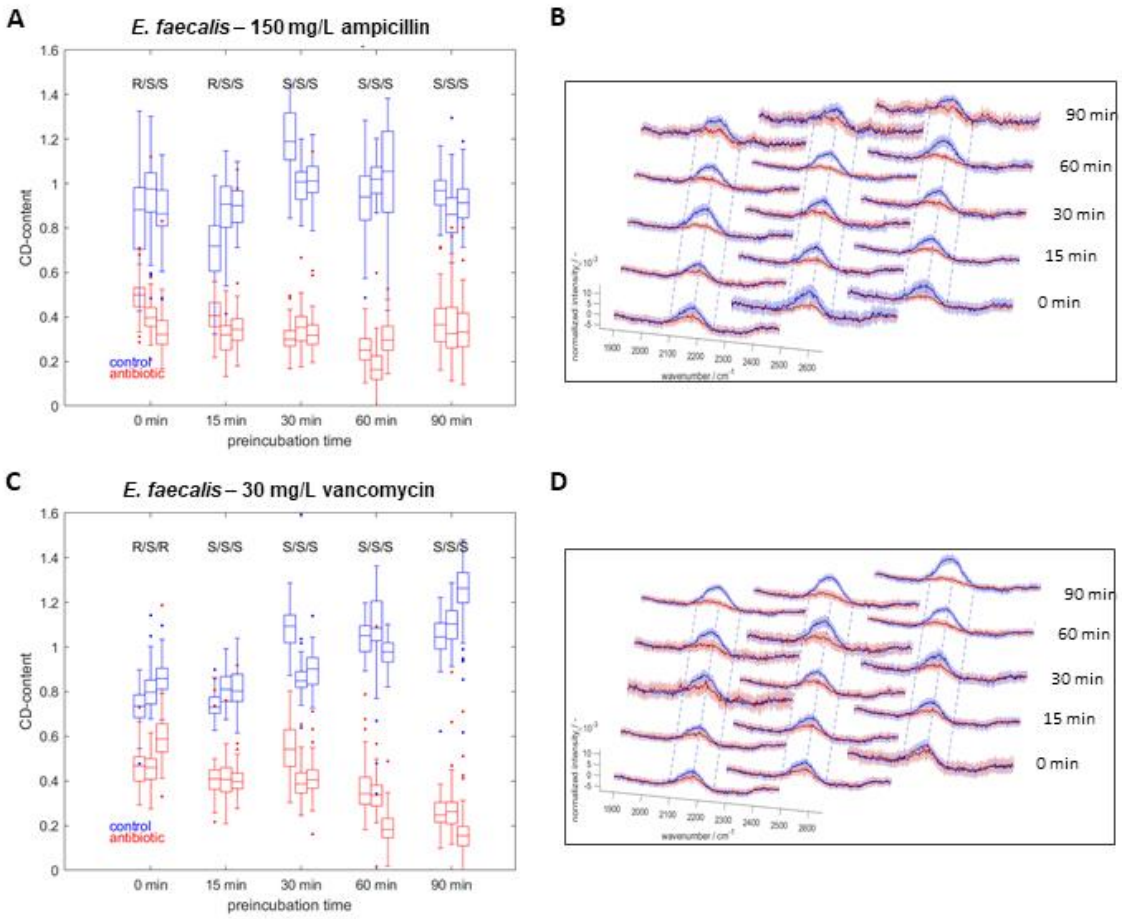

Figure 18: Preincubation of *E. faecalis* with ampicillin or vancomycin.

These results allow definition of a minimum preincubation time of 30 minutes needed in order to obtain a reliable classification in the case of these bug-drug combinations. Considering the variability of the minimum preincubation time required for different bug-drug combinations and its effect on the accuracy of the classification result, a general preincubation of 90 minutes was chosen for all following experiments. Adding to that the 60 additional minutes for treatment with D_2O-containing medium, additional 30 to 45 minutes for sample preparation and the time of the Raman measurement, a result can be obtained within 3.5 to 4 hours. This is still faster than any of the AST methods that are currently commercially available.[145, 151]

4.1.5 Test of Clinical Samples

To apply the developed protocol on clinical isolates of susceptible as well as resistant bacteria, 52 clinical isolates (30 *E. coli* and 22 *E. faecalis* or *E. faecium*) were taken from the MVP stock and tested for the MIC via E-tests and in comparison with the Raman-deuterium based AST. Exemplary E-tests of *E. coli* with ampicillin are shown in Figure 19. As mentioned in section 2.4.3, the E-tests are the gold-standard AST but require 16 hours before results can be obtained.

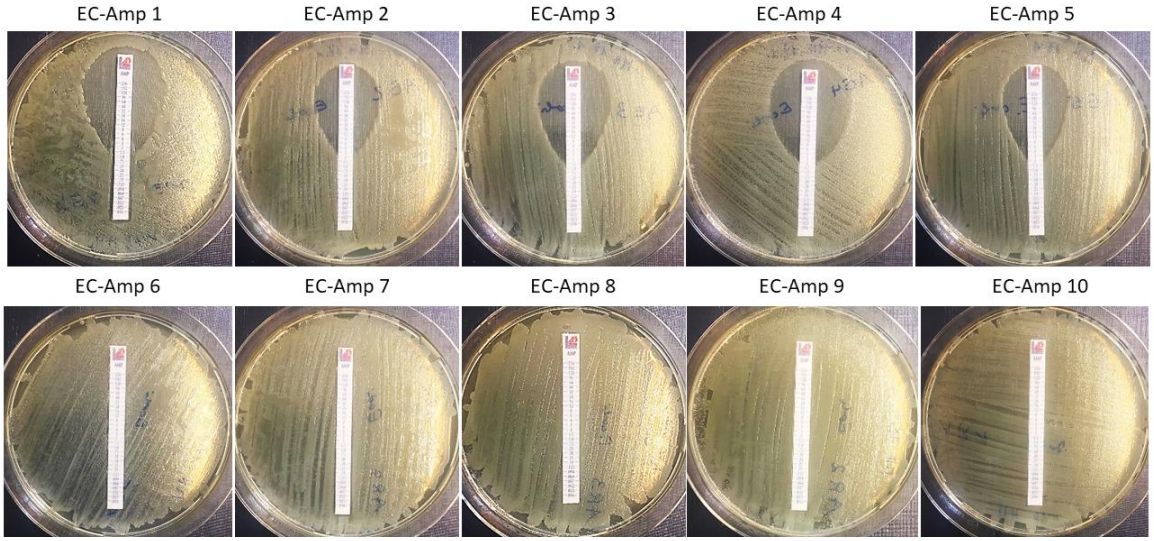

Figure 19: E-tests of clinical isolates of *E. coli* with ampicillin.

The complete list of the chosen isolates with the determined MIC values is given in Table 9 together with the number of Raman spectra recorded for the control/antibiotic-treated sample of each isolate. The results of the two ASTs are summarized in Figure 20 and 21 for *E. coli* and in Figure 23 for the Gram-positive isolates. In the table, isolates that could be clearly identified as heteroresistant via the E-test are marked with two asterisks (**) and MIC values for subpopulations with higher MIC than the main population are given in brackets. In the case of *Enterococci,* isolates of *E. faecium* are marked with one asterisk (*).

Table 9: List of MIC values and number of recorded Raman spectra (control/antibiotic) of clinical isolates of *E. coli* and *Enterococci*. ** Heteroresistant isolates with corresponding MIC values; * *E. faecium*.

E. coli								
Ampicillin			Ciprofloxacin			Meropenem		
Label	MIC (mg/L)	# specs	Label	MIC (mg/L)	# specs	Label	MIC (mg/L)	# specs
EC Amp 1	1.3	53/62	EC Cip 1	0.012	67/72	EC Mer 1	0.023	56/42
EC Amp 2	2	36/63	EC Cip 2	0.016	53/58	EC Mer 2	0.016	70/51
EC Amp 3	1.3	56/54	EC Cip 3	0.023	60/75	EC Mer 3	< 0.016	67/41
EC Amp 4	1.8	73/65	EC Cip 4	0.016	50/72	EC Mer 4	< 0.016	66/63
EC Amp 5	2	53/47	EC Cip 5	0.016	71/60	EC Mer 5	< 0.016	72/53
EC Amp 6	> 256	40/68	EC Cip 6	**0.032 (1)	74/66	EC Mer 6	4	59/48
EC Amp 7	> 256	53/67	EC Cip 7	> 32	74/67	EC Mer 7	1	63/41
EC Amp 8	> 256	58/48	EC Cip 8	> 32	63/61	EC Mer 8	**0.5 (32)	53/56
EC Amp 9	> 256	53/63	EC Cip 9	> 32	74/71	EC Mer 9	8	53/31
EC Amp 10	> 256	38/51	EC Cip 10	>32	71/72			

E. faecalis/ faecium (*)					
Ampicillin			Vancomycin		
Label	MIC (mg/L)	# specs	Label	MIC (mg/L)	# specs
EF Amp 1	0.75 - 1	79/73	EF* Van 1	1.5	67/61
EF Amp 2	1	78/57	EF Van 2	2	68/71
EF Amp 3	0.38	74/87	EF Van 3	1.7	79/52
EF Amp 4	0.5	74/51	EF Van 4	1.5	67/89
EF Amp 5	1	52/85	EF Van 5	0.38	70/75
EF* Amp 6	2	72/53	EF Van 6	0.5	74/76
EF* Amp 7	> 256	46/69	EF Van 7	> 256	59/61
EF* Amp 8	> 256	62/55	EF Van 8	> 256	77/67
EF* Amp 9	> 256	72/76	EF* Van 9	> 256	64/55
EF* Amp 10	> 256	72/67	EF* Van 10	> 256	76/73
EF* Amp 11	> 256	55/111	EF* Van 11	> 256	68/76

In Figure 20, Figure 21 and Figure 23, the results of AST for each bug-drug combination are depicted. The bar plot on top shows the data from the E-tests, and the Raman-based AST results (lower boxplots) using the 2σ criterion are indicated for each isolate by the letter S for susceptible and R for resistant at the top. For the E-tests, the bars provide the obtained MIC. The EUCAST clinical breakpoint for the corresponding bug-drug is indicated by a horizontal line. On the right, the corresponding mean Raman spectra are plotted. In Figure 20, the spectra along the complete range are given, and in the following ones, only the range of the CD band (1900 – 2500 cm^{-1}) is shown.

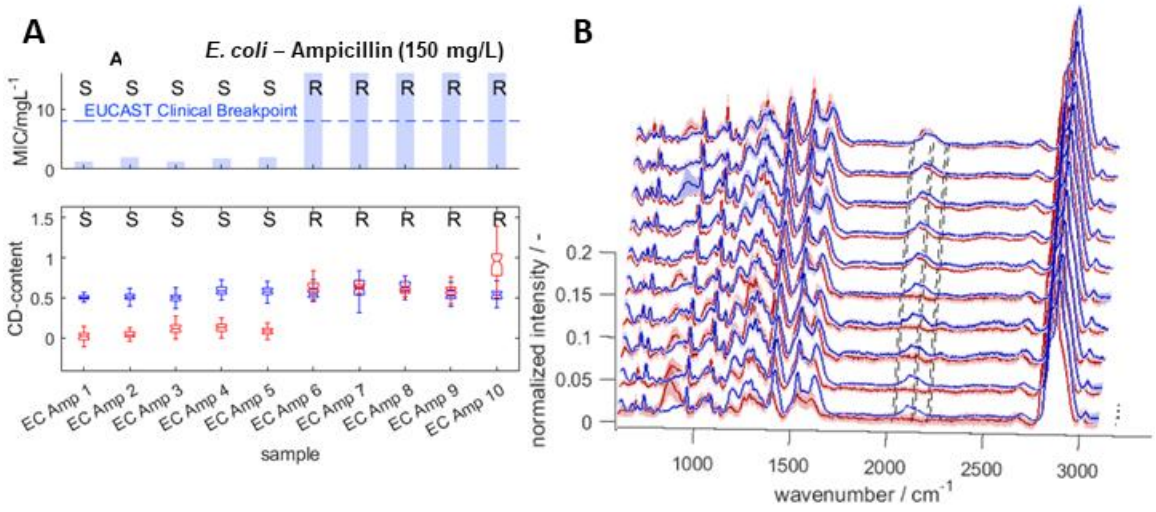

Figure 20: AST test results of ampicillin-susceptible and resistant clinical *E. coli* isolates.

In the case of *E. coli* treated with ampicillin, perfect agreement between both AST results is observed. The tests of *E. coli* with ciprofloxacin (Figure 21A and B on the next page) concur for all isolates, too. Only EC-Cip 6 shows a discrepancy. For the E-test-based MIC of this isolate, two values, 0.032 and 1 mg/L, are given. This is due to the heteroresistance. One MIC, the one at a lower antibiotic concentration, shows inhibition of the majority of colonies on the plate. However, a subpopulation, able to grow even under higher concentrations of antibiotic is present, too. The BP for *E. coli* and ciprofloxacin lies at a value of 0.5. Thus, the isolate is classified as resistant.

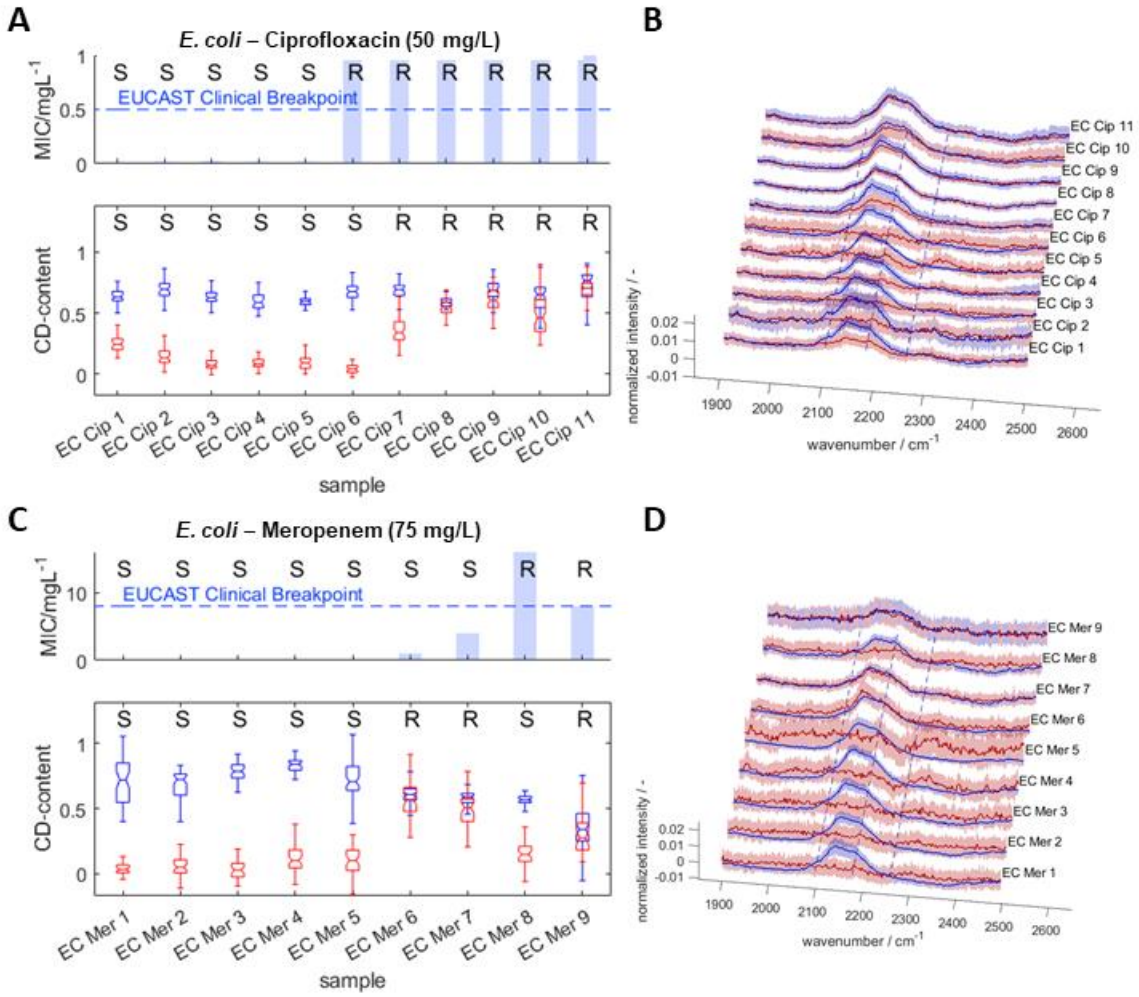

Figure 21: AST test results of susceptible and resistant clinical *E. coli* isolates with ciprofloxacin and meropenem.

Since the Raman-based test is carried out with a concentration of 50 mg/L ciprofloxacin, which exceeds the MIC also of the resistant cells (MIC = 1 mg/L), the result of the Raman AST is “susceptible”.

In the tests with meropenem, depicted in Figure 21C and D, the same occurs with EC-Mer 8. Here too, heteroresistance could be identified by the E-test. The corresponding plates are shown in Figure 22. In contrast, EC Mer 6 and 7 show resistance in the Raman-based test and are identified as susceptible by the E-test. For the other isolates, both tests are in good agreement.

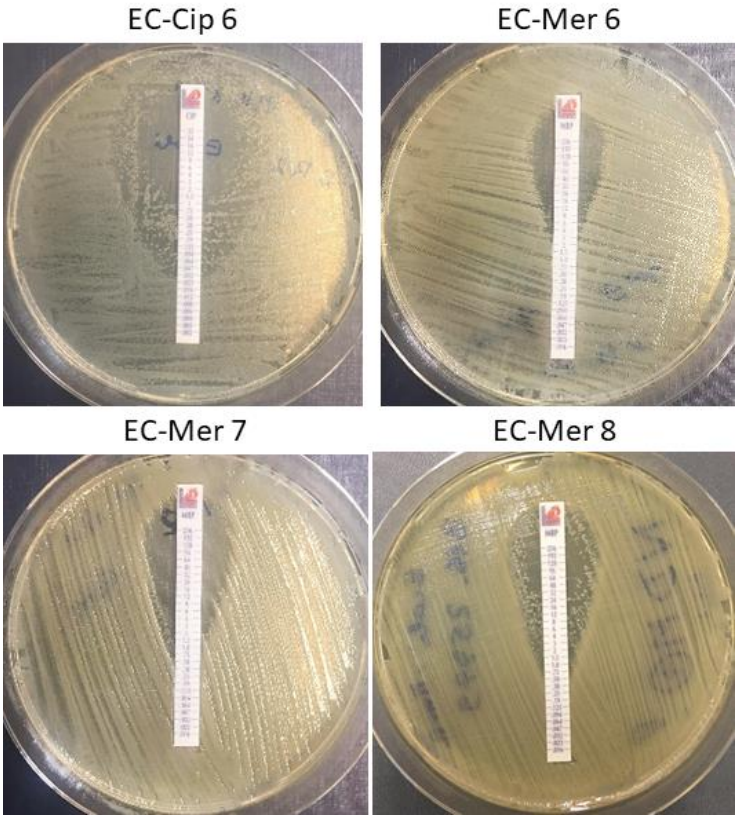

Figure 22: E-tests for isolates with contradicting results between MIC-based E-test and Raman-based AST.

In the case of EC-Cip 6 and EC-Mer 8, the subpopulation with higher MIC can be clearly identified. For EC-Mer 6 and 7, however, no unambiguous decision on heteroresistance can be made using the E-tests, since no clear subpopulation like in the other two cases is visible. Looking closely at the image of EC-Mer 6, only a few colonies are visible inside the inhibition zone. Compared to the plates of ampicillin-susceptible isolates shown above in Figure 19, the edges formed by the colonies that developed on the plate are not perfectly straight. This indicates the presence of heteroresistant cells, but it is not easy to make out, even by a trained physician. In this case, more elaborate tests that are not explained in detail here would be necessary to reliably identify heteroresistance in these cases.[8, 129, 132]

The results of the Gram-positive isolates tested against ampicillin (Figure 23A and B) are again in perfect agreement between the two tests.

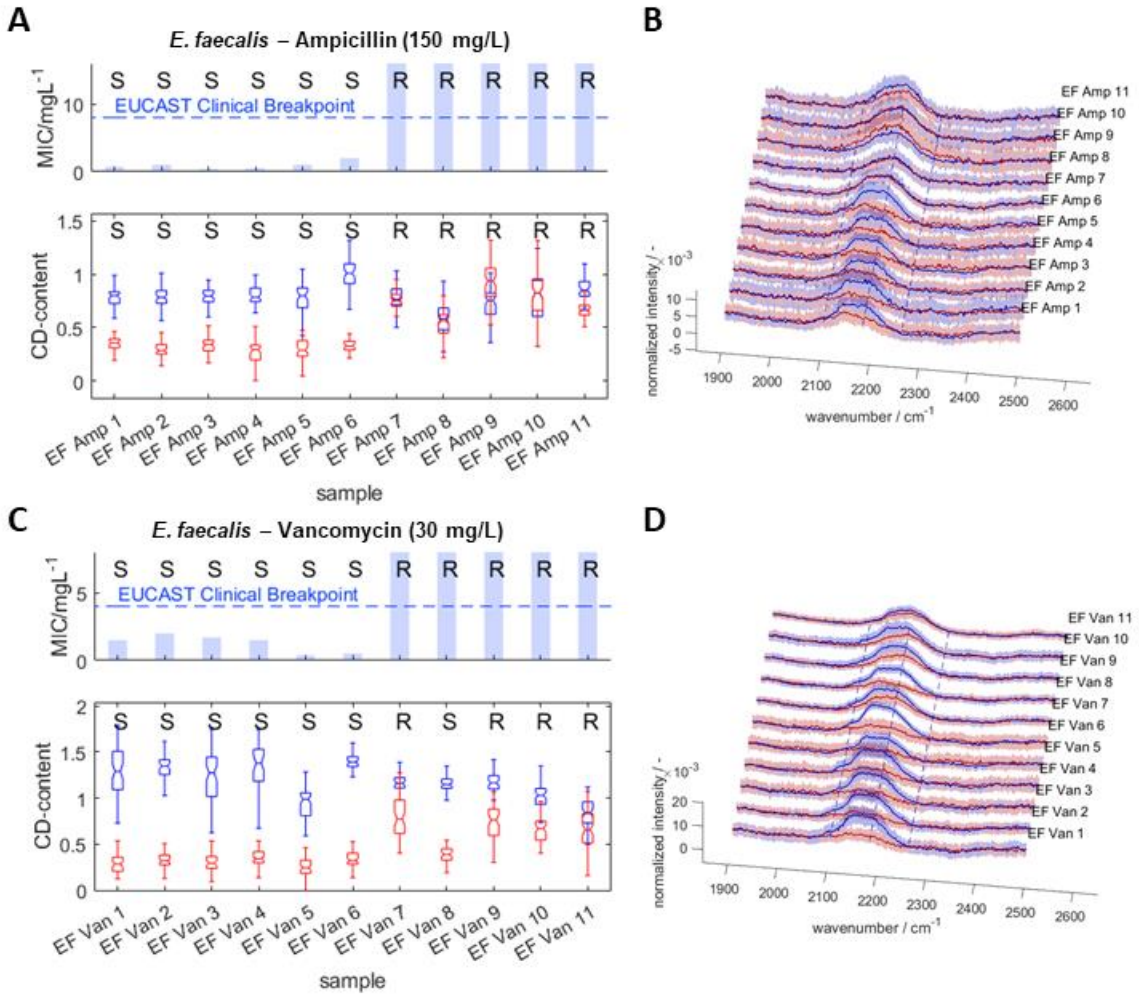

Figure 23: AST test results of ampicillin- and of vancomycin- susceptible and resistant clinical isolates of *E. faecalis* and *E. faecium*.

The results of Raman-based and E-test ASTs of all but one isolate of *Enterococci* tested with vancomycin are in good agreement. For EF Van 8, the E-test gave a MIC above the maximum concentration on the E-test strip (256 mg/L), whereas the Raman-based AST shows susceptibility. A repeated E-test, depicted in Figure 24, indicates that a heteroresistant culture is present here also, although it is again difficult to identify it as heteroresistant by the naked eye. The colonies of *Enterococci* did not grow as densely as *E. coli*. Thus, the two different populations (susceptible and resistant) are not as distinct as for the Gram-negative ones, EC-Cip 6 and EC-Mer 8.

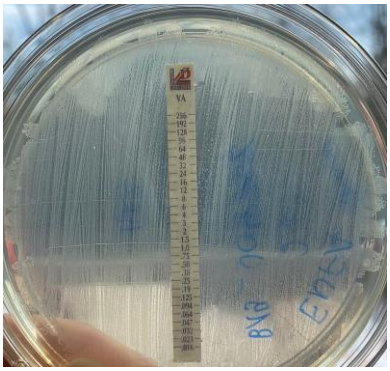

Figure 24: E-test of EF-Van 8.

In summary, the Raman-based AST demonstrated good performance and good agreement with the E-test used as a reference AST method.

4.1.6 Extended Tests for Heteroresistant Isolates

In order to further investigate the detection of metabolic activity in heteroresistant isolates, the incubation time was increased to 2, 3 and 4 hours and, also, varying concentrations of antibiotics were used.

The results of the experiments for *E. coli* isolates EC-Cip 6, EC-Mer 6, EC-Mer 7 and EC-Mer 8 are shown in Figure 25A to C, respectively. In the case of isolate EC-Cip 6 (Figure 25A), antibiotic concentrations of 0 (control), 0.5 (BP), 5, and 50 mg/L were chosen. An increase of the CD band is detected for the control and also for the lowest concentration of antibiotic (0.5 mg/L). This is in perfect agreement with the E-test shown above in Figure 22, which gave a MIC of 1 mg/L for the heteroresistant culture.

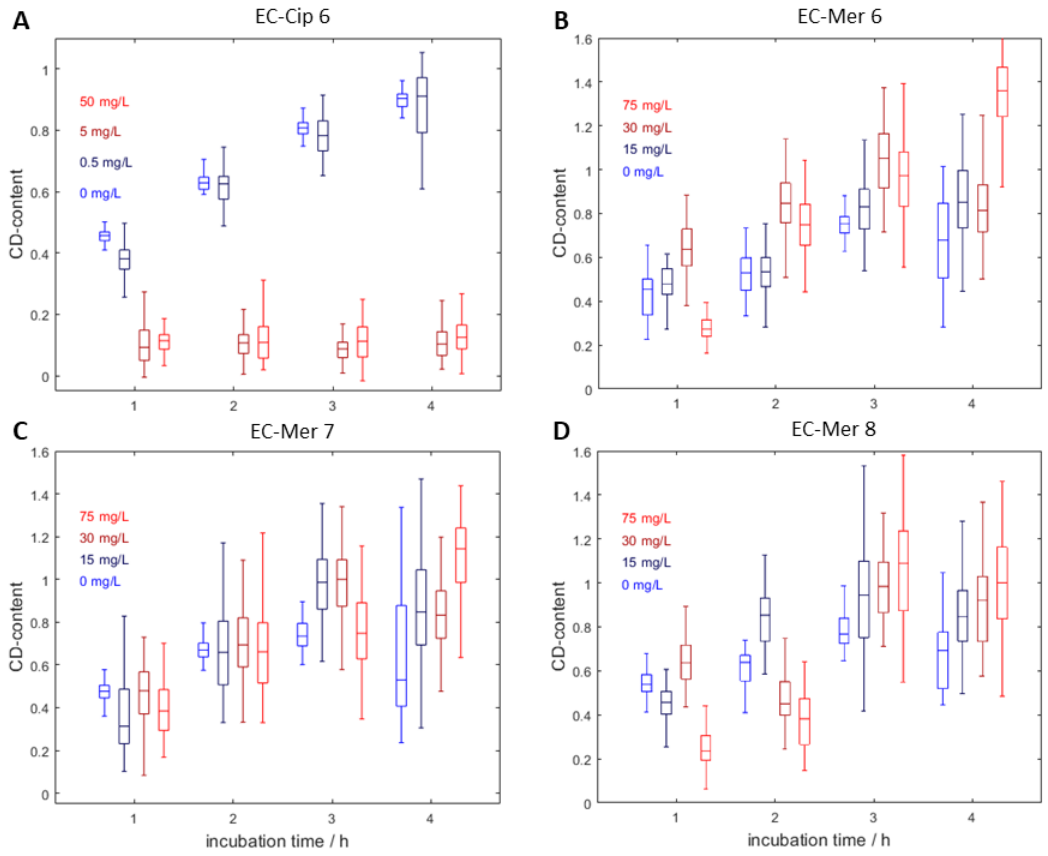

Figure 25: Raman-based AST with extended incubation time (1, 2, 3, 4 hours) and various concentrations of antibiotics for EC-Cip 6 (A), EC-Mer 6 (B), EC-Mer 7 (C) and EC-Mer 8 (D).

In the case of the samples treated with meropenem, concentrations of 0 (control), 15, 30 and 75 mg/L were chosen. The BP for the bug-drug combination *E. coli*-meropenem lies at 8 mg/L. For the isolates investigated here (Figure 25B – D), the CD content of 15 and 30 mg/L meropenem are at comparable values to the control. The dose-dependent evolution of the CD content is useful for pinning down the causative mechanism of the heteroresistance, its stability and more details on the behavior of the bacteria. Thus, especially the metabolic activity in the presence of antibiotics at concentrations well above the BP, like 75 mg/L (i.e ~10-fold the BP) here, were investigated and used in the AST presented and discussed in section 4.1.4. At this high concentration, only EC-Mer 7 shows an equal level of CD content for the treated sample and the control after an incubation time of one hour. In contrast, EC-Mer 6 and EC-Mer 8 have a considerably lower CD content than the control. However, for EC-Mer 6, the CD band is at the same level as the control after two hours incubation time. The intensity even exceeds the value of the control, which

indicates a high rate of deuterium uptake and metabolic activity. The same effect can be observed for EC-Mer 8 after three hours. Compared to the control in all three cases, the CD band of the antibiotic-treated samples exceeds that of the control after four hours of incubation time. This higher deuterium uptake indicates stimulation of metabolic activity by the antibiotic. From the database of the MVP, the presence of a New-Delhi metallo-beta-lactamase-1 (NDM-1) encoding gene was confirmed for these isolates via polymerase chain reaction. NDM-1 is an enzyme that belongs to the carbapenemases and is known to cause heteroresistance.[8, 220-222] In the case of this specific resistance mechanism enhanced metabolic activity in the presence of the antibiotic compared to non-antibiotic conditions has also been reported.[8, 220] Most worrisome is the possibility of this gene being forwarded to other microorganisms via horizontal gene transfer.[130, 223-225] In this process, genetic information is passed on from one cell to another by plasmids (short ring-formed DNA parts) directly and not by "normal" reproduction and corresponding DNA doubling. Thus, with these properties, the NDM-1-carrying isolates can be categorized as polyclonal and unstable, according to the definition given by Andersson *et al*., and can complicate the detection of resistance with the conventional testing methods.[129] The data obtained from the dose-dependent metabolic activity monitoring indicates that the Raman-D_2O-based AST is a promising tool with which to characterize this kind of resistance mechanism.

To investigate the difference between resistant and susceptible bacteria, meropenem-susceptible isolates (EC-Mer 1, EC-Mer 2 and EC-Mer 3) were incubated for the extended incubation time (1, 2, 3 and 4 hours) using 75 mg/L meropenem, too. The corresponding boxplots are depicted in Figure 26A. A Wilcoxon rank sum test (also known as Mann-Whitney U test) was used to test if the CD content values between one and four hours incubation are significantly different (the null hypothesis is that data are from continuous distributions with equal median).[226] Only for EC-Mer 3 was a p-value between 0.01 and 0.001 obtained, and it is indicated in the figure with two asterisks (**). This is still above the significance of 0.001 that should be reached for this test to be conclusive. The other two measurements provide no significant difference (n.s.) between the values (the criterion is that the p-value is larger than 0.05). Consequently, in the case of a susceptible isolate, the CD content does not change, even for an increased incubation time of up to four hours.

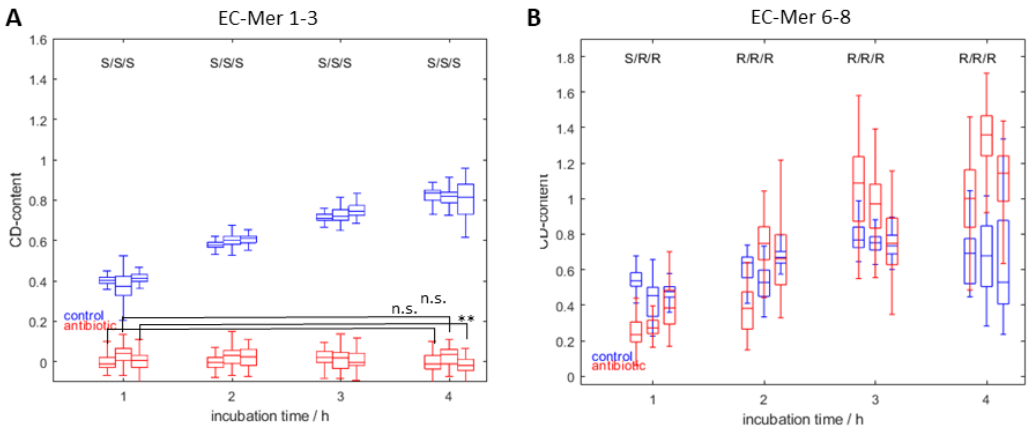

Figure 26: CD content obtained by Raman-based AST of meropenem-susceptible isolates EC-Mer 1-3 (A) and meropenem-heteroresistant ones EC-Mer 6-8 (B) treated with 75 mg/L meropenem for extended incubation time of 1, 2, 3 and 4 hours.

In the case of the slower growing *Enterococci*, a corresponding test was carried out using the reference strain ATCC 29212 of *E. faecalis*, which is susceptible to vancomycin, and the clinical isolate EF-Van 8 (Figure 27A and B, respectively). Both were tested with 0, 4, 16 and 30 mg/L vancomycin, again after one, two, three, and four hours of incubation. The boxplots obtained from the analysis of the CD content of the susceptible culture *E. faecalis* ATCC 29212 show that there were slight increases of the CD band, which indicated CD contents far below the values of the control. In the case of the heteroresistant culture EF Van-8, after one hour, no increase of CD content can be noted at any concentration. The values of the quartiles of the three different concentrations range from 0.2 to 0.4, which is just slightly above the values of the susceptible sample. However, in contrast to the latter, the CD content of the heteroresistant sample clearly increases for longer incubations times, which proves the growth of the cells.

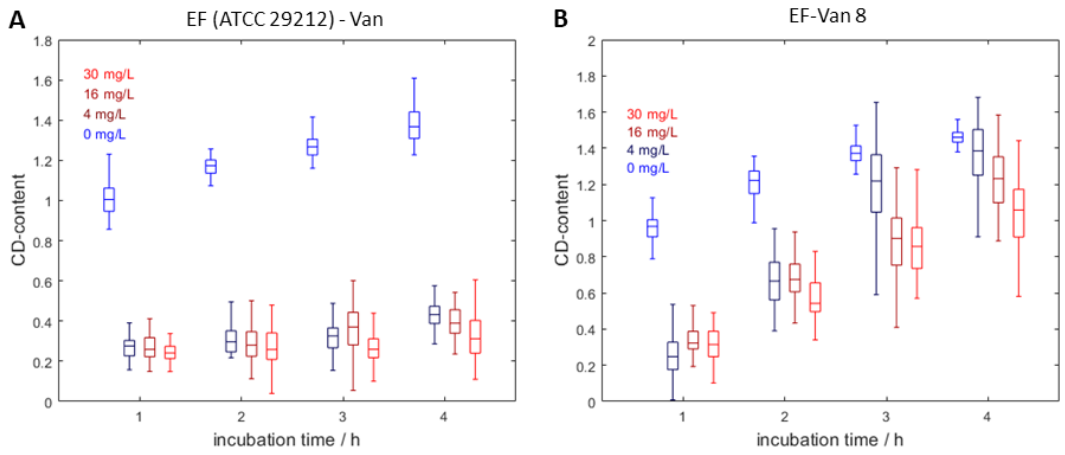

Figure 27: CD content obtained by Raman-based AST of vancomycin-susceptible isolate EF-Van 1 (A) and vancomycin-heteroresistant isolate EF-Van 8 (B) treated with 0, 4, 16 and 30 mg/L vancomycin for extended incubation times of 1, 2, 3 and 4 hours.

In summary, these experiments demonstrated how fast-growing Gram-negative as well as slower-growing Gram-positive heteroresistant bacteria can be identified as such within a maximum of four hours. Not only the short time for identification in comparison to E-tests, but especially the potential to deduce different resistance-mechanisms make this method promising for fast detection of NDM-1-carrying bacteria.

4.1.7 Frequency-Dependent Detection of Heteroresistant Cultures

As demonstrated above, heteroresistance can be difficult to detect using standard AST methods. This is especially true for unstable heteroresistance, which is the case for NDM-1-carrying isolates, or if the frequency of resistance is low.[129] There are methods to determine the frequency of heteroresistant cultures, however, they are based on repeated plate counts.[137] This is a rather slow process requiring at least 24 hours and time-intensive cultivation. In this context, a method to directly quantify the frequency of the resistant cells in a heteroresistant culture would be useful. Hence, heteroresistant cultures with frequencies of 10^{-1}, $2 \cdot 10^{-2}$, 10^{-2}, 10^{-3} and 10^{-4} were modelled from fully ampicillin-susceptible and ampicillin-resistant bacteria in the corresponding ratios. The CD band intensities for heteroresistant *E. coli* cells treated with 150 mg/L ampicillin relative to the control group are shown in Figure 28.

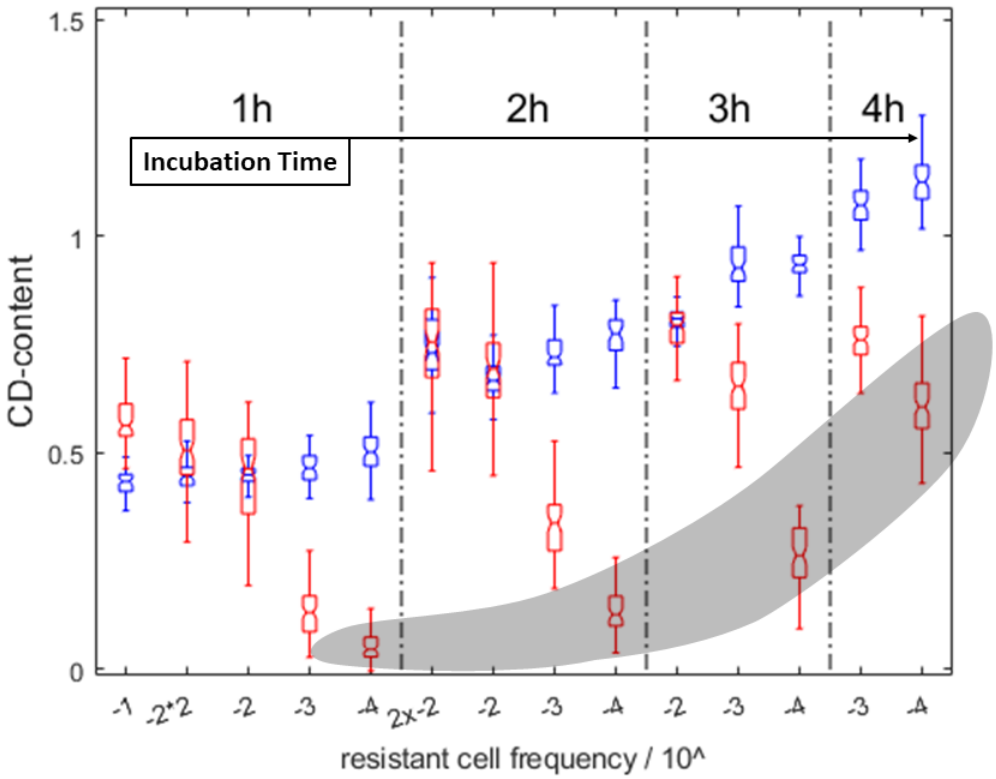

Figure 28: Boxplots of experimentally simulated heteroresistant cultures with defined frequencies.

While frequencies of 10^{-2} can easily be detected within one hour of incubation time, lower frequencies of 10^{-3} and 10^{-4} require an extension of incubation time up to three and four hours, respectively. As can be seen, the samples with a frequency of 10^{-4} show significant progress in deuterium uptake after longer incubation time. The data for this frequency is highlighted in Figure 28 in gray, showing the exponential growth of the resistant cells with increasing incubation time.

However, to apply the Raman-based AST to identify heteroresistance, an additional criterion and measurements at longer incubation times need to be the introduced. Figure 29 contains an approach by which to realize such a criterion via a decision tree. It is based on and refers to the observations depicted above in Figure 28.

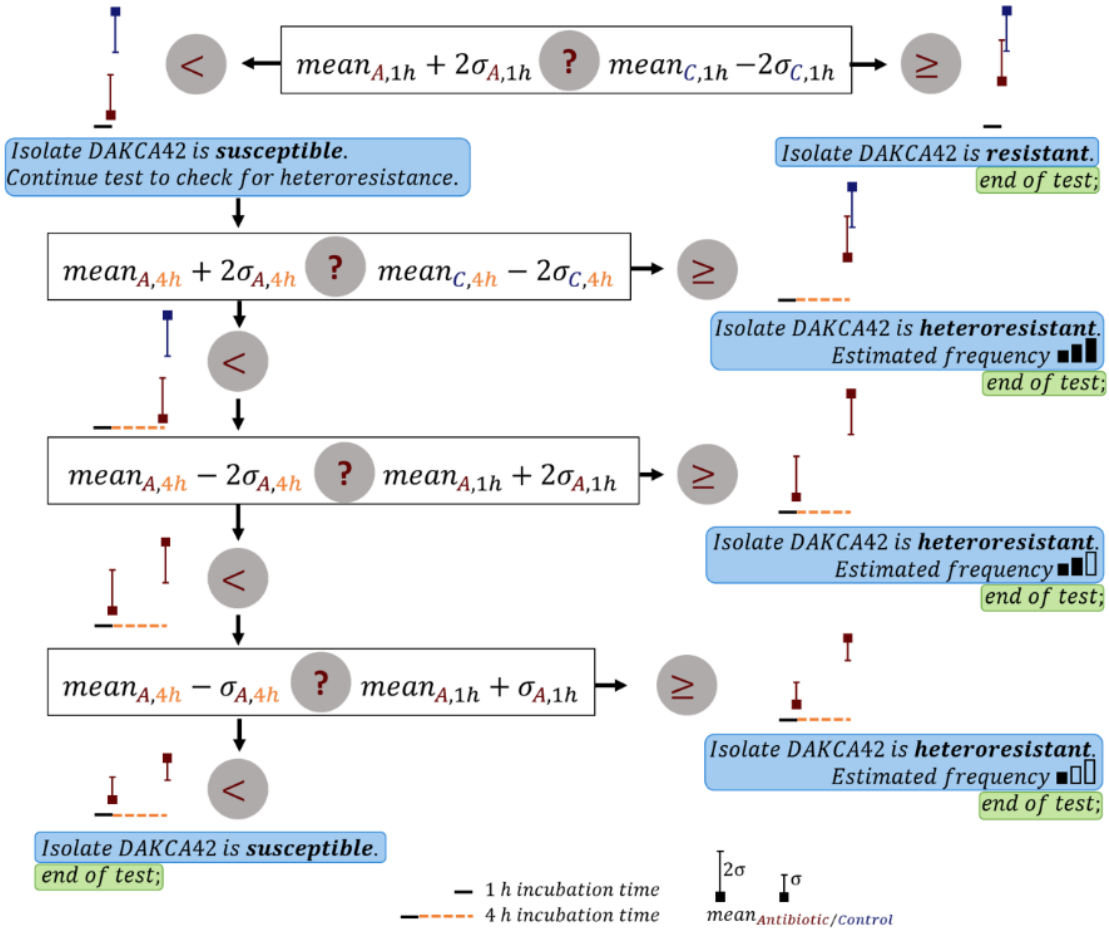

Figure 29: Decision tree for the detection of susceptible, resistant and heteroresistant isolates. (D) Intensities of the CD band for frequencies 10^{-3}-10^{-4} of resistant cells for 1 and 4 hours of incubation time.

The decision tree consists of four decision nodes to classify susceptible, resistant, and heteroresistant isolates. First, resistant and susceptible cells are classified based on the 2σ criterion described in equation 11. At this point, the isolate that tests susceptible may still be heteroresistant. The following three decision nodes require a longer incubation time but allow an estimation of the frequency of the resistant subpopulation, and, hence, to discriminate heteroresistant from susceptible isolates. Based on the data of modeled heteroresistant cultures depicted in Figure 28, an extended incubation time of 4 hours in total is necessary to cover resistant cell frequencies down to 10^{-4} and possibly lower. The second decision in the decision tree is based upon the 2σ criterion applied to cells that have been incubated for 4 hours in D_2O-containing medium. If the mean of the CD content of

the control group ("$mean_C$") minus its twofold standard deviation ("$2\sigma_C$") is smaller than the mean CD content of the antibiotic-treated aliquot ("$mean_A$") plus its twofold standard deviation ("$2\sigma_A$"), the isolate is classified as heteroresistant with a high frequency of resistant cells ($\geq 10^{-2}$). Otherwise, the test continues to the next decision node. Based on the assumption that the CD band of susceptible bacteria does not increase between 1 h and 4 h of incubation (see Figure 26A), another 2σ criterion is applied to classify heteroresistant isolates with lower frequency of resistant cells ($10^{-4} \leq$ frequency $< 10^{-2}$). The final decision differentiates between susceptible and heteroresistant isolates with very low frequencies ($< 10^{-4}$). The isolate is classified as heteroresistant if the single standard deviation of the CD content of cells treated with antibiotic after 1 h and 4 h do not overlap. This last criterion may be replaced or extended by a statistical test comparing the mean value after 1 h and 4 h of incubation time, as demonstrated for the samples depicted above in Figure 26A. If statistical testing reveals a significant difference and the CD content at 4 h is increasing compared to 1 h, then heteroresistance cannot be excluded.

In order to relate the measured data of CD content of antibiotic-treated samples to the frequency, the corresponding number of cells was calculated (see Figure 30). In the presence of antibiotic, only the resistant cells are growing. An exponential growth function according to Allen *et al.* as given in equation 12 was used to calculate the cell numbers.[120] Here, n_t is the number of cells at time t, n_0 number of cells at the beginning of the growth and td is the doubling time. A typical td for *E. coli*, 20 minutes, was used.[120]

$$n_t = n_0 \cdot 2^{t \cdot \frac{1}{td}} \tag{12}$$

With this equation, the number of cells containing deuterium and those without a CD band can be estimated. For the frequencies used in the experiment described above (10^{-1}, $2 \cdot 10^{-2}$, 10^{-2}, 10^{-3} and 10^{-4}) and further frequencies of 10^{-5}-10^{-8}, the resulting curves are given in the graph in Figure 30A. Here, the number of cells is traced over time. The resistant cells are depicted by the blue curves and the susceptible cells are represented by the horizontal black lines. The vertical red lines indicate the time points of deuterium addition (90 minutes) and the sampling after 1, 2, 3, and 4 hours incubation. In the graph in Figure 30B, blue curves depict the ratio of susceptible and resistant cells for the same frequencies. This

plot can help to explain the appearance of the CD band observed in the plots in Figure 28 (on page 68). As a matter of fact, the susceptible bacteria show no CD band. However, they contribute to the measured biomass. Its portion is low for the high frequency of 10^{-1} in the case of the 1 hour sample. However, for the lower frequency of 10^{-2}, it makes up even one third of the biomass as can be conducted from the value of 2 for the Ratio of Resistant and susceptible cells in Figure 30B (highlighted with red circles). While in this case the CD content of the corresponding sample in Figure 28 on page 68 with a value of 0.5 equals that of the control sample, the next smaller frequency of 10^{-3} comes with a significantly lower CD content at a value of 0.2. For the next sampling time of two hours, it is already at a considerably higher value of 0.3. The same applies to the 10^{-4} sample for two and three hours of incubation time. Here, the ratio of resistant and susceptible cells lies at a value of one (i.e. 1:1) in Figure 30B. Again, it is indicated in the graph by a red circle. Thus, this ratio of 1:1 of cells containing deuterium and not deuterated biomass can be assumed to be necessary at a minimum in order to detect growth by means of the CD band. Consequently, for frequencies down to 10^{-5}, detection after 4 hours of incubation time, and after 6-7 hours for 10^{-6} and 10^{-7}, should be possible.

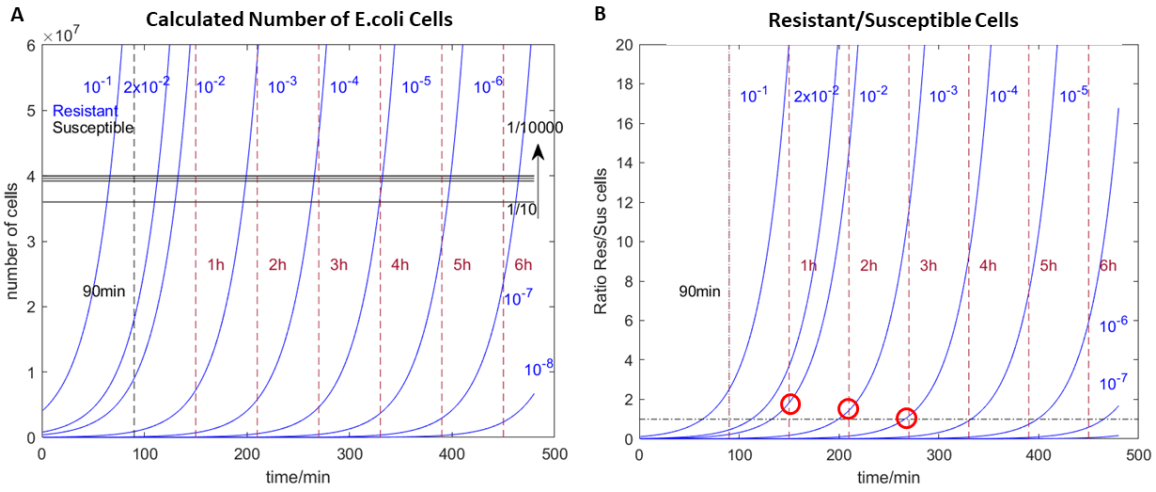

Figure 30: (A) Calculated number of cells under antibiotic treatment with frequencies used in the experiment and extended for 10^{-5} to 10^{-8}. Susceptible cells (black) are supposed to stay constant, while resistant ones (blue) to grow exponentially. (B) Respective ratio of resistant to susceptible cells calculated from numbers in (A). The timepoints of the AST protocol (90 min preincubation, 1, 2, 3, 4 h sampling) are indicated by lines and extended to 5 and 6 hours.

Nevertheless, it has to be taken into account that this simulated case is only valid for cultures with stable heteroresistance (i.e. where the ratio of resistant to susceptible cells remains stable). This is usually the case for polyclonal populations.[129, 137] If horizontal gene transfer is involved instead, as in case of NDM-1-carrying bacteria, the resistance is not passed on during replication of the cells, but by plasmids or bacteriophages. Thus, the frequency of resistant cells does not remain constant, but increases. Therefore, resistance might be detected even faster, as was observed in the clinical isolates described above (EC-Mer 6, EC-Mer 7, and EC-Mer 8). Furthermore, as already mentioned in section 4.1.6, the antibiotic treatment can induce enhanced metabolic activity due to the stress. Hence, an enhanced deuterium uptake can take place and the CD content does not increase according to "normal" growth conditions.

4.1.8 Classification of Bacteria

Although not yet established in certified clinical systems, it has been shown in numerous studies that Raman spectroscopy allows for differentiation of bacteria even down to the strain level based on the unique spectral fingerprint.[99, 100, 227, 228] This classification is typically done using a broad range of chemometric tools. Supervised classification models are trained to correctly identify the species or group. Hence, they are typically more suitable for complex classification tasks than unsupervised ones.[88, 227, 228] Here, a support vector machine (SVM) was chosen for the classification of three bacterial strains. In this study, a dataset consisting of 4152 spectra of the three microorganisms (*E. coli, E. faecalis* and *E. faecium*) was used. As can be seen in Figure 31A, while the spectral fingerprint of *E. coli* might exhibit certain specific spectral features that allow for straightforward distinction from the other spectra, the classification of the two *Enterococci* requires a more complex classification algorithm. SVM can be trained to look at subtle differences between classes and is also efficient with regard to the computing time and power.

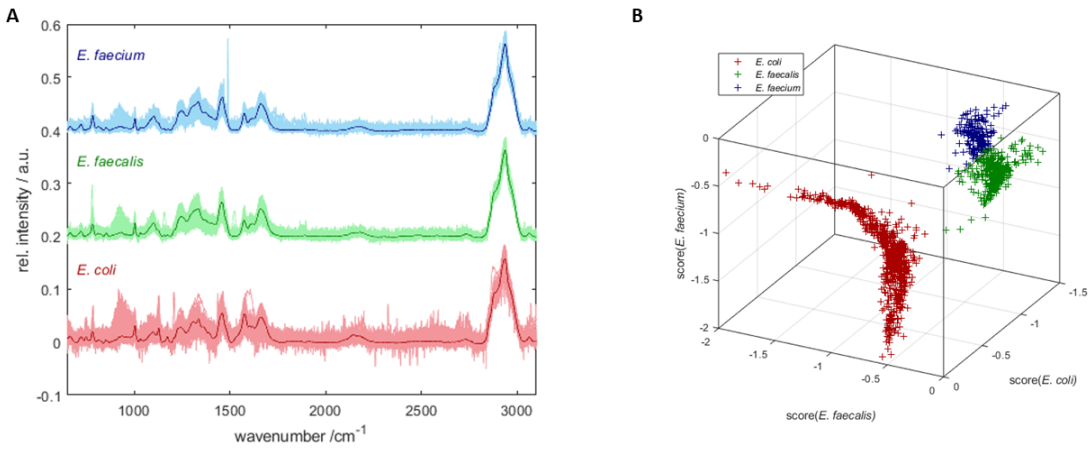

Figure 31: (A) Raman spectra of the bacteria used for classification. Average spectrum is shown in pronounced color, while the collective of all single spectra are depicted with higher transparency. (B) Scores of the different spectra according to the employed SVM model.

The spectral region between 650 and 3150 cm^{-1} of the baseline-corrected and normalized dataset (Figure 31A) was selected for data analysis. Two-thirds of the spectra of each microorganism (i.e. 1123 spectra of *E. coli*, 715 of *E. faecalis*, and 294 of *E. faecium*) were used to train the SVM using a cubic function with Matlab's "fitcecoc" tool for classification of multiple class problems, and a five-fold cross validation was performed. The established model was then applied on the other third of the data. The classification result shown in Figure 31B indicates good performance of the classifier, which is confirmed by a specificity of > 97 % and a sensitivity of ≥ 89 % for all classes, as summarized in Table 10.

Table 10: Results of the SVM-based classification. An accuracy of 95.7% was reached and can be calculated from the values listed here. Columns from left to right contain the bacterium species, the number of spectra per species and the results of the SVM classification: number of correctly classified - true positive (TP) and true negative (TN) - and misclassified - false positive (FP) and false negative (FN) - spectra.

Species	# Spectra	TP	FP	TN	FN	Sensitivity	Specificity
E. coli	736	735	0	647	1	100%	100%
E. faecalis	451	432	40	892	19	92%	98%
E. faecium	196	157	19	1168	39	89%	97%

The 3-dimensional score plot (Figure 31B) underlines that *E. coli* spectra can be clearly isolated from *E. faecium* and *E. faecalis*, while the latter two are more difficult to distinguish from each other. This was to be expected, as *E. faecium* and *E. faecalis* are closely related species of the same genus. These results are especially interesting for the development of an AST. They demonstrate that the simultaneous identification and antibiotic testing can be achieved within one measurement. This makes Raman spectroscopy an attractive alternative compared to currently available automated AST techniques, where the identification of bacteria is carried out in a separate test.[145, 151]

4.2 Identification of the Dormant State in *Mycobacterium Smegmatis*

4.2.1 Cultivation and sample preparation of *M. smegmatis*

Mycobacteria are typically known because their representative *M. tuberculosis* causes tuberculosis, which has the highest death rate among bacterial infections.[9] A non-pathogenic member of this family is *M. smegmatis*.[199] However, it is similar with regard to the cell structure and also the ability to reach a dormant state. Wild type *M. smegmatis* with a generation time of three hours can be cultivated well in M7H9 medium, and bacteria can be brought to the dormant state by an acidification protocol according to Kudykina *et al.*.[229, 230] One milliliter of bacteria from an overnight culture in M7H9 medium are used as inoculum for 100 mL of Sauton's medium at a starting pH value of 6.0. Within 21 days, the pH goes further down to a value of 4.0 - 4.5 because of the release of organic acids and other acidic metabolites. The dormant state was verified by measurement of ATP levels and MALDI-TOF analysis by the project partners from the Wieser group of the MVP.

In the context of this work, Raman microscopic analysis and evaluation of the spectra was carried out. For the fixation of live mycobacteria on glass slides, no standardized techniques exist.[231] In Raman microscopy and microscopic analysis in general, chemical fixation is employed or bacteria are fixed by drying. Both ways lead to cell death. In order to observe viable microorganisms, fixation can be realized by optical tweezing or with surface-modified slides.[231, 232] However, optical tweezing requires elaborate instrumentation. Typical surface modifications on glass slides, like poly-L-lysine or

electrostatic surfaces, lead to adhesive binding of cells or tissues. However, because of their highly hydrophobic cell wall, this binding is inefficient in the case of mycobacteria. For biosynthetic reactions using live mycobacteria, hydrophobic silicone rubbers have been used to immobilize mycobacteria.[233] Similarly, the hydrophobic nature of the cell wall was exploited for sample preparation. Thus, they could be fixed on a hydrophobic glass slide through non-covalent interaction between the two nonpolar materials. In order to keep them in a physiologically favored environment, the bacteria fixed on the cover slide were positioned over a chamber filled with sterile 0.9% NaCl solution.

4.2.2 Single Cell Raman and SEM Measurements

To analyze single cells, the microscopic images were processed with a Matlab script (see Appendix 1.2.1). It allows detection of the bacteria from a binary image using the built-in function "bwconncomp". The binary image was achieved after background detection and contrast enhancement with the built-in functions "imopen", "graythresh" and "im2bw". Thus, by loading the coordinates into the "Point Viewer" of WITec's Control FIVE software (WITec GmbH, Ulm, Germany), a semi-automated measurement could be carried out. For best depth resolution and due to the use of a cover glass, the 63x oil-immersion objective with a numerical aperture of 1.4 was employed. Microscopic images of dormant and wild type cultures are depicted in Figure 32A and C, respectively. The Raman spectra acquired from the single cells are shown in Figure 32B and D. Spectra of several single cells were obtained from three different batches. After selection by a signal-to-noise ratio filter of the CH stretching band with a minimum threshold value of 5, 60 spectra of wild type (WT) cells and 77 of dormant ones were selected for further analysis. Before further processing steps, the spectra were cropped to the region from 750 to 3050 cm^{-1}. They are shown in Figure 32B and D for the wild type and the dormant bacteria respectively. The broad band at 924 cm^{-1} can be attributed to the cover glass. The rest of the spectrum represents typical Raman bands found in literature for *M. smegmatis*.[186, 188, 189]

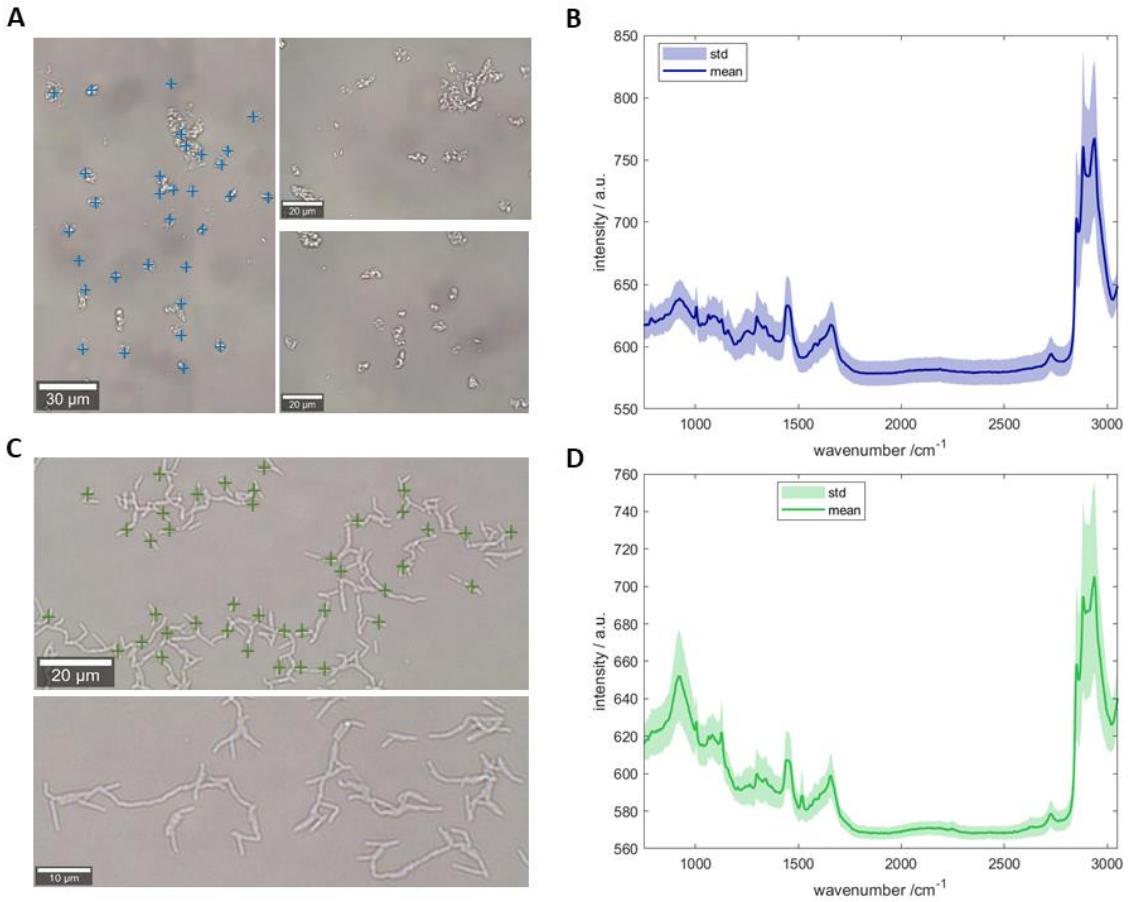

Figure 32: Microscopic images and Raman spectra of *M. smegmatis* dormant (A and B, respectively) and as wild type (C and D, respectively).

The microscopic images in Figure 32 show that already the morphological appearance of the cells is different in the dormant state compared to the WT bacteria. The cells are shorter, deformed and agglomerated. These phenotypic differences were confirmed in more detail by scanning electron microscopy. A selection of the corresponding images of WT and dormant bacteria is shown in Figure 33 A and B, respectively.

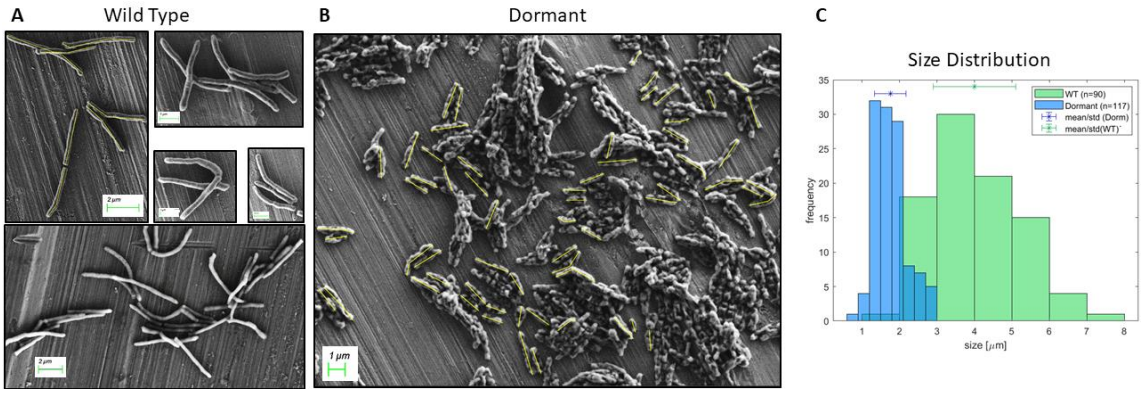

Figure 33: SEM images of *M.smegmatis* wild type (A) and in the dormant state (B). The yellow lines on a few bateria indicate the size measurement that was performed (on all bacteria). The corresponding size distribution is shown in (C).

The length distribution of bacteria was analyzed on several SEM images using the measuring tool of the ImageJ software (indicated by yellow lines in the images). The results are depicted in the bar graph in Figure 33C. Thus, as indicated by the mean and standard deviation plot above the bars, the average size of WT cells (n = 90) is in the range of 4.00 ±1.10 μm and for dormant ones (n = 117), it is 1.76 ± 0.42 μm.

4.2.3 Cluster Analysis-Based Classification

The Raman spectra shown in Figure 32 were further processed in order to carry out hierarchical cluster analysis.

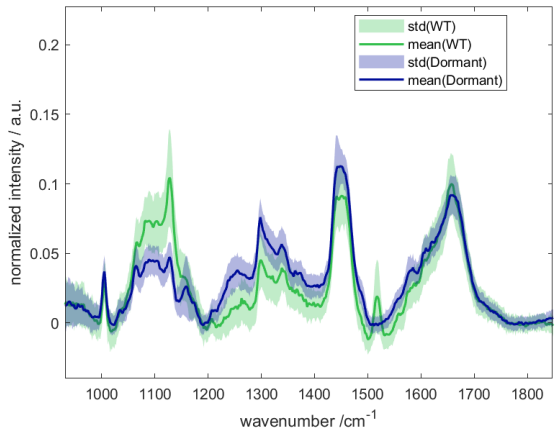

Figure 34: Processed Raman spectra of mycobacteria single cells. Mean spectra and standard deviation of WT (green) and dormant (blue) cells after background subtraction (4th order polynomial, asymmetric truncated quadratic fitting function, 0.065 noise threshold) and normalization of the Euclidean length of the spectrum.

Cluster analysis has proved to be useful for grouping spectra of mycobacteria down to the strain level.[21, 22] To avoid the influence of the glass band at 924 cm^{-1}, the region of the fingerprint between 950 and 1850 cm^{-1} was selected and background correction was carried out using a 4th order polynomial function in combination with an asymmetric truncated quadratic function and a threshold value of 0.065 for the noise level of the function. The spectra resulting after normalization of the Euclidean length are depicted in Figure 34.

After mean centering, the spectra were analyzed using the Euclidean distance with Ward's clustering algorithm. The resulting cluster tree is depicted in Figure 35A. It can be seen that two main clusters with a distance of almost 100 are found. After labeling the single branches with a color scheme, it can be seen that they represent the two different cultivation conditions well.

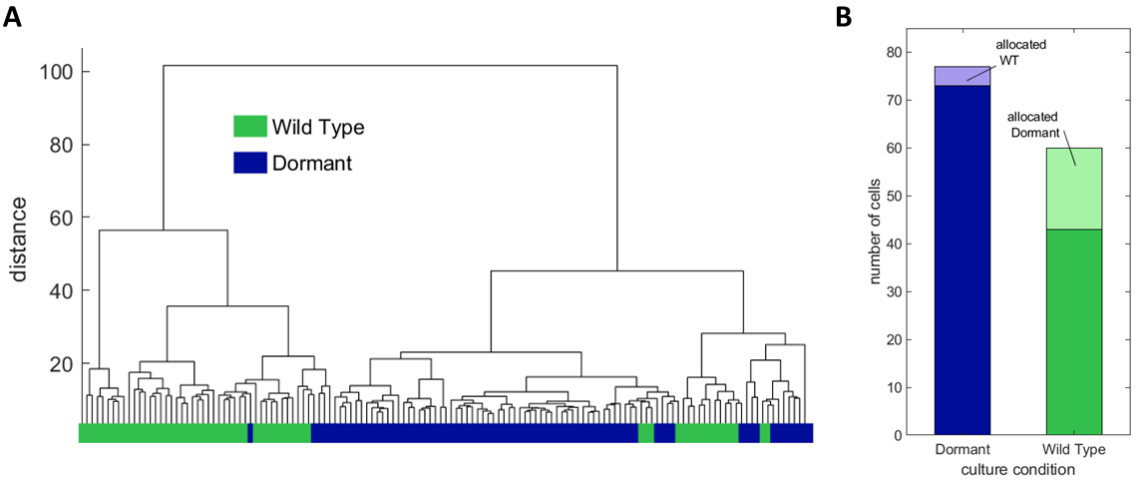

Figure 35: (A) Dendrogram of hierarchical cluster analysis of Raman spectra of mycobacteria in dormant (red) and wild type (blue) state. The Euclidean distance and Ward' algorithm were used. (B). Result of cluster analysis allocation compared to cultivation conditions.

Thus, 64 of 71 spectra (~90%) classified as dormant and 48 out of 60 (80%) as WT cells. Since no reference method revealing dormancy on a single-organism basis, it is not possible to verify a 100% efficiency of each cultivation protocol. Assuming that in an ensemble of wild-type organisms some individual cells are dormant, and even in the dormant culture some cells may remain wild type the particular value of Raman spectroscopy becomes evident. It is the only technique allowing for a non-destructive assessment of the chemical composition of individual microorganisms. Thus, it has already been used to sort individual cells based on the Raman allocation into groups with different

biological properties.[174, 234-239] Considering that hierarchical cluster analysis is an unsupervised method and therefore does not require calibration, setting up a large training dataset or validation of the classification, these results underline the potential of Raman microscopy as a straightforward analytical method for broad applications in microbiology, biotechnology and pharmacology.

5 CONCLUSION

Raman spectroscopy is a valuable analytical tool especially in the field of microbiology. This work demonstrates the potential of the technique in two main fields of clinical microbiology: the fast detection of resistant and heteroresistant Gram-positive and Gram-negative bacteria by monitoring of the deuterium uptake and the differentiation between dormant and wild type *M. smegmatis*.

One of the most threatening global health issues is the evolution of multi-drug resistant bacteria. Modern systems used in clinical microbiology for antibiotic susceptibility testing (AST) are preferably combined with an identification (ID) method in one instrument. They can deliver AST/ID results within 5 – 12 hours. This time is still too long for point-of-care diagnostics and often fails to detect heteroresistance. Heteroresistant cultures come with a subpopulation with a higher resistance towards an antibiotic in an otherwise genetically identical population. This often leads to a wrong AST classification and ultimately to treatment failure. In this work, a Raman-based AST protocol exploiting the evolution of the CD band from metabolically active bacteria in the otherwise empty region between 2050 and 2350 cm^{-1} was developed. It takes into account that certain bacteria-antibiotic combinations require a preincubation with antibiotic before addition of D_2O in order to obtain unambiguous results. This protocol gives a reliable AST result within 3.5 hours. In order to demonstrate the practical use, 52 clinical isolates were investigated with this protocol. Gram-negative *E. coli* were tested against ampicillin, ciprofloxacin and meropenem, while Gram-positive *E. faecalis* and *E. faecium* against ampicillin and vancomycin. The results for fully resistant and fully susceptible phenotypes were in good agreement with AST results obtained via state-of-the-art E-tests. In the case of heteroresistant isolates, the Raman-based approach yields reliable results at extended incubation times of two to three hours. In this work, the usefulness of the Raman-based monitoring of deuterium uptake could be demonstrated. Furthermore, an experimental modeling of heteroresistant cultures with frequencies between 10^{-2} and 10^{-4} indicates the possibility of directly measuring the frequency of heteroresistance in a straightforward way. Simulations based on these experiments indicate that heteroresistance of a stable frequency down to 10^{-7} can be detected within 6 to 7 hours.

One prerequisite for the development of a clinical routine instrument is the automated and reliable acquisition of a sufficient number of spectra. This was realized by the sample preparation on a hydrophobic slide, on which the sample is obtained as an assembled biomass. Hence, straightforward spectral acquisition was possible.

Furthermore, the obtained datasets of Raman spectra of the three different bacteria, *E. coli*, *E. faecalis* and *E. faecium*, were used to test their identification by a supervised machine learning algorithm. Namely, a support vector machine was employed to carry out the identification and obtained an accuracy of identification of 95.7%.

To sum up, the Raman-deuterium-based AST proved to be a promising tool for clinical use, since it is one of the primary methods for the identification of heteroresistant cultures. Furthermore, the recorded spectra can be used for identification of the species of bacteria. However, in order to bring it to a clinical application, a broad range of other bacteria-antibiotic combinations needs to be tested.

In this work, Raman microscopy was used in a second context of high clinical relevance. It was applied to investigate the so-called dormant state of *Mycobacteria*. In this genus of bacteria *M. tuberculosis* is the most relevant one. It is known that this dormant state in which the metabolism of the cells is reduced, passivates them and they become even more resistant towards antibiotics or the immune system in vivo. This warrants further investigations and the development of straightforward detection methods. In this work, the Raman-based single cell measurement in combination with cluster analysis was carried out on dormant versus wild type *M. smegmatis*. The metabolic state was confirmed by the microbiology project partners using orthogonal methods like ATP measurement, microbiological cultivation and MALDI-TOF. Employing hierarchical cluster analysis in combination with Raman spectroscopy allowed assignment of the majority of the cells to the corresponding metabolic state. Thus, 90% of dormant cells and 60% of wild type cells were categorized into the group expected by the cultivation protocol. However, it can be assumed that a certain portion of the cells is in a different than the proposed metabolic state. The high potential of Raman spectroscopy as a non-destructive method allowing for chemical characterization of individual cells and therefore its usefulness for clinical microbiology has been demonstrated in this work.

6 BIBLIOGRAPHY

1. O'Neill, J. A., Tackling Drug-Resistant Infections Globally: final report and recommendations. *Review on Antimicrobial Resistance* **2016**.

2. ECDC *Surveillance of antimicrobial resistance in Europe – 2017*; EARS-Net: Stockholm, 2018.

3. WHO *Global antimicrobial resistance surveillance system (GLASS) report: early implementation 2016-2017*; World Health Organization: Geneva, 2017.

4. Krause, M.; Radt, B.; Rosch, P.; Popp, J., The investigation of single bacteria by means of fluorescence staining and Raman spectroscopy. *Journal of Raman Spectroscopy* **2007,** *38* (4), 369-372.

5. Foxman, B.; Barlow, R.; D'Arcy, H.; Gillespie, B.; Sobel, J. D., Urinary tract infection: Self reported incidence and associated costs. *Ann Epidemiol* **2000,** *10* (8), 509-515.

6. Simmering, J. E.; Tang, F.; Cavanaugh, J. E.; Polgreen, L. A.; Polgreen, P. M., The Increase in Hospitalizations for Urinary Tract Infections and the Associated Costs in the United States, 1998-2011. *Open Forum Infect Di* **2017,** *4* (1).

7. Leclercq, R.; Canton, R.; Brown, D. F. J.; Giske, C. G.; Heisig, P.; MacGowan, A. P.; Mouton, J. W.; Nordmann, P.; Rodloff, A. C.; Rossolini, G. M.; Soussy, C. J.; Steinbakk, M.; Winstanley, T. G.; Kahlmeter, G., EUCAST expert rules in antimicrobial susceptibility testing. *Clin Microbiol Infec* **2013,** *19* (2), 141-160.

8. El-Halfawy, O. M.; Valvano, M. A., Antimicrobial Heteroresistance: an Emerging Field in Need of Clarity. *Clinical Microbiology Reviews* **2015,** *28* (1), 191-207.

9. https://www.who.int/tb/publications/global_report/en/ Global Tuberculosis Report 2019. (accessed 5/1/2020).

10. Dheda, K.; Ruhwald, M.; Theron, G.; Peter, J.; Yam, W. C., Point-of-care diagnosis of tuberculosis: Past, present and future. *Respirology* **2013,** *18* (2), 217-232.

11. Gordon, S. V.; Parish, T., Microbe Profile: Mycobacterium tuberculosis: Humanity's deadly microbial foe. *Microbiology* **2018,** *164* (4), 437-439.

12. Gomez, J. E.; McKinney, J. D., M. tuberculosis persistence, latency, and drug tolerance. *Tuberculosis* **2004,** *84* (1), 29-44.

13. Lipworth, S.; Hammond, R. J. H.; Baron, V. O.; Hu, Y. M.; Coates, A.; Gillespie, S. H., Defining dormancy in mycobacterial disease. *Tuberculosis* **2016,** *99*, 131-142.

14. Raman, C. V., A new radiation. *Indian J. Phys.* **1928,** *2*, 387-398.

15. Strutt, J. W., XV. On the light from the sky, its polarization and colour. *The London, Edinburgh, and Dublin Philosophical Magazine and Journal of Science* **1871,** *41* (271), 107-120.

16. Strutt, J. W., LVIII. On the scattering of light by small particles. *The London, Edinburgh, and Dublin Philosophical Magazine and Journal of Science* **1871,** *41* (275), 447-454.

17. Landsberg, G. M., L., Eine neue Erscheinung bei der Lichtzerstreuung in Krystallen. *Naturwissenschaften* **1928,** *16* (28), 557-558.

18. Vandenabeele, P., *Practical Raman Spectroscopy - An Introduction*. John Wiley & Sons, Ltd: 2013.

19. Horiba; Ltd Raman Bands List (pdf). https://www.horiba.com/fileadmin/uploads/Scientific/Documents/Raman/bands.pdf (accessed 05/29/2020).

20. Smith, E.; Dent, G., The Theory of Raman Spectroscopy. In *Modern Raman Spectroscopy – A Practical Approach*, John Wiley & Sons, Ltd: 2005; pp 71-92.

21. Buijtels, P. C. A. M.; Willemse-Erix, H. F. M.; Petit, P. L. C.; Endtz, H. P.; Puppels, G. J.; Verbrugh, H. A.; van Belkum, A.; van Soolingen, D.; Maquelin, K., Rapid identification of mycobacteria by Raman spectroscopy. *J Clin Microbiol* **2008,** *46* (3), 961-965.

22. Kirschner, C.; Maquelin, K.; Pina, P.; Thi, N. A. N.; Choo-Smith, L. P.; Sockalingum, G. D.; Sandt, C.; Ami, D.; Orsini, F.; Doglia, S. M.; Allouch, P.; Mainfait, M.; Puppels, G. J.; Naumann, D., Classification and identification of enterococci: a comparative phenotypic, genotypic, and vibrational spectroscopic study. *J Clin Microbiol* **2001,** *39* (5), 1763-1770.

23. Maquelin, K.; Choo-Smith, L. P.; van Vreeswijk, T.; Endtz, H. P.; Smith, B.; Bennett, R.; Bruining, H. A.; Puppels, G. J., Raman spectroscopic method for identification of clinically relevant microorganisms growing on solid culture medium. *Analytical Chemistry* **2000,** *72* (1), 12-19.

24. Maquelin, K.; Kirschner, C.; Choo-Smith, L. P.; van den Braak, N.; Endtz, H. P.; Naumann, D.; Puppels, G. J., Identification of medically relevant microorganisms by vibrational spectroscopy. *Journal of Microbiological Methods* **2002,** *51* (3), 255-271.

25. Harz, M.; Rosch, P.; Peschke, K. D.; Ronneberger, O.; Burkhardt, H.; Popp, J., Micro-Raman spectroscopic identification of bacterial cells of the genus Staphylococcus and dependence on their cultivation conditions. *Analyst* **2005,** *130* (11), 1543-1550.

26. Penney, C. M.; Goldman, L. M.; Lapp, M., Raman Scattering Cross Sections. *Nature Physical Science* **1972,** *235* (58), 110-112.

27. Hadrich, S.; Hefter, S.; Pfelzer, B.; Doerk, T.; Jauernik, P.; Uhlenbusch, J., Determination of the absolute Raman cross section of methyl. *Chemical Physics Letters* **1996,** *256* (1-2), 83-86.

28. Kneipp, K.; Kneipp, H.; Kneipp, J., Surface-enhanced Raman scattering in local optical fields of silver and gold nanoaggregatess - From single-molecule Raman spectroscopy to ultrasensitive probing in live cells. *Accounts Chem Res* **2006,** *39* (7), 443-450.

29. Fung, K. H.; Tang, I. N., Relative Raman Scattering Cross-Section Measurements with Suspended Particles. *Appl Spectrosc* **1991,** *45* (5), 734-737.

30. Dieing, T.; Hollricher, O.; Toporski, J., *Confocal Raman Microscopy*. Springer: Berlin Heidelberg, 2011; Vol. 158, p 292.

31. Smith, E.; Dent, G., The Raman Experiment – Raman Instrumentation, Sample Presentation, Data Handling and Practical Aspects of Interpretation. In *Modern Raman Spectroscopy – A Practical Approach*, John Wiley & Sons, Ltd: 2005; pp 23-70.

32. Demtröder, W., *Laserspektroskopie 1*. 6 ed.; Springer Spektrum: Berlin, Heidelberg, 2011; Vol. 1, p 307.

33. Amos, B.; McConnell, G.; Wilson, T., 2.2 Confocal Microscopy. In *Comprehensive Biophysics*, Egelman, E. H., Ed. Elsevier: Amsterdam, 2012; pp 3-23.

34. Everall, N. J., Confocal Raman Microscopy: Why the Depth Resolution and Spatial Accuracy Can Be Much Worse Than You Think. *Appl Spectrosc* **2000,** *54* (10), 1515-1520.

35. Everall, N. J., Modeling and Measuring the Effect of Refraction on the Depth Resolution of Confocal Raman Microscopy. *Appl Spectrosc* **2000,** *54* (6), 773-782.

36. Everall, N.; Lapham, J.; Adar, F.; Whitley, A.; Lee, E.; Mamedov, S., Optimizing depth resolution in confocal Raman microscopy: A comparison of metallurgical, dry corrected, and oil immersion objectives. *Appl Spectrosc* **2007,** *61* (3), 251-259.

37. Everall, N., Optimising image quality in 2D and 3D confocal Raman mapping. *Journal of Raman Spectroscopy* **2014,** *45* (1), 133-138.

38. Owens, J. C., Optical Refractive Index of Air: Dependence on Pressure, Temperature and Composition. *Applied Optics* **1967,** *6* (1), 51-59.

39. Rottenfusser, R.; Dragoo, T.; Davidson, M. W. Oil Immersion and Refractive Index. https://www.zeiss.com/microscopy/int/solutions/reference/all-tutorials/basic-microscopy/oil-immersion-and-refractive-index.html (accessed 06/06/2020).

40. Vyörykkä, J.; Halttunen, M.; Iitti, H.; Tenhunen, J.; Vuorinen, T.; Stenius, P., Characteristics of Immersion Sampling Technique in Confocal Raman Depth Profiling. *Appl Spectrosc* **2002,** *56*, 776-782.

41. Adar, F., Lee, E., Mamedov, S., Whitley, A., Experimental Evaluation of the Depth Resolution of a Raman Microscope. *Microscopy and Microanalysis* **2010,** *16* (S02), 360-361.

42. Adar, F. Depth Resolution of the Raman Microscope: Optical Limitations and Sample Characteristics.

43. Opilik, L.; Schmid, T.; Zenobi, R., Modern Raman Imaging: Vibrational Spectroscopy on the Micrometer and Nanometer Scales. *Annual Review of Analytical Chemistry* **2013,** *6* (1), 379-398.

44. Park, J.; Kim, J.; Kwon, H., Evaluation of Lateral Resolution for Confocal Raman Microscopy Using Gold Nano-Lines Made by Electron Beam Lithography. *Bulletin of the Korean Chemical Society* **2020,** *41* (1), 34-37.

45. Everall, N. J., Confocal Raman microscopy: common errors and artefacts. *Analyst* **2010,** *135* (10), 2512-2522.

46. Mauricio-Iglesias, M.; Guillard, V.; Gontard, N.; Peyron, S., Raman depth-profiling characterization of a migrant diffusion in a polymer. *Journal of Membrane Science* **2011,** *375* (1), 165-171.

47. https://www.witec.de/resources-and-education/knowledge-base/show/raman-basics/how-is-the-spatial-resolution-defined (accessed 05.05.2020).

48. What is the spatial resolution of a Raman microscope? https://www.horiba.com/uk/scientific/products/raman-spectroscopy/raman-academy/raman-faqs/what-is-the-spatial-resolution-of-a-raman-microscope/ (accessed 04/05/2020).

49. Esposito, R.; Scherillo, G.; Pannico, M.; Musto, P.; DeNicola, S.; Mensitieri, G., Depth profiles in confocal optical microscopy: a simulation approach based on the second Rayleigh-Sommerfeld diffraction integral. *Opt Express* **2016,** *24* (12), 12565-12576.

50. Phillips, G. R.; Harris, J. M., Polynomial Filters for Data Sets with Outlying or Missing Observations - Application to Charge-Coupled-Device-Detected Raman-Spectra Contaminated by Cosmic-Rays. *Analytical Chemistry* **1990,** *62* (21), 2351-2357.

51. Cappel, U. B.; Bell, I. M.; Pickard, L. K., Removing Cosmic Ray Features from Raman Map Data by a Refined Nearest Neighbor Comparison Method as a Precursor for Chemometric Analysis. *Appl Spectrosc* **2010,** *64* (2), 195-200.

52. Schulze, H. G.; Turner, R. F. B., A Two-Dimensionally Coincident Second Difference Cosmic Ray Spike Removal Method for the Fully Automated Processing of Raman Spectra. *Appl Spectrosc* **2014,** *68* (2), 185-191.

53. Leger, M. N.; Ryder, A. G., Comparison of derivative preprocessing and automated polynomial baseline correction method for classification and quantification of narcotics in solid mixtures. *Appl Spectrosc* **2006,** *60* (2), 182-193.

54. Keating, M. E.; Nawaz, H.; Bonnier, F.; Byrne, H. J., Multivariate statistical methodologies applied in biomedical Raman spectroscopy: assessing the validity of partial least squares regression using simulated model datasets. *Analyst* **2015,** *140* (7), 2482-2492.

55. Byrne, H. J.; Knief, P.; Keating, M. E.; Bonnier, F., Spectral pre and post processing for infrared and Raman spectroscopy of biological tissues and cells. *Chemical Society Reviews* **2016,** *45* (7), 1865-1878.

56. Ling, Y. C.; Vickers, T. J.; Mann, C. K., Background correction in Raman-spectroscopic determination of Dimethylsulfone, Sulfate, and Bisulfate. *Appl Spectrosc* **1985,** *39* (3), 463-470.

57. Schulze, G.; Jirasek, A.; Yu, M. M. L.; Lim, A.; Turner, R. F. B.; Blades, M. W., Investigation of selected baseline removal techniques as candidates for automated implementation. *Appl Spectrosc* **2005,** *59* (5), 545-574.

58. Afseth, N. K.; Segtnan, V. H.; Wold, J. P., Raman spectra of biological samples: A study of preprocessing methods. *Appl Spectrosc* **2006,** *60* (12), 1358-1367.

59. Leon-Bejarano, M.; Dorantes-Mendez, G.; Ramirez-Elias, M.; Mendez, M. O.; Alba, A.; Rodriguez-Leyva, I.; Jimenez, M., Fluorescence background removal method for biological Raman spectroscopy based on Empirical Mode Decomposition. In *38th Annual International Conference of the IEEE Engineering in Medicine and Biology Society*, IEEE: New York, 2016; pp 3610-3613.

60. Liland, K. H.; Almoy, T.; Mevik, B. H., Optimal Choice of Baseline Correction for Multivariate Calibration of Spectra. *Appl Spectrosc* **2010,** *64* (9), 1007-1016.

61. Mazet, V.; Carteret, C.; Brie, D.; Idier, J.; Humbert, B., Background removal from spectra by designing and minimising a non-quadratic cost function. *Chemometr Intell Lab* **2005,** *76* (2), 121-133.

62. Krishna, H.; Majumder, S. K.; Gupta, P. K., Range-independent background subtraction algorithm for recovery of Raman spectra of biological tissue. *Journal of Raman Spectroscopy* **2012,** *43* (12), 1884-1894.

63. Chan, J. W.; Winhold, H.; Corzett, M. H.; Ulloa, J. M.; Cosman, M.; Balhorn, R.; Huser, T., Monitoring dynamic protein expression in living E-coli. Bacterial Cells by laser tweezers raman spectroscopy. *Cytom Part A* **2007,** *71a* (7), 468-474.

64. Muhamadali, H.; Chisanga, M.; Subaihi, A.; Goodacre, R., Combining Raman and FT-IR Spectroscopy with Quantitative Isotopic Labeling for Differentiation of E. coli Cells at Community and Single Cell Levels. *Analytical Chemistry* **2015,** *87* (8), 4578-4586.

65. Chisanga, M.; Muhamadali, H.; Kimber, R.; Goodacre, R., Quantitative detection of isotopically enriched E. coli cells by SERS. *Faraday Discussions* **2017**.

66. Clarke, R. H.; Londhe, S.; Premasiri, W. R.; Womble, M. E., Low-resolution Raman spectroscopy: Instrumentation and applications in chemical analysis. *Journal of Raman Spectroscopy* **1999,** *30* (9), 827-832.

67. Grow, A. E. Raman optrode processes and devices for detection of chemicals and microorganisms. 11. Jan. 1999, 2000.

68. Pelletier, M. J., Quantitative analysis using Raman spectrometry. *Appl Spectrosc* **2003,** *57* (1), 20a-42a.

69. Heinemann, M.; Meinberg, H.; Büchs, J.; Koß, H.-J.; Ansorge-Schumacher, M. B., Method for Quantitative Determination of Spatial Polymer Distribution in Alginate Beads Using Raman Spectroscopy. *Appl Spectrosc* **2005,** *59* (3), 280-285.

70. Rantanen, J., Process analytical applications of Raman spectroscopy. *J Pharm Pharmacol* **2007,** *59* (2), 171-177.

71. Johansson, J.; Claybourn, M.; Folestad, S., Raman Spectroscopy: A Strategic Tool in the Process Analytical Technology Toolbox. *Biol Med Phys Biomed* **2010**, 241-262.

72. Yang, D. T.; Ying, Y. B., Applications of Raman Spectroscopy in Agricultural Products and Food Analysis: A Review. *Applied Spectroscopy Reviews* **2011,** *46* (7), 539-560.

73. Assi, S.; Watt, R. A.; Moffat, A. C., On the quantification of ciprofloxacin in proprietary Ciproxin tablets and generic ciprofloxacin tablets using handheld Raman spectroscopy. *Journal of Raman Spectroscopy* **2012,** *43* (8), 1049-1057.

74. Chen, D.; Chen, Z. W.; Grant, E. R., Adaptive multiscale regression for reliable Raman quantitative analysis. *Analyst* **2012,** *137* (1), 237-244.

75. Li, B. Y.; Casamayou-Boucau, Y.; Calvet, A.; Ryder, A. G., Chemometric approaches to low-content quantification (LCQ) in solid-state mixtures using Raman mapping spectroscopy. *Anal Methods-Uk* **2017,** *9* (44), 6293-6301.

76. Smith, E.; Dent, G., Applications. In *Modern Raman Spectroscopy – A Practical Approach*, John Wiley & Sons, Ltd: 2005; pp 135-179.

77. Farkas, A.; Vajna, B.; Soti, P. L.; Nagy, Z. K.; Pataki, H.; Van der Gucht, F.; Marosi, G., Comparison of multivariate linear regression methods in micro-Raman spectrometric quantitative characterization. *Journal of Raman Spectroscopy* **2015,** *46* (6), 566-576.

78. Schmid, T.; Schäfer, N.; Levcenko, S.; Rissom, T.; Abou-Ras, D., Orientation-distribution mapping of polycrystalline materials by Raman microspectroscopy. *Sci Rep-Uk* **2015,** *5* (1), 18410.

79. Neil, E., Depth Profiling With Confocal Raman Microscopy, Part I. *Spectroscop Online* **2004,** *19* (10), 22 - 27.

80. Neil, E., Depth Profiling With Confocal Raman Microscopy, Part II. *Spectroscop Online* **2004,** *19* (11), 22 - 27.

81. Perez-Marin, D.; Garrido-Varo, A.; Guerrero, J. E., Non-linear regression methods in NIRS quantitative analysis. *Talanta* **2007,** *72* (1), 28-42.

82. Sorensen, J. A.; Thompson, L. C.; Glass, G. E., Quantitative-Analysis of Aqueous Species Using Raman Spectrometry and Equilibrium-Model Calculations. *Analytical Chemistry* **1985,** *57* (6), 1087-1091.

83. Freedman, D. A., *Statistical Models: Theory and Practice*. 2nd ed.; Cambridge University Press: 2009.

84. Mark, H.; Workman, J., *Chemometrics in Spectroscopy*. Elsevier Academic Press Inc: San Diego, 2007; p 1-544.

85. Chatterjee, S.; Hadi, A. S., Influential Observations, High Leverage Points, and Outliers in Linear Regression. *Statist. Sci.* **1986,** *1* (3), 379-393.

86. Gautam, R.; Vanga, S.; Ariese, F.; Umapathy, S., Review of multidimensional data processing approaches for Raman and infrared spectroscopy. *EPJ Techniques and Instrumentation* **2015,** *2* (1), 8.

87. Brereton, R. G., *Chemometrics : Data Driven Extraction for Science*. John Wiley & Sons, Incorporated: Newark, UNITED KINGDOM, 2018.

88. Rosch, P.; Harz, M.; Schmitt, M.; Peschke, K. D.; Ronneberger, O.; Burkhardt, H.; Motzkus, H. W.; Lankers, M.; Hofer, S.; Thiele, H.; Popp, J., Chemotaxonomic identification of single bacteria by micro-Raman spectroscopy: Application to clean-room-

relevant biological contaminations. *Applied and Environmental Microbiology* **2005,** *71* (3), 1626-1637.

89. Gaus, K.; Rosch, P.; Petry, R.; Peschke, K. D.; Ronneberger, O.; Burkhardt, H.; Baumann, K.; Popp, J., Classification of lactic acid bacteria with UV-resonance Raman spectroscopy. *Biopolymers* **2006,** *82* (4), 286-290.

90. Devos, O.; Ruckebusch, C.; Durand, A.; Duponchel, L.; Huvenne, J.-P., Support vector machines (SVM) in near infrared (NIR) spectroscopy: Focus on parameters optimization and model interpretation. *Chemometr Intell Lab* **2009,** *96* (1), 27-33.

91. Cortes, C.; Vapnik, V., Support-Vector Networks. *Mach Learn* **1995,** *20* (3), 273-297.

92. Boser, B. E.; Guyon, I. M.; Vapnik, V. N., A training algorithm for optimal margin classifiers. In *Proceedings of the fifth annual workshop on Computational learning theory*, ACM: Pittsburgh, Pennsylvania, USA, 1992; pp 144-152.

93. Vapnik, V. N., *The Nature of Statistical Learning Theory*. Springer: New York, 1995; p 188.

94. Burges, C. J. C., A tutorial on Support Vector Machines for pattern recognition. *Data Min Knowl Disc* **1998,** *2* (2), 121-167.

95. Allwein, E. L.; Schapire, R. E.; Singer, Y., Reducing multiclass to binary: A unifying approach for margin classifiers. *J Mach Learn Res* **2001,** *1* (2), 113-141.

96. Furnkranz, J., Round robin classification. *J Mach Learn Res* **2002,** *2* (4), 721-747.

97. Escalera, S.; Pujol, O.; Radeva, P., On the Decoding Process in Ternary Error-Correcting Output Codes. *Ieee T Pattern Anal* **2010,** *32* (1), 120-134.

98. Popp, J.; Harz, A.; Rosch, P., Vibrational Spectroscopy-A Powerful Tool for the Rapid Identification of Microbial Cells at the Single-Cell Level. *Cytom Part A* **2009,** *75A* (2), 104-113.

99. Kusic, D.; Kampe, B.; Rosch, P.; Popp, J., Identification of water pathogens by Raman microspectroscopy. *Water Research* **2014,** *48*, 179-189.

100. Yogesha, M.; Chawla, K.; Bankapur, A.; Acharya, M.; D'Souza, J. S.; Chidangil, S., A micro-Raman and chemometric study of urinary tract infection-causing bacterial pathogens in mixed cultures. *Analytical and Bioanalytical Chemistry* **2019,** *411* (14), 3165-3177.

101. Juan, A. d.; Piqueras, S.; Maeder, M.; Hancewicz, T.; Duponchel, L.; Tauler, R., Chemometric Tools for Image Analysis. In *Infrared and Raman Spectroscopic Imaging*, Wiley-VCH Verlag GmbH & Co. KGaA: 2014; pp 57-110.

102. Wierzchoń, S. K., Mieczyslaw, *Modern Algorithms of Cluster Analysis*. Springer: Cham, 2018; Vol. 34.

103. De Gelder, J.; De Gussem, K.; Vandenabeele, P.; Moens, L., Reference database of Raman spectra of biological molecules. *Journal of Raman Spectroscopy* **2007,** *38* (9), 1133-1147.

104. Delgado, F. F.; Cermak, N.; Hecht, V. C.; Son, S.; Li, Y. Z.; Knudsen, S. M.; Olcum, S.; Higgins, J. M.; Chen, J. Z.; Grover, W. H.; Manalis, S. R., Intracellular Water Exchange for Measuring the Dry Mass, Water Mass and Changes in Chemical Composition of Living Cells. *Plos One* **2013,** *8* (7).

105. Neugebauer, U.; Rosch, P.; Schmitt, M.; Popp, J.; Julien, C.; Rasmussen, A.; Budich, C.; Deckert, V., On the way to nanometer-sized information of the bacterial surface by tip-enhanced Raman spectroscopy. *Chemphyschem* **2006,** *7* (7), 1428-1430.

106. Neugebauer, U.; Schmid, U.; Baumann, K.; Ziebuhr, W.; Kozitskaya, S.; Deckert, V.; Schmitt, M.; Popp, J., Towards a detailed understanding of bacterial metabolism - Spectroscopic characterization of Staphylococcus epidermidis. *Chemphyschem* **2007,** *8* (1), 124-137.

107. Neugebauer, U.; Kloß, S.; Schröder, U.-C.; Rösch, P.; Popp, J., Fast and Selective Against Bacteria. *Optik & Photonik* **2013,** *8* (4), 36-39.

108. Schröder, U.-C.; Bokeloh, F.; O'Sullivan, M.; Glaser, U.; Wolf, K.; Pfister, W.; Popp, J.; Ducrée, J.; Neugebauer, U., Rapid, culture-independent, optical diagnostics of centrifugally captured bacteria from urine samples. *Biomicrofluidics* **2015,** *9* (4), 044118.

109. Berry, D.; Loy, A., Stable-Isotope Probing of Human and Animal Microbiome Function. *Trends in Microbiology* **2018,** *26* (12), 999-1007.

110. Escoriza, M. F.; Vanbriesen, J. M.; Stewart, S.; Maier, J., Studying bacterial metabolic states using Raman spectroscopy. *Appl Spectrosc* **2006,** *60* (9), 971-976.

111. Hlaing, M. M.; Dunn, M.; Stoddart, P. R.; McArthur, S. L., Raman spectroscopic identification of single bacterial cells at different stages of their lifecycle. *Vibrational Spectroscopy* **2016,** *86*, 81-89.

112. Strola, S. A.; Marcoux, P. R.; Schultz, E.; Perenon, R.; Simon, A. C.; Espagnon, I.; Allier, C. P.; Dinten, J. M., Differentiating the growth phases of single bacteria using Raman spectroscopy. *Biomedical Vibrational Spectroscopy Vi: Advances in Research and Industry* **2014,** *8939*.

113. Stöckel, S.; Kirchhoff, J.; Neugebauer, U.; Rösch, P.; Popp, J., The application of Raman spectroscopy for the detection and identification of microorganisms. *Journal of Raman Spectroscopy* **2016,** *47* (1), 89-109.

114. Wainwright, M., Moulds in ancient and more recent medicine. *Mycologist* **1989,** *3* (1), 21-23.

115. Nelson, M. L.; Dinardo, A.; Hochberg, J.; Armelagos, G. J., Brief Communication: Mass Spectroscopic Characterization of Tetracycline in the Skeletal Remains of an Ancient Population From Sudanese Nubia 350-550 CE. *Am J Phys Anthropol* **2010,** *143* (1), 151-154.

116. Gould, K., Antibiotics: from prehistory to the present day. *J Antimicrob Chemoth* **2016,** *71* (3), 572-575.

117. Fleming, A., On the Antibacterial Action of Cultures of a Penicillium, with Special Reference to their Use in the Isolation of B. influenzæ. *Br J Exp Pathol* **1929,** *10* (3), 226-236.

118. Högberg, L. D.; Heddini, A.; Cars, O., The global need for effective antibiotics: challenges and recent advances. *Trends in Pharmacological Sciences* **2010,** *31* (11), 509-515.

119. Parker, N.; Schneegurt, M.; Thi Tu, A.-H.; Lister, P.; Forster, B. M., *Microbiology*. OpenStax: Houston, Texas, 2016.

120. Allen, R. J.; Waclaw, B., Bacterial growth: a statistical physicist's guide. *Reports on Progress in Physics* **2019,** *82* (1).

121. Baietto, L.; Corcione, S.; Pacini, G.; Di Perri, G.; D'Avolio, A.; De Rosa, F. G., A 30-years Review on Pharmacokinetics of Antibiotics: Is the Right Time for Pharmacogenetics? *Curr Drug Metab* **2014,** *15* (6), 581-598.

122. Tortora, G. J.; Funke, B. R.; Case, C. L., *Microbiology*. 10 ed.; Pearson Education Inc.: San Francisco, CA, 2010.

123. Franklin, T. J.; Snow, G. A., *Biochemistry and Molecular Biology of Antimicrobial Drug Action*. 6 ed.; Springer US: 2005; p 182.

124. Mendez, A. S. L.; Dalomo, J.; Steppe, M.; Schapoval, E. E. S., Stability and degradation kinetics of meropenem in powder for injection and reconstituted sample. *Journal of Pharmaceutical and Biomedical Analysis* **2006,** *41* (4), 1363-1366.

125. Blumer, J. L., Meropenem: Evaluation of a new generation carbapenem. *Int J Antimicrob Ag* **1997,** *8* (2), 73-92.

126. Bradley, J. S., Meropenem: A new, extremely broad spectrum beta-lactam antibiotic for serious infections in pediatrics. *Pediatr Infect Dis J* **1997,** *16* (3), 263-268.

127. Yao, Z. Z.; Kahne, D.; Kishony, R., Distinct Single-Cell Morphological Dynamics under Beta-Lactam Antibiotics. *Mol Cell* **2012,** *48* (5), 705-712.

128. Cohen, N. R.; Lobritz, M. A.; Collins, J. J., Microbial Persistence and the Road to Drug Resistance. *Cell Host Microbe* **2013,** *13* (6), 632-642.

129. Andersson, D. I.; Nicoloff, H.; Hjort, K., Mechanisms and clinical relevance of bacterial heteroresistance. *Nature Reviews Microbiology* **2019,** *17* (8), 479-496.

130. Balaban, N. Q.; Helaine, S.; Lewis, K.; Ackermann, M.; Aldridge, B.; Andersson, D. I.; Brynildsen, M. P.; Bumann, D.; Camilli, A.; Collins, J. J.; Dehio, C.; Fortune, S.; Ghigo, J. M.; Hardt, W. D.; Harms, A.; Heinemann, M.; Hung, D. T.; Jenal, U.; Levin, B. R.; Michiels, J.; Storz, G.; Tan, M. W.; Tenson, T.; Van Melderen, L.; Zinkernagel, A., Definitions and guidelines for research on antibiotic persistence. *Nature Reviews Microbiology* **2019,** *17* (7), 441-448.

131. Band, V. I.; Satola, S. W.; Burd, E. M.; Farley, M. M.; Jacob, J. T.; Weiss, D. S., Carbapenem-Resistant Klebsiella pneumoniae Exhibiting Clinically Undetected Colistin Heteroresistance Leads to Treatment Failure in a Murine Model of Infection. *Mbio* **2018,** *9* (2).

132. Falagas, M. E.; Makris, G. C.; Dimopoulos, G.; Matthaiou, D. K., Heteroresistance: a concern of increasing clinical significance? *Clin Microbiol Infec* **2008,** *14* (2), 101-104.

133. Khosrovaneh, A.; Riederer, K.; Saeed, S.; Tabriz, M. S.; Shah, A. R.; Hanna, M. M.; Sharma, M.; Johnson, L. B.; Fakih, M. G.; Khatib, R., Frequency of reduced vancomycin susceptibility and heterogeneous subpopulation in persistent or recurrent methicillin-resistant Staphylococcus aureus bacteremia. *Clin Infect Dis* **2004,** *38* (9), 1328-1330.

134. Meletis, G.; Tzampaz, E.; Sianou, E.; Tzavaras, I.; Sofianou, D., Colistin heteroresistance in carbapenemase-producing Klebsiella pneumoniae. *J Antimicrob Chemoth* **2011,** *66* (4), 946-947.

135. Saravolatz, S. N.; Martin, H.; Pawlak, J.; Johnson, L. B.; Saravolatz, L. D., Ceftaroline-Heteroresistant Staphylococcus aureus. *Antimicrob Agents Ch* **2014,** *58* (6), 3133-3136.

136. Adams-Sapper, S.; Nolen, S.; Donzelli, G. F.; Lal, M.; Chen, K.; da Silva, L. H. J.; Moreira, B. M.; Rile, L. W., Rapid Induction of High-Level Carbapenem Resistance in Heteroresistant KPC-Producing Klebsiella pneumoniae. *Antimicrob Agents Ch* **2015,** *59* (6), 3281-3289.

137. Nicoloff, H.; Hjort, K.; Levin, B. R.; Andersson, D. I., The high prevalence of antibiotic heteroresistance in pathogenic bacteria is mainly caused by gene amplification. *Nat Microbiol* **2019,** *4* (3), 504-514.

138. Band, V. I.; Weiss, D. S., Heteroresistance: A cause of unexplained antibiotic treatment failure? *PLoS Pathog* **2019,** *15* (6), e1007726.

139. Breakpoint tables for interpretation of MICs and zone diameters. Breakpoint tables for interpretation of MICs and zone diameters ed.; The European Committee on Antimicrobial Susceptibility Testing: 2019; Vol. 2019.

140. ESCMID MIC determination of non-fastidious and fastidious organisms. http://www.eucast.org/ast_of_bacteria/mic_determination/?no_cache=1 (accessed 2019/10/15).

141. EUCAST *Determination of minimum inhibitory concentrations (MICs) of antibacterial agents by broth dilution*; 1469-0691; Wiley Online Library: 2003; pp ix-xv.

142. Boehme, M. S.; Somsel, P. A.; Downes, F. P., Systematic Review of Antibiograms: A National Laboratory System Approach for Improving Antimicrobial Susceptibility Testing Practices in Michigan. *Public Health Rep* **2010,** *125*, 63-72.

143. EUCAST Setting breakpoints. https://www.eucast.org/clinical_breakpoints_and_dosing/eucast_setting_breakpoints/ (accessed 1/5/2020).

144. Bauer, A. W.; Kirby, W. M. M.; Sherris, J. C.; Turck, M., Antibiotic Susceptibility Testing by a Standardized Single Disk Method. *Am J Clin Pathol* **1966,** *45* (4), 493-&.

145. Behera, B.; Vishnu, G. K. A.; Chatterjee, S.; Sitaramgupta, V. V. S. N.; Sreekumar, N.; Nagabhushan, A.; Rajendran, N.; Prathik, B. H.; Pandya, H. J., Emerging technologies for antibiotic susceptibility testing. *Biosensors and Bioelectronics* **2019,** *142*.

146. EUCAST Antimicrobial wild type distributions of microorganisms. https://mic.eucast.org/Eucast2/regShow.jsp?Id=1529 (accessed 08/05/2020).

147. Eigner, U.; Schmid, A.; Wild, U.; Bertsch, D.; Fahr, A.-M., Analysis of the Comparative Workflow and Performance Characteristics of the VITEK 2 and Phoenix Systems. *J Clin Microbiol* **2005,** *43* (8), 3829-3834.

148. Junkins, A. D.; Arbefeville, S. S.; Howard, W. J.; Richter, S. S., Comparison of BD Phoenix AP Workflow with Vitek 2. *J Clin Microbiol* **2010,** *48* (5), 1929-1931.

149. Lo-Ten-Foe, J. R.; de Smet, A. M. G. A.; Diederen, B. M. W.; Kluytmans, J. A. J. W.; van Keulen, P. H. J., Comparative evaluation of the VITEK 2, disk diffusion, etest, broth microdilution, and agar dilution susceptibility testing methods for colistin in clinical isolates, including heteroresistant Enterobacter cloacae and Acinetobacter baumannii strains. *Antimicrob Agents Ch* **2007,** *51* (10), 3726-3730.

150. Woodford, N.; Eastaway, A. T.; Ford, M.; Leanord, A.; Keane, C.; Quayle, R. M.; Steer, J. A.; Zhang, J. C.; Livermore, D. M., Comparison of BD Phoenix, Vitek 2, and MicroScan Automated Systems for Detection and Inference of Mechanisms Responsible for Carbapenem Resistance in Enterobacteriaceae. *J Clin Microbiol* **2010,** *48* (8), 2999-3002.

151. Puttaswamy, S.; Kishore Gupta, S.; Regunath, H.; Smith, L.; Sengupta, S., A Comprehensive Review of the Present and Future Antibiotic Susceptibility Testing (AST) Systems. **2018,** *09*.

152. Tannert, A.; Grohs, R.; Popp, J.; Neugebauer, U., Phenotypic antibiotic susceptibility testing of pathogenic bacteria using photonic readout methods: recent achievements and impact. *Appl Microbiol Biot* **2019,** *103* (2), 549-566.

153. van Belkum, A.; Bachmann, T. T.; Ludke, G.; Lisby, J. G.; Kahlmeter, G.; Mohess, A.; Becker, K.; Hays, J. P.; Woodford, N.; Mitsakakis, K.; Moran-Gilad, J.; Vila, J.; Peter, H.; Rex, J. H.; Dunne, W. M.; Grp, J. A.-R. W., Developmental roadmap for antimicrobial susceptibility testing systems. *Nature Reviews Microbiology* **2019,** *17* (1), 51-62.

154. Lopez-Diez, E. C.; Winder, C. L.; Ashton, L.; Currie, F.; Goodacre, R., Monitoring the mode of action of antibiotics using Raman spectroscopy: Investigating subinhibitory effects of amikacin on Pseudomonas aeruginosa. *Analytical Chemistry* **2005,** *77* (9), 2901-2906.

155. Liu, T.-T.; Lin, Y.-H.; Hung, C.-S.; Liu, T.-J.; Chen, Y.; Huang, Y.-C.; Tsai, T.-H.; Wang, H.-H.; Wang, D.-W.; Wang, J.-K.; Wang, Y.-L.; Lin, C.-H., A High Speed Detection Platform Based on Surface-Enhanced Raman Scattering for Monitoring Antibiotic-Induced Chemical Changes in Bacteria Cell Wall. *Plos One* **2009,** *4* (5), e5470.

156. Walter, A.; Reinicke, M.; Bocklitz, T.; Schumacher, W.; Rosch, P.; Kothe, E.; Popp, J., Raman spectroscopic detection of physiology changes in plasmid-bearing *Escherichia coli* with and without antibiotic treatment. *Analytical and Bioanalytical Chemistry* **2011,** *400* (9), 2763-2773.

157. Munchberg, U.; Rosch, P.; Bauer, M.; Popp, J., Raman spectroscopic identification of single bacterial cells under antibiotic influence. *Analytical and Bioanalytical Chemistry* **2014,** *406* (13), 3041-3050.

158. Schroder, U. C.; Beleites, C.; Assmann, C.; Glaser, U.; Hubner, U.; Pfister, W.; Fritzsche, W.; Popp, J.; Neugebauer, U., Detection of vancomycin resistances in enterococci within 3 1/2 hours. *Sci Rep-Uk* **2015,** *5*.

159. Assmann, C.; Kirchhoff, J.; Beleites, C.; Hey, J.; Kostudis, S.; Pfister, W.; Schlattmann, P.; Popp, J.; Neugebauer, U., Identification of vancomycin interaction with Enterococcus faecalis within 30 min of interaction time using Raman spectroscopy. *Analytical and Bioanalytical Chemistry* **2015,** *407* (27), 8343-8352.

160. Liu, C. Y.; Han, Y. Y.; Shih, P. H.; Lian, W. N.; Wang, H. H.; Lin, C. H.; Hsueh, P. R.; Wang, J. K.; Wang, Y. L., Rapid bacterial antibiotic susceptibility test based on simple surface-enhanced Raman spectroscopic biomarkers. *Sci Rep* **2016,** *6*, 23375.

161. Premasiri, W. R.; Chen, Y.; Williamson, P. M.; Bandarage, D. C.; Pyles, C.; Ziegler, L. D., Rapid urinary tract infection diagnostics by surface-enhanced Raman spectroscopy (SERS): identification and antibiotic susceptibilities. *Analytical and Bioanalytical Chemistry* **2017,** *409* (11), 3043-3054.

162. Tao, Y.; Wang, Y.; Huang, S.; Zhu, P.; Huang, W. E.; Ling, J.; Xu, J., Metabolic-Activity-Based Assessment of Antimicrobial Effects by D2O-Labeled Single-Cell Raman Microspectroscopy. *Analytical Chemistry* **2017,** *89* (7), 4108-4115.

163. Dekter, H. E.; Orelio, C. C.; Morsink, M. C.; Tektas, S.; Vis, B.; te Witt, R.; van Leeuwen, W. B., Antimicrobial susceptibility testing of Gram-positive and -negative bacterial isolates directly from spiked blood culture media with Raman spectroscopy. *Eur J Clin Microbiol* **2017,** *36* (1), 81-89.

164. Xuan Nguyen, N. T.; Sarter, S.; Hai Nguyen, N.; Daniel, P., Detection of molecular changes induced by antibiotics in Escherichia coli using vibrational spectroscopy. *Spectrochimica Acta Part A: Molecular and Biomolecular Spectroscopy* **2017,** *183* (Supplement C), 395-401.

165. Song, Y.; Cui, L.; López, J. Á. S.; Xu, J.; Zhu, Y.-G.; Thompson, I. P.; Huang, W. E., Raman-Deuterium Isotope Probing for in-situ identification of antimicrobial resistant bacteria in Thames River. *Sci Rep-Uk* **2017,** *7* (1), 16648.

166. Schröder, U.-C.; Kirchhoff, J.; Hübner, U.; Mayer, G.; Glaser, U.; Henkel, T.; Pfister, W.; Fritzsche, W.; Popp, J.; Neugebauer, U., On-chip spectroscopic assessment of microbial susceptibility to antibiotics within 3.5 hours. *Journal of Biophotonics* **2017,** *10* (11), 1547-1557.

167. Hong, W.; Karanja, C. W.; Abutaleb, N. S.; Younis, W.; Zhang, X.; Seleem, M. N.; Cheng, J.-X., Antibiotic Susceptibility Determination within One Cell Cycle at Single-Bacterium Level by Stimulated Raman Metabolic Imaging. *Analytical Chemistry* **2018,** *90* (6), 3737-3743.

168. Novelli-Rousseau, A.; Espagnon, I.; Filiputti, D.; Gal, O.; Douet, A.; Mallard, F.; Josso, Q., Culture-free Antibiotic-susceptibility Determination From Single-bacterium Raman Spectra. *Sci Rep-Uk* **2018,** *8*.

169. Yang, K.; Li, H. Z.; Zhu, X.; Su, J. Q.; Ren, B.; Zhu, Y. G.; Cui, L., Rapid Antibiotic Susceptibility Testing of Pathogenic Bacteria Using Heavy-Water-Labeled

Single-Cell Raman Spectroscopy in Clinical Samples. *Analytical Chemistry* **2019,** *91* (9), 6296-6303.

170. Stosch, R.; Henrion, A.; Schiel, D.; Guttler, B., Surface enhanced Raman scattering based approach for quantitative determination of creatinine in human serum. *Analytical Chemistry* **2005,** *77* (22), 7386-7392.

171. Huang, Y. S.; Nakatsuka, T.; Hamaguchi, H. O., Behaviors of the "Raman Spectroscopic Signature of Life" in single living fission yeast cells under different nutrient, stress, and atmospheric conditions. *Appl Spectrosc* **2007,** *61* (12), 1290-1294.

172. Wagner, M.; Whiteley, A. S., Single cell stable isotope probing with FISH-Raman spectroscopy for deciphering the ecophysiology of uncultured bacteria. *Febs J* **2007,** *274*, 13-13.

173. Xu, J.; Zhu, D.; Ibrahim, A. D.; Allen, C. C. R.; Gibson, C. M.; Fowler, P. W.; Song, Y.; Huang, W. E., Raman Deuterium Isotope Probing Reveals Microbial Metabolism at the Single-Cell Level. *Analytical Chemistry* **2017,** *89* (24), 13305-13312.

174. Berry, D.; Mader, E.; Lee, T. K.; Woebken, D.; Wang, Y.; Zhu, D.; Palatinszky, M.; Schintlmeister, A.; Schmid, M. C.; Hanson, B. T.; Shterzer, N.; Mizrahi, I.; Rauch, I.; Decker, T.; Bocklitz, T.; Popp, J.; Gibson, C. M.; Fowler, P. W.; Huang, W. E.; Wagner, M., Tracking heavy water (D2O) incorporation for identifying and sorting active microbial cells. *Proceedings of the National Academy of Sciences* **2015,** *112* (2), E194-E203.

175. Lester, W.; Sun, S. H.; Seber, A., Observations on the Influence of Deuterium on Bacterial Growth. *Annals of the New York Academy of Sciences* **1960,** *84* (16), 667-677.

176. Lovett, S., Effect of Deuterium on Starving Bacteria. *Nature* **1964,** *203*, 429.

177. Feng, J. J.; Yao, W. R.; Guo, Y. H.; Cheng, Y. L.; Qian, H.; Xie, Y., Incorporation of Heavy Water for Rapid Detection of Salmonella typhimurium by Raman Microspectroscopy. *Food Analytical Methods* **2018,** *11* (12), 3551-3557.

178. Olaniyi, O. O.; Yang, K.; Zhu, Y. G.; Cui, L., Heavy water-labeled Raman spectroscopy reveals carboxymethylcellulose-degrading bacteria and degradation activity at the single-cell level. *Appl Microbiol Biot* **2019,** *103* (3), 1455-1464.

179. Kline, K. A.; Lewis, A. L., Gram-Positive Uropathogens, Polymicrobial Urinary Tract Infection, and the Emerging Microbiota of the Urinary Tract. *Microbiol Spectr* **2016,** *4* (2).

180. Xie, X.; Zubarev, R. A., Effects of Low-Level Deuterium Enrichment on Bacterial Growth. *Plos One* **2014,** *9* (7), e102071.

181. Xie, X.; Zubarev, R. A., Isotopic Resonance Hypothesis: Experimental Verification by Escherichia coli Growth Measurements. *Sci Rep-Uk* **2015,** *5*, 9215.

182. Kushner, D. J.; Baker, A.; Dunstall, T. G., Pharmacological uses and perspectives of heavy water and deuterated compounds. *Can J Physiol Pharm* **1999,** *77* (2), 79-88.

183. Yakes, B. J.; Lipert, R. J.; Bannantine, J. P.; Porter, M. D., Detection of Mycobacterium avium subsp paratuberculosis by a sonicate immunoassay based on surface-enhanced Raman scattering. *Clin Vaccine Immunol* **2008,** *15* (2), 227-234.

184. Silva, L. B.; Veigas, B.; Doria, G.; Costa, P.; Inacio, J.; Martins, R.; Fortunato, E.; Baptista, P. V., Portable optoelectronic biosensing platform for identification of mycobacteria from the Mycobacterium tuberculosis complex. *Biosensors and Bioelectronics* **2011,** *26* (5), 2012-2017.

185. Tang, M. J.; McEwen, G. D.; Wu, Y. Z.; Miller, C. D.; Zhou, A. H., Characterization and analysis of mycobacteria and Gram-negative bacteria and co-culture mixtures by Raman microspectroscopy, FTIR, and atomic force microscopy. *Analytical and Bioanalytical Chemistry* **2013,** *405* (5), 1577-1591.

186. Rivera-Betancourt, O. E.; Karls, R.; Grosse-Siestrup, B.; Helms, S.; Quinn, F.; Dluhy, R. A., Identification of mycobacteria based on spectroscopic analyses of mycolic acid profiles. *Analyst* **2013,** *138* (22), 6774-6785.

187. Sathyavathi, R.; Dingari, N. C.; Barman, I.; Prasad, P. S. R.; Prabhakar, S.; Rao, D. N.; Dasari, R. R.; Undamatla, J., Raman spectroscopy provides a powerful, rapid diagnostic tool for the detection of tuberculous meningitis in ex vivo cerebrospinal fluid samples. *Journal of Biophotonics* **2013,** *6* (8), 567-572.

188. Stöckel, S.; Stanca, A. S.; Helbig, J.; Rösch, P.; Popp, J., Raman spectroscopic monitoring of the growth of pigmented and non-pigmented mycobacteria. *Analytical and Bioanalytical Chemistry* **2015,** *407* (29), 8919-8923.

189. Kumar, S.; Matange, N.; Umapathy, S.; Visweswariah, S. S., Linking carbon metabolism to carotenoid production in mycobacteria using Raman spectroscopy. *FEMS Microbiology Letters* **2015,** *362* (3), 1-6.

190. Hanson, C.; Bishop, M. M.; Barney, J. T.; Vargis, E., Effect of growth media and phase on Raman spectra and discrimination of mycobacteria. *Journal of Biophotonics* **2019**.

191. Baranowski, C.; Welsh, M. A.; Sham, L. T.; Eskandarian, H. A.; Lim, H. C.; Kieser, K. J.; Wagner, J. C.; McKinney, J. D.; Fantner, G. E.; Ioerger, T. R.; Walker, S.; Bernhardt, T. G.; Rubin, E. J.; Rego, E. H., Maturing Mycobacterium smegmatis peptidoglycan requires non-canonical crosslinks to maintain shape. *Elife* **2018,** *7*.

192. Dhillon, J.; Fourie, P. B.; Mitchison, D. A., Persister populations of Mycobacterium tuberculosis in sputum that grow in liquid but not on solid culture media. *J Antimicrob Chemoth* **2014,** *69* (2), 437-440.

193. Nikitushkin, V. D.; Shleeva, M. O.; Zinin, A. I.; Trutneva, K. A.; Ostrovsky, D. N.; Kaprelyants, A. S., The main pigment of the dormant Mycobacterium smegmatis is porphyrin. *Fems Microbiol Lett* **2016,** *363* (19), fnw206-fnw206.

194. Cohn, D. L.; Catlin, B. J.; Peterson, K. L.; Judson, F. N.; Sbarbaro, J. A., A 62-Dose, 6-Month Therapy for Pulmonary and Extrapulmonary Tuberculosis: A Twice-Weekly, Directly Observed, and Cost-Effective Regimen. *Annals of Internal Medicine* **1990,** *112* (6), 407-415.

195. Grosset, J. H., Present Status of Chemotherapy for Tuberculosis. *Reviews of Infectious Diseases* **1989,** *11* (Supplement_2), S347-S352.

196. Byrne, S. T.; Gu, P. H.; Zhou, H. B.; Denkin, S. M.; Chong, C.; Sullivan, D.; Liu, J. O.; Zhang, Y., Pyrrolidine dithiocarbamate and diethyldithiocarbamate are active against growing and nongrowing persister Mycobacterium tuberculosis. *Antimicrob Agents Ch* **2007,** *51* (12), 4495-4497.

197. Ueno, H.; Kato, Y.; Tabata, K. V.; Noji, H., Revealing the Metabolic Activity of Persisters in Mycobacteria by Single-Cell D2O Raman Imaging Spectroscopy. *Analytical Chemistry* **2019,** *91* (23), 15171-15178.

198. Neumann, A. C.; Bauer, D.; Hoelscher, M.; Haisch, C.; Wieser, A., Identifying Dormant Growth State of Mycobacteria by Orthogonal Analytical Approaches on a Single Cell and Ensemble Basis. *Analytical Chemistry* **2019,** *91* (1), 881-887.

199. Hammond, R. J.; Baron, V. O.; Oravcova, K.; Lipworth, S.; Gillespie, S. H., Phenotypic resistance in mycobacteria: is it because I am old or fat that I resist you? *The Journal of antimicrobial chemotherapy* **2015,** *70* (10), 2823-7.

200. Standardization, D. G. I. f., Clinical laboratory testing and in vitro diagnostic test systems - Susceptibility testing of infectious agents and evaluation of performance of antimicrobial susceptibility test devices - Part 1: Broth micro-dilution reference method for testing the in vitro activity of antimicrobial agents against rapidly growing aerobic bacteria involved in infectious diseases (ISO/DIS 20776-1:2018); German and English version prEN ISO 20776-1:2018. Beuth Verlag GmbH: Germany, 2018.

201. ImageJ - Fiji. https://imagej.net/Fiji (accessed 04/12/2020).

202. Bhattacharya, S., Early diagnosis of resistant pathogens How can it improve antimicrobial treatment? *Virulence* **2013,** *4* (2), 172-184.

203. Magistro, G.; Gratzke, C.; Stief, C. G.; Weidner, W.; Wagenlehner, F., Management of multiresistant pathogens in urology. *Urologe* **2015,** *54* (2), 267-274.

204. Tandogdu, Z.; Bartoletti, R.; Cai, T.; Cek, M.; Grabe, M.; Kulchavenya, E.; Koves, B.; Menon, V.; Naber, K.; Perepanova, T.; Tenke, P.; Wullt, B.; Johansen, T. E.; Wagenlehner, F., Antimicrobial resistance in urosepsis: outcomes from the multinational, multicenter global prevalence of infections in urology (GPIU) study 2003-2013. *World J Urol* **2016,** *34* (8), 1193-200.

205. Otsuka, Y., Potent Antibiotics Active against Multidrug-Resistant Gram-Negative Bacteria. *Chem Pharm Bull* **2020,** *68* (3), 182-190.

206. Kirchhoff, J.; Glaser, U.; Bohnert, J. A.; Pletz, M. W.; Popp, J.; Neugebauer, U., Simple Ciprofloxacin Resistance Test and Determination of Minimal Inhibitory Concentration within 2 h Using Raman Spectroscopy. *Analytical Chemistry* **2018,** *90* (3), 1811-1818.

207. Baltekin, O.; Boucharin, A.; Tano, E.; Andersson, D. I.; Elf, J., Antibiotic susceptibility testing in less than 30 min using direct single-cell imaging. *P Natl Acad Sci USA* **2017,** *114* (34), 9170-9175.

208. Bhosale, P.; Teredesai, P. V.; Lihong, J.; Ermakov, I. V.; Gellermann, W.; Bernstein, P. S., Production of Deuterated Zeaxanthin by Flavobacterium Multivorum and its Detection by Resonance Raman and Mass Spectrometric Methods. *Biotechnol Lett* **2005,** *27* (21), 1719-1723.

209. Paliy, O.; Bloor, D.; Brockwell, D.; Gilbert, P.; Barber, J., Improved methods of cultivation and production of deuteriated proteins from E. coli strains grown on fully deuteriated minimal medium. *J Appl Microbiol* **2003,** *94* (4), 580-586.

210. Sezonov, G.; Joseleau-Petit, D.; D'Ari, R., Escherichia coli physiology in Luria-Bertani broth. *J Bacteriol* **2007,** *189* (23), 8746-8749.

211. Vu, J.; Carvalho, J., Enterococcus: review of its physiology, pathogenesis, diseases and the challenges it poses for clinical microbiology. *Frontiers in Biology* **2011,** *6* (5), 357.

212. Holt, J. F.; Kiedrowski, M. R.; Frank, K. L.; Du, J.; Guan, C. H.; Broderick, N. A.; Dunny, G. M.; Handelsman, J., Enterococcus faecalis 6-Phosphogluconolactonase Is Required for Both Commensal and Pathogenic Interactions with Manduca sexta. *Infection and Immunity* **2015,** *83* (1), 396-404.

213. Ren, Y.; Ji, Y. T.; Teng, L.; Zhang, H. P., Using Raman spectroscopy and chemometrics to identify the growth phase of Lactobacillus casei Zhang during batch culture at the single-cell level. *Microb Cell Fact* **2017,** *16*.

214. Wang, P.; Robert, L.; Pelletier, J.; Dang, W. L.; Taddei, F.; Wright, A.; Jun, S., Robust Growth of Escherichia coli. *Curr Biol* **2010,** *20* (12), 1099-1103.

215. Reshes, G.; Vanounou, S.; Fishov, I.; Feingold, M., Timing the start of division in E-coli: a single-cell study. *Phys Biol* **2008,** *5* (4).

216. Monod, J., The Growth of Bacterial Cultures. *Annual Review of Microbiology* **1949,** *3*, 371-394.

217. Llorens, J. M. N.; Tormo, A.; Martinez-Garcia, E., Stationary phase in gram-negative bacteria. *Fems Microbiology Reviews* **2010,** *34* (4), 476-495.

218. Miksch, G.; Dobrowolski, P., Growth Phase-Dependent Induction of Stationary-Phase Promoters of Escherichia-Coli in Different Gram-Negative Bacteria. *J Bacteriol* **1995,** *177* (18), 5374-5378.

219. Basul, A.; Parentez, A. C.; Bryant, Z., Structural Dynamics and Mechanochemical Coupling in DNA Gyrase. *J Mol Biol* **2016,** *428* (9), 1833-1845.

220. Sully, E. K.; Geller, B. L.; Li, L.; Moody, C. M.; Bailey, S. M.; Moore, A. L.; Wong, M.; Nordmann, P.; Daly, S. M.; Sturge, C. R.; Greenberg, D. E., Peptide-conjugated phosphorodiamidate morpholino oligomer (PPMO) restores carbapenem susceptibility to NDM-1-positive pathogens in vitro and in vivo. *The Journal of antimicrobial chemotherapy* **2017,** *72* (3), 782-790.

221. Nordmann, P.; Poirel, L.; Carrer, A.; Toleman, M. A.; Walsh, T. R., How To Detect NDM-1 Producers. *J Clin Microbiol* **2011,** *49* (2), 718-721.

222. Yong, D.; Toleman, M. A.; Giske, C. G.; Cho, H. S.; Sundman, K.; Lee, K.; Walsh, T. R., Characterization of a New Metallo-beta-Lactamase Gene, bla(NDM-1), and

a Novel Erythromycin Esterase Gene Carried on a Unique Genetic Structure in Klebsiella pneumoniae Sequence Type 14 from India. *Antimicrob Agents Ch* **2009,** *53* (12), 5046-5054.

223. Fauvart, M.; De Grootet, V. N.; Michiels, J., Role of persister cells in chronic infections: clinical relevance and perspectives on anti-persister therapies. *J Med Microbiol* **2011,** *60* (6), 699-709.

224. Cavalie, L.; Mantion, B.; Fayet, O.; Prere, M. F., bla(NDM-1)-positive Citrobacter sedlakii: emergence after horizontal gene transfer from Klebsiella pneumoniae in the human intestinal tract. *Int J Antimicrob Ag* **2016,** *47* (5), 411-413.

225. Warnes, S. L.; Highmore, C. J.; Keevil, C. W., Horizontal Transfer of Antibiotic Resistance Genes on Abiotic Touch Surfaces: Implications for Public Health. *Mbio* **2012,** *3* (6).

226. Hastie, T. T., Robert; Friedman, Jerome, *The Elements of Statistical Learning: Data Mining, Inference, and Prediction*. 2 ed.; Springer: New York, NY, 2009.

227. Strola, S. A.; Baritaux, J. C.; Schultz, E.; Simon, A. C.; Allier, C.; Espagnon, I.; Jary, D.; Dinten, J. M., Single bacteria identification by Raman spectroscopy. *Journal of Biomedical Optics* **2014,** *19* (11).

228. Kloss, S.; Kampe, B.; Sachse, S.; Rosch, P.; Straube, E.; Pfister, W.; Kiehntopf, M.; Popp, J., Culture Independent Raman Spectroscopic Identification of Urinary Tract Infection Pathogens: A Proof of Principle Study. *Analytical Chemistry* **2013,** *85* (20), 9610-9616.

229. Kudykina, Y. K.; Shleeva, M. O.; Artsabanov, V. Y.; Suzina, N. E.; Kaprelyants, A. S., Generation of dormant forms by Mycobacterium smegmatis in the poststationary phase during gradual acidification of the medium. *Microbiology* **2011,** *80* (5), 638-649.

230. Shleeva, M.; Goncharenko, A.; Kudykina, Y.; Young, D.; Young, M., Cyclic Amp-Dependent Resuscitation of Dormant Mycobacteria by Exogenous Free Fatty Acids (vol 8, e82914, 2013). *Plos One* **2014,** *9* (5).

231. Hobro, A. J.; Smith, N. I., An evaluation of fixation methods: Spatial and compositional cellular changes observed by Raman imaging. *Vibrational Spectroscopy* **2017,** *91*, 31-45.

232. Wagner, M., Single-Cell Ecophysiology of Microbes as Revealed by Raman Microspectroscopy or Secondary Ion Mass Spectrometry Imaging. *Annual Review of Microbiology* **2009,** *63* (1), 411-429.

233. Claudino, M. J. C.; Soares, D.; Van Keulen, F.; Marques, M. P. C.; Cabral, J. M. S.; Fernandes, P., Immobilization of mycobacterial cells onto silicone – Assessing the feasibility of the immobilized biocatalyst in the production of androstenedione from sitosterol. *Bioresource Technol* **2008,** *99* (7), 2304-2311.

234. Lee, K. S.; Palatinszky, M.; Pereira, F. C.; Nguyen, J.; Fernandez, V. I.; Mueller, A. J.; Menolascina, F.; Daims, H.; Berry, D.; Wagner, M.; Stocker, R., An automated Raman-based platform for the sorting of live cells by functional properties. *Nat Microbiol* **2019,** *4* (6), 1035-1048.

235. Zhang, Q.; Zhang, P. R.; Gou, H. L.; Mou, C. B.; Huang, W. E.; Yang, M. L.; Xu, J.; Ma, B., Towards high-throughput microfluidic Raman-activated cell sorting. *Analyst* **2015,** *140* (18), 6163-6174.

236. Zhang, P. R.; Ren, L. H.; Zhang, X.; Shan, Y. F.; Wang, Y.; Ji, Y. T.; Yin, H. B.; Huang, W. E.; Xu, J.; Ma, B., Raman-Activated Cell Sorting Based on Dielectrophoretic Single-Cell Trap and Release. *Analytical Chemistry* **2015,** *87* (4), 2282-2289.

237. Yun Wang, Y. S., Di Zhu, Yuetong Ji, Tingting Wang, David McIlvenna, Huabing Yin,; Huanga, J. X. a. W. E., Probing and sorting single cells - the application of a Raman-activated cell sorter. *Spectroscopy Europe* **2013,** *25* (5), 16 - 20.

238. Ramoji, A.; Neugebauer, U.; Bocklitz, T.; Foerster, M.; Kiehntopf, M.; Bauer, M.; Poppt, J., Toward a Spectroscopic Hemogram: Raman Spectroscopic Differentiation of the Two Most Abundant Leukocytes from Peripheral Blood. *Analytical Chemistry* **2012,** *84* (12), 5335-5342.

239. Li, M.; Xu, J.; Romero-Gonzalez, M.; Banwart, S. A.; Huang, W. E., Single cell Raman spectroscopy for cell sorting and imaging. *Curr Opin Biotech* **2012,** *23* (1), 56-63.

APPENDIX

List of Abbreviations

Amp	ampicillin
AST	Antibiotic susceptibility test
ATCC	American type culture collection
BP	Breakpoint
CCD	charged coupled device
CD	carbon deuterium
CH	carbon hydrogen
Cip	ciprofloxacin
CLSI	Clinical laboratory standards institute
DNA	Desoxyribonucleic acid
ECOC	error correcting output codecs
E-test	Epsilometer test
EUCAST	European committee on antibiotic susceptibility testing
ISO	International Organisation for Standardization
LB	Lysogeny broth
MALDI-TOF	Matrix assisted Laser desorption/ionization-Time of flight
Mer	meropenem

MH	Mueller Hinton
MIC	Minimum inhibitory concentration
MLR	Multiple linear regression
MVP	Max von Pettenkofer
NA	Numerical aperture
NB	Nutrient broth
OADC	Oleic Albumin Dextrose Catalase
OD600	Optical density at 600 nm
Q1	25% percentile
Q3	25% percentile
RNA	Ribonucleic acid
rpm	rounds per minute
SEM	Scanning electron microscopy
SNR	Signal-to-noise ratio
SVM	Support vector machine
TB/TSB	Tryptic soy broth
UTI	Urinary tract infection
Van	vancomycin
WHO	World Health Organisation

List of Figures